University of California

Los Angeles

Electromagnetic Wave Interaction with the Auroral Plasma

A dissertation submitted in partial satisfaction

of the requirements for the degree

Doctor of Philosophy in Physics

by

Jacqueline Tze-Ho Pau

2003

The dissertation of Jacqueline Tze-Ho Pau is approved.

Francis Chen

Steven Cowley

Warren Mori

Ralph Wuerker

Alfred Y. Wong, Committee Chair

University of California, Los Angeles

2003

Table of Contents

List of Figures

List of Tables

Acknowledgments

I would like to acknowledge the many and important people behind the scenes that have made this thesis possible. First, I would like to give thanks to God for He has given me strength, wisdom, and endurance. As printed in the Bible, the Book of Philippians 4:13, "I can do everything through Him who gives me strength".

I would like to express my deepest gratitude to my thesis advisor, Professor Alfred Wong, for giving me the opportunity to engage in this research, for his support, guidance, and patience with me.

I am grateful to the staff of the HIPAS Observatory and the HAARP facility for their all-time supports in performing the experiments, without which, this thesis could not be completed.

I would like to acknowledge many fruitful conversations and insightful suggestions from Dr. Ralph Wuerker, Dr. Peter Cheung, Dr. Thomas Leyser, Dr. Glenn Rosenthal, and Dr. Viktor K. Decyk. They have helped me in an extent more than they probably know.

I thank Dr. Terry Bullet for his collaboration in providing ionograms, Dr. Bill Bristow and Dr. John M. Hughes for providing the SuperDARN data, Dr. Paul Bernhardt and Dr. Craig Selcher for the support in using the NRL SEE receiver.

Thanks also to all of my friends for their warmest friendship and belief in me at all times. Their friendship and encouragement have helped me to live through all the ups and downs throughout the course of this project.

Last but not least, I would like to thank my family for their patience, constant support, incessant prayers for me, and for giving me the freedom to pursue my

interest.

This research was supported by the Office of Naval Research. The HIPAS Observatory is operated by the University of California, Los Angeles and is financially supported by the Office of Naval Research. The HAARP facility is managed jointly by the Air Force Research Laboratory and the Office of Naval Research.

The article in the appendix is reprinted with the permission of the publisher:

-P. Y. Cheung, A. Y. Wong, J. Pau, and E. Mjølhus, Physical Review Letters, Vol.80, 4891-4 (1998).

Vita

1968	Born, Hong Kong
1990	B.S. (Physics) and B.S. (Applied Mathematics), UCLA, Los Angeles, California.
1992	M.S. (Physics), UCLA, Los Angeles, California.
1994–2002	Research Assistant, Department of Physics and Astronomy, UCLA.

Publications and Presentations

B. Song, A. Y. Wong, J. Villaseñor, G. Rosenthal, M. McCarrick, J. Pau, and D. Sentman, *Experimental study of double resonance parametric excitations in the ionosphere* Radio Sci., 30, 1875–83 (1995).

J. Pau, A. Y. Wong, J. Villaseñor, B. Song, and H. Zwi, *Matching the critical plasma frequencies in the ionosphere with the HIPAS heater array*, Paper presented at the meeting of the High Power RF Ionospheric Modification Workshop, Santa Fe, New Mexico, April 1995.

J. Pau, A. Y. Wong, G. Rosenthal, J. Villaseñor, and B. Song, *Generation of density perturbations by frequency matching at the peak of the ionospheric density profile*,

J. Pau, J. Villaseñor, H. R. Zwi, B. Song, E. Nichols, A. Y. Wong, and T. Tanikawa, *Preliminary results on HIPAS imaging riometer ionospheric studies*, Paper presented at the Fall meeting of the High Power RF Ionospheric Modification Workshop, Santa Fe, New Mexico, April 1996.

Paper presented at the Fall meeting of the High Power RF Ionospheric Modification Workshop, Santa Fe, New Mexico, April 1996.

J. Pau, A. Y. Wong, J. Villaseñor, T. Berkey, and L. C. Tsai, *Generation of Large Density Perturbations by Frequency Matching at the Peak of the Ionospheric Density Profile*, Paper presented at the meeting of the 26th Annual Anomalous Absorption Conference, Fairbanks, Alaska, August 1996.

J. Pau, J. Villaseñor, H. R. Zwi, B. Song, A.Y. Wong, and T. Tanikawa, *Preliminary Results on HIPAS Imaging Riometer Ionospheric Studies*, Paper presented at the meeting of the 26th Annual Anomalous Absorption Conference, Fairbanks, Alaska, August 1996.

J. Pau, A. Y. Wong, J. Villaseñor, P. Y. Cheung, T. Berkey, and L. C. Tsai, *Observations of HF Ionospheric Modification at the Peak of the Ionospheric Density Profile*, Paper presented at the Fall meeting of the American Geophysical Union (AGU), San Francisco, California, December 1996.

J. Villaseñor, A. Y. Wong, B. Song, J. Pau, M. McCarrick, and D. Sentman *Comparison of ELF/VLF generation modes in the ionosphere by the HIPAS heater array* Radio Sci., 31, 211–26 (1996).

J. Pau, P. Y. Cheung, A.Y. Wong, and W. T. Armstrong, *Beat Wave Heating of the F-Layer Auroral Ionosphere*, Paper presented at the meeting of the RF Ionospheric Interactions Workshop, Santa Fe, New Mexico, April 1997.

J. Pau, H. Zwi, A. Y. Wong, R. Wuerker , and P.Y. Cheung *Recent Results on ELF Excitations at HIPAS*, Paper presented at the meeting of the RF Ionospheric Interactions Workshop, Santa Fe, New Mexico, April 1997.

P. Y. Cheung, E. Mjølhus, D. F. DuBois, J. Pau, H. Zwi, and A. Y. Wong, *Stimulated radiation from strong Langmuir turbulence in ionospheric modification*, Phys. Rev. Lett., 79, 1273–6 (1997).

J. Pau, A. Y. Wong, and P. Y. Cheung, *Observations of HF Ionospheric Pre-conditioning near* f_oF_2, Paper presented at the meeting of the RF Ionospheric Interactions Workshop, Santa Fe, New Mexico, April 1998.

P. Y. Cheung, A. Y. Wong, J. Pau, and E. Mjølhus, *Controlled ionospheric preconditioning and stimulated electromagnetic radiation*, Phys. Rev. Lett., 80, 4891–4 (1998).

P. Y. Cheung, J. Pau, and W. T. Armstrong, *Dual-site ionospheric modification experiments*, Paper presented at the meeting of the RF Ionospheric Interactions

Workshop, Santa Fe, New Mexico, April 1999.

J. Pau, P. Y. Cheung, and A. Y. Wong, *SEE experiments at HAARP*, Paper presented at the meeting of the RF Ionospheric Interactions Workshop, Santa Fe, New Mexico, April 1999.

J. Pau, A. Y. Wong, and P. Y. Cheung, *Optimization of Ionospheric Modification near the Peak of the Ionospheric Density Profile*, Paper presented at the 41st Annual Meeting of the American Physical Society Division of Plasma Physics, Seattle, Washington, November 1999.

A. Y. Wong and J. pau, *Generation of ELF/VLF Using Frequency Sweeping Method*, Paper presented at the meeting of the RF Ionospheric Interactions Workshop, Santa Fe, New Mexico, April 2000.

J. Pau, T.B. Leyser, and A. Y. Wong, *Effects of Preconditioning of HAARP Interaction near* f_oF_2, Paper presented at the meeting of the RF Ionospheric Interactions Workshop, Santa Fe, New Mexico, April 2001.

J. Pau, A. Y. Wong, R. Wuerker, V. K.Decyk, and T. B. Leyser, *Generation of Vertical Current and ELF/VLF by Controlled Frequency sweep of HAARP*, Paper presented at the 43rd Annual Meeting of the American Physical Society Division of Plasma Physics, Long Beach, California, November 2001.

L-C. Tsai, F. T. Berkey, A. Y. Wong, and J. Pau, *Dynasonde observations of ionospheric modification experiments with the HIPAS observatory*, J. Atmos.

Sol. Terr. Phys., 63, 107–16 (2001).

J. Pau and A. Y. Wong, E. A. Gerken, U. S. Inan, and W. Bristow, *SEE and Radar Observations during the February 2002 HAARP Optical Campaign*, Paper presented at the meeting of the RF Ionospheric Interactions Workshop, Santa Fe, New Mexico, April 2002.

J. Pau, A. Y. Wong, G. Rosenthal, K. E. Koziar, and K. Stone, *Enhancement of EM-Ionospheric Interaction through Plasma Lens and Frequency Chirping*, Paper presented at the 44th Annual Meeting of the American Physical Society Division of Division of Plasma Physics, Orlando, Florida, November 2002.

J. Pau and A. Y. Wong, *SEE at near 2nd gyroharmonics*, Paper presented at the meeting of the RF Ionospheric Interactions Workshop, Santa Fe, New Mexico, April 2003.

Abstract of the Dissertation

Electromagnetic Wave Interaction with the Auroral Plasma

by

Jacqueline Tze-Ho Pau

Doctor of Philosophy in Physics

University of California, Los Angeles, 2003

Professor Alfred Y. Wong, Chair

High power radio electromagnetic waves interaction with the auroral plasma have been investigated. Plasma in this auroral region can be illuminated by EM waves for a prolonged period of time and thus, experience accumulative perturbations and resonances because of its long plasma lifetime, slow transport rates, and weak convection, especially near the peak of the ionospheric electron density profile. A plasma resonance at a specific height in the ionosphere has a corresponding EM wave frequency. These plasma resonances can enhance the local electromagnetic fields, and therefore their interactions with plasma particles leading to turbulences, local heating, density perturbations, and field aligned striations. These effects are more pronounced when the EM wave frequency is near f_oF_2, the frequency for the resonance near the peak of the ionospheric electron density profile. Optical emissions are also enhanced under such conditions.

The non-linear process at the resonance layer can stimulate emission of electromagnetic waves which appear as the sidebands of the reflected EM wave. When the ionosphere is pre-conditioned first with high power EM wave, the threshold level of this non-linear process is reduced. The spectral features of the sidebands

can then be excited with an effective radiation power (ERP) level of 24 dB less than that normally required. In particular, pre-conditioning near the f_oF_2 resonant layer can further enhance the non-linear process. At this layer, density perturbation is stronger and can affect a larger region as the density scale length is largest. Consequently, the density needs a longer time to recover.

This thesis also discusses the capability at the HIPAS facility and attempts to study interactions at the second harmonic of the ionospheric electron cyclotron frequency. This is the first investigation to date on this critical resonance. EM waves from the ground facility can reach this layer without much loss by a mode conversion from the right-circular to left-circular polarization. The plasma resonance and the cyclotron resonance can now occur in the same layer. As a result, new spectral features manifest in the sidebands of the reflected EM wave from this layer. A simple model is introduced to explain the generation mechanism of this new spectral feature.

CHAPTER 1

Introduction

1.1 The Earth's Ionosphere

The ionosphere is an example of naturally occurring plasma formed by solar photo-ionization and soft x-ray radiation. Ultraviolet radiation from the sun ionizes the atmospheric constituents. Free thermal ($1 < eV$) electrons and ions are present in the earth's upper atmosphere between 50 km and 6000 km approximately. In this region, the atmospheric temperature first increases with altitude to an overall maximum value ($\sim 900\ K$) and then becomes constant with altitude (see Figure 1.1). In the ionosphere, a balance between photo-ionization and various loss mechanisms gives rise to an equilibrium density of free electrons and ions with a horizontal stratified structure. The density of these electrons is a function of the height above the earth's surface and is dramatically affected by the effects of sunrise and sunset, especially at the lower altitudes. The presence of these free electrons in the ionosphere can influence the propagation of radio waves.

In comparison with laboratory plasmas, the ionospheric plasma is long-lived and effectively unbounded. The transport rate is low such that cumulative turbulent and radiation effects can occur. As a result, a moderate power of approximately 1 MW can excite a wide range of temporal and spatial plasma instabilities. At an altitude of 100 km, the energy flux is $\sim 0.56\ mW/m^2$, neglecting ionospheric

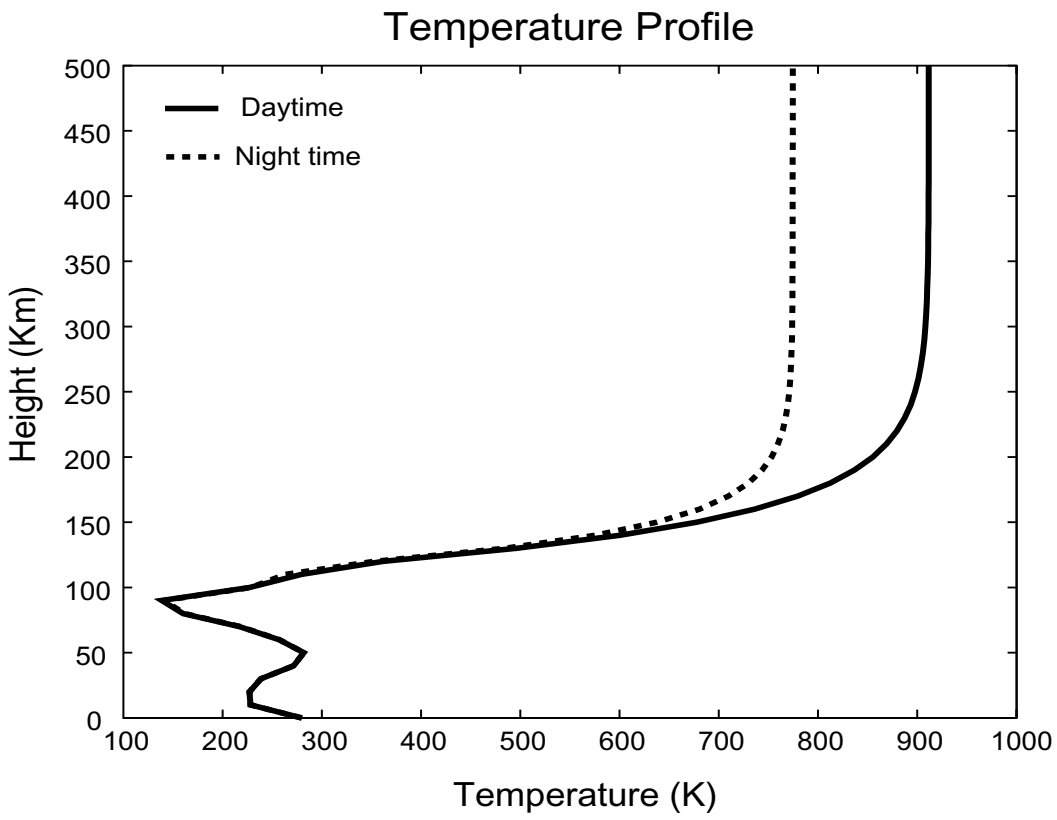

Figure 1.1: The earth's atmospheric temperature profiles calculated from the MSIS-E-90 Atmospheric Model at HIPAS, Alaska.

absorption. Even though the transmitted power is more powerful than that used in the laboratory plasma experiments, this pumping energy is rather weak when compared to the ionospheric plasma thermal energy. The ratio is on order of 10^{-4} – 10^{-3}. The characteristic scale lengths of many plasma phenomena are much smaller than the size of the ionospheric plasma, therefore experiments can be conducted in a very homogeneous environment.

1.2 Structure of the Ionosphere

The ionosphere is conventionally divided into the D-, E-, and F-regions (see Figure 1.2). The D-region lies between 60 and 95 km, the E-region between 95 and 150 km, and the F-region lies above 150 km. In daylight, it is possible to distinguish two separate layers within the F-region, the F1 (lower) and the F2 (upper) layers. During nighttime, these two layers combine into one single layer. The combined effect of gravitationally decreasing densities of neutral atoms and molecules and increasing intensity of ionizing solar ultra-violet radiation with increasing altitudes (see Figure 1.3, 1.4) , gives a maximum plasma density during daytime in the F-region at a few hundred kilometers altitude. During daytime, the ratio of charged particles to neutral particles concentration can vary from 10^{-8} at 100 km to 10^{-4} at 300 km and 10^{-1} at 1000 km altitude.

The D-region is both a refracting and an absorbing medium for radio waves. When a radio wave travels through the ionosphere, it interacts with the electrons and sets them into oscillation. With the high concentration of both molecular and atomic gas particles in the D-region, these oscillations are damped by collisions between electrons and gas molecules. Throughout the D-region the collision frequency decreases exponentially with height, roughly proportional to the neutral gas pressure, whereas electron density increases rapidly with height. In this

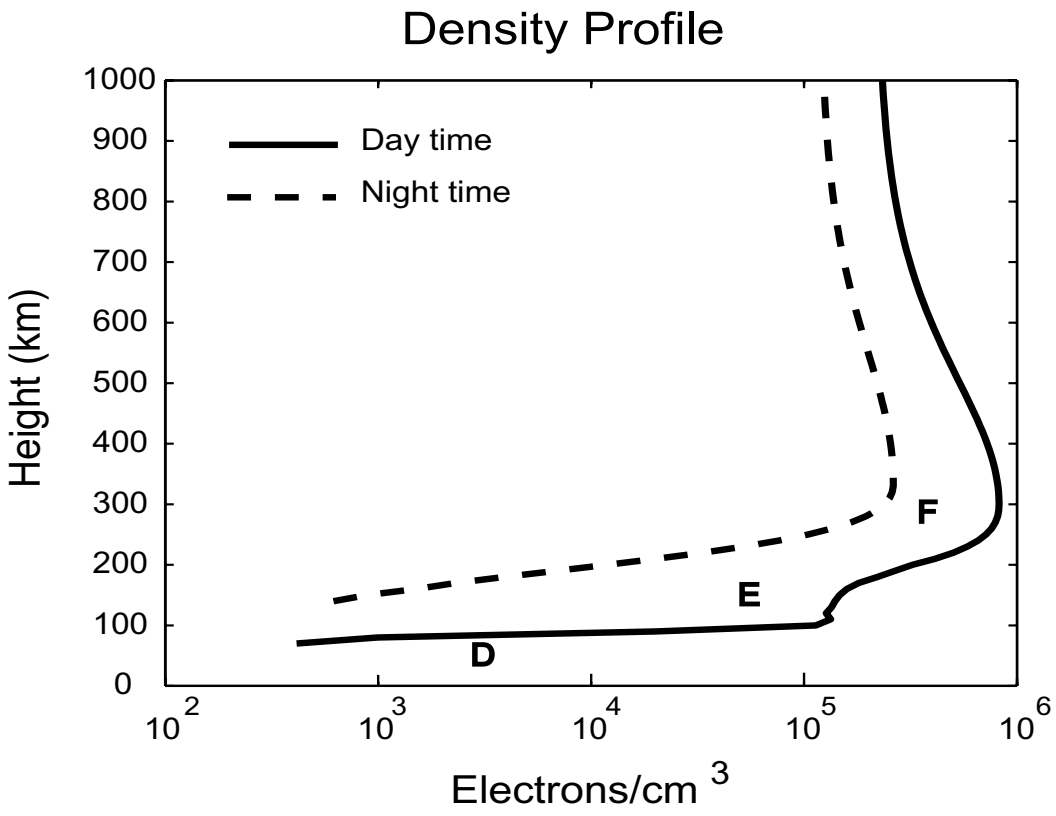

Figure 1.2: Various layers of the ionosphere. Actual electron density profiles vary over a wide range and depend markedly on time of day, season, sun-spot number and whether or not the ionosphere is disturbed.

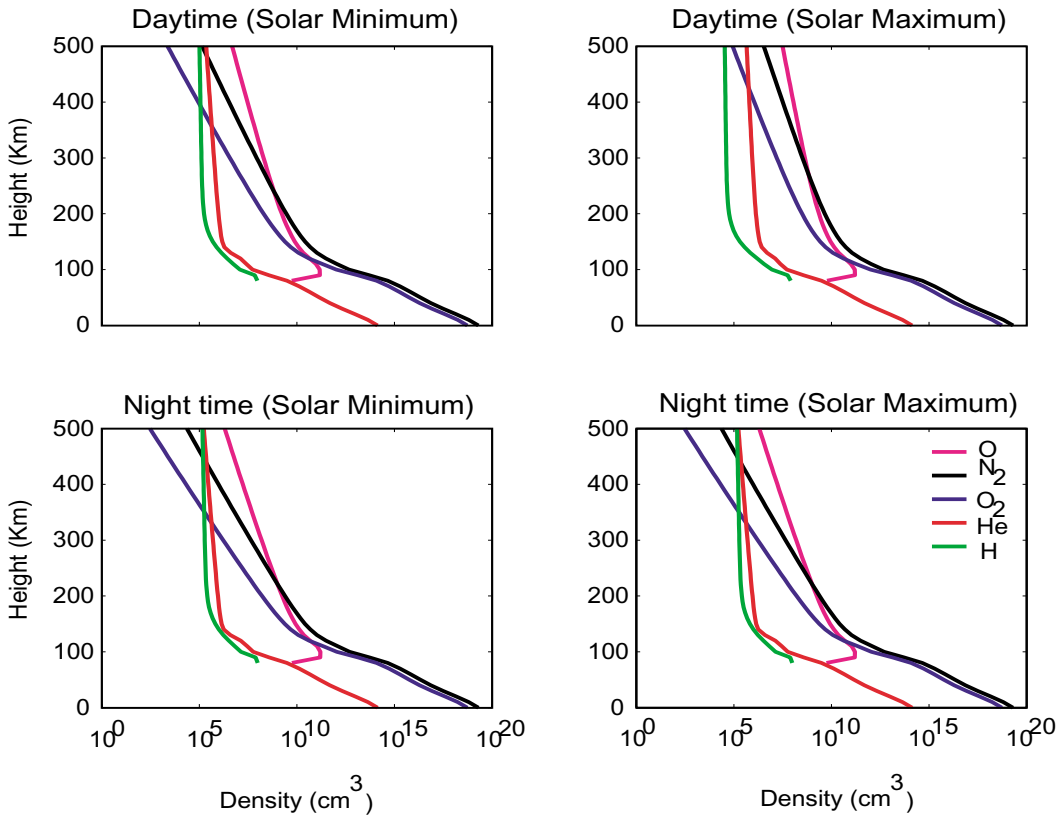

Figure 1.3: Neutral density profiles calculated from the MSIS-E-90 Atmospheric Model for both solar maximum and solar minimum period at HIPAS.

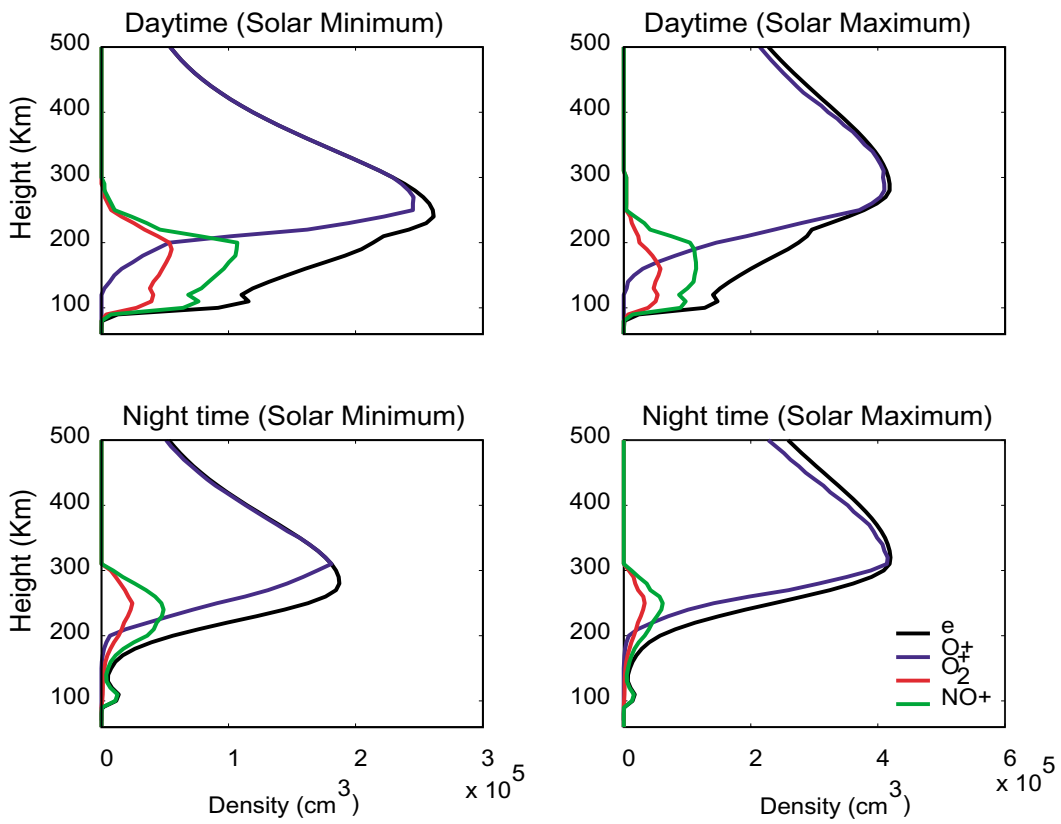

Figure 1.4: Atomic, and molecular ion profiles calculated from the International Reference Ionosphere IRI-2001 model for both solar maximum and solar minimum period at HIPAS.

region, chemical processes are most important, molecular ions dominate, and N_2, O_2, and O are the most abundant neutral species. The electron density is sharply reduced at night because molecular ions have a much higher recombination rate with electrons than atomic ions. Thus, the linear absorption of radio waves in this region varies from a typical 4 – 10 times (or 6 – 10 dB) during daytime to a much lower rate during nighttime.

The behavior of the E-region is subject to close solar control. In this region, the basic chemical reactions are not as complicated as those in the D-region. The major ions are NO^+, O_2^+, and N_2^+. The total ion density is of the order of 10^5 cm^{-3}, while the neutral density is greater than 10^{11} cm^{-3}. Therefore, the E-region plasma is weakly ionized, and collisions between charged particles are not important. The sporadic E layer consists largely of relatively dense patches of electrons with a horizontal extent of tens of kilometers and are thought to be produced by meteoric particles. In addition to photo-ionization, energetic particles from the solar wind collide with the neutral gas resulting in additional plasma production in the E-region.

The F-region is much thicker than the E-region and heavily ionized, where maximum electron density locates in the range 200 – 400 km. In this region, the O^+ and O atomic species dominate. In daylight, a subsidiary bulge is observed in the curve of electron density just below the maximum. This is the F1-layer. The layer where the main maximum electron density locates is the F2-layer. The F2-layer's maximum ionospheric electron plasma frequency is the critical frequency "f_oF_2". The peak ion density in the F2-layer is roughly a factor of 10 greater than that in the E-region, while the neutral density (10^8 cm^{-3}) is still orders of magnitude greater than the ion density. The plasma in this region is partially ionized and collisions among charged and neutral particles must be taken into

account. The effective electron collision frequency is $\nu_e \sim 500\ Hz$ at 200 km altitude and the thermal electron mean free path is about 1 km. The scale height of the ambient plasma density profile is defined as the height differences for the density to increase by a factor of e from its reference value. At the bottom boundary of F-region, where the pump wave is reflected, the scale height is typically 50 km. It is much larger than the vacuum pump wavelength of ~ 30 – 100 m.

Sunrise and sunset have little or no influence in the F-region. However, the geomagnetic field plays an important role in the structure and dynamics of this region. As charged particles collisions are sufficiently less frequent in this region, the motion of charged particles is constrained by the earth's magnetic field. At high latitudes, where the geomagnetic field is nearly perpendicular to the earth's surface the field lines can extend into the interplanetary medium. Charged particles ejected from the sun are thus guided down into the ionosphere and depicted as the aurora.

The electron distribution throughout these layers is subject to diurnal, daily, seasonal, and geographical variations as well as the magnetic disturbance associates with solar activities. Among these layers, the F2 layer is the most variable. When a solar flare occurs, the sudden increase of x-ray emission will result in a large increase of ionization in the lower D-, E- and F-regions of the ionosphere, on the sunlit side of the earth. Sufficiently large or long-lived solar flares will produce geomagnetic storms that may result in ionospheric disturbances.

The earth's magnetic field varies partly due to the external currents and the induced earth currents. "Quiet days" are days when the transient magnetic variations are regular, while on "disturbed" days they are magnetically disturbed. During these disturbed days, additional currents circulate in the ionosphere. In

addition to the visible aurora, the ionization process is enhanced, corresponding to the increase in sporadic E and D-region absorption.

1.3 Propagation of Waves in the Ionosphere

The presence of the earth's magnetic field makes the ionosphere a double refractive medium. When an electromagnetic (EM) wave of frequency f_o from the ground enters the ionospheric D-region its refraction depends on the initial polarization state of the incident wave. Two types of waves are most commonly used in the ionospheric modification experiments, namely ordinary (O-mode) and extraordinary (X-mode) waves.

At high latitudes such as Alaska, the magnetic field is directed nearly vertically downwards. When a right-handed circularly polarized (O-mode) pump wave is propagating upwards which is anti-parallel to the earth's magnetic field, its polarization becomes left-handed after reflection in the ionosphere. An X-mode pump has a polarization opposite to the O-mode pump and is the same direction as an electron cyclotron rotation.

Using the Appleton-Hartree dispersion relation, the refractive index n, neglecting collisions, is

$$n^2 = 1 - \frac{X(1-X)}{(1-X) - \frac{1}{2}Y_T^2 \pm [\frac{1}{4}Y_T^4 + (1-X)^2 Y_L^2]^{\frac{1}{2}}} \tag{1.1}$$

where $X = \omega_{pe}^2/\omega^2$, $Y = \omega_{ce}/\omega$, $Y_L = Y\cos\theta$, $Y_T = Y\sin\theta$, ω_{pe} and ω_{ce} are the plasma and cyclotron frequencies, and θ is the angle between the direction of propagation and the magnetic field. The "+" sign refers to the O-mode wave and the "-" sign refer to the X-mode wave [72]. From equation 1.1, an O-mode wave will reflect at the height where $\omega_o = \omega_{pe}$, and an X-mode wave will reflect when it's frequency satisfies the relation of $\omega_{pe}^2 - \omega_{pe}\omega_{ce} = \omega_o^2$, where ω_o is the EM

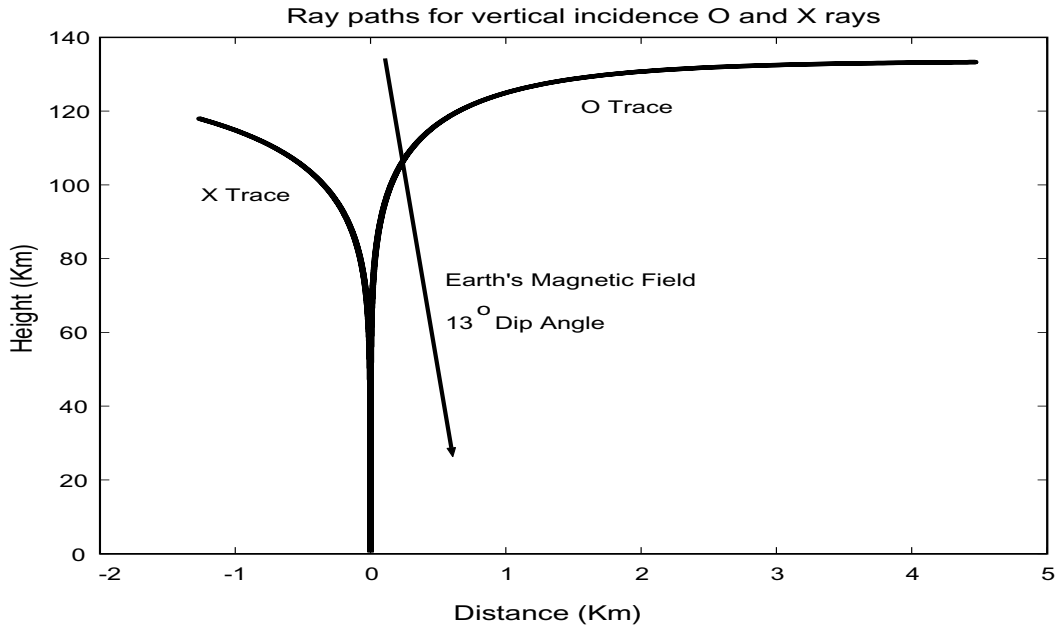

Figure 1.5: The ray paths computed from a cold-plasma theory. The Earth's magnetic field makes an angle of 13° with the density gradient at HIPAS.

wave frequency. Hence, an upward directed X-mode wave will reflect at a lower altitude than an upward directed O-mode wave (Figure 1.5). The separation of the O- and X-mode critical frequencies is approximately $f_{ce}/2$. Raytracing calculations indicate that their ray paths are very different and well-separated laterally [8].

The angle between the pump electric field and the ambient geomagnetic field determines the nature of the plasma turbulence and the induced plasma waves. Langmuir turbulence is most strongly excited in the plasma resonance region parallel to the geomagnetic field. With the larger magnetic field angle at lower latitudes the parallel electric field component remains parallel to the magnetic

field over a larger altitude range below the reflection height. Therefore, the excitation of the Langmuir turbulence is more important in the lower latitudes. Upper-hybrid (UH) turbulence occurs where the electric field is perpendicular to the geomagnetic field. At higher latitudes, the UH resonance region is only a few kilometers below the plasma resonance region.

Not only are there differences in the excitation locations, the physical processes and temporal scales are also very different between the Langmuir and UH turbulence. The Langmuir turbulence involves ponderomotive interactions between the Langmuir and ion-acoustic oscillations whereas UH turbulence involves both ponderomotive and transport processes. The Langmuir turbulence includes dynamics at the short time scale of electron fluctuations and at long time scale of ion fluctuations. Meanwhile, the UH turbulence also includes the much slower dynamics of transport processes.

A vertical incident pump wave is partially or totally reflected in the reflection region of a monotonically increasing plasma density with height. The incident and the reflected waves interact with each other and form a standing wave pattern [61, 62]. As the pump wave approaches the reflection region, the wavelength of the pump increases and the wave slows down. Because the energy flow must be constant, the decrease in the wave velocity leads to an increase in the wave amplitude. This is usually referred to as "swelling". This swelling causes an enhancement in the intensity of the pump wave electric field, and thus a tendency towards the Langmuir turbulence. Swelling only occurs in the parallel component of the electric field. Therefore, the maximum electric field strength is located just below the reflection level where the pump electric field is almost parallel to the geomagnetic field. The angle between the pump electric field and the geomagnetic field increases below the reflection region. At the UH resonance

layer, the electric field is almost perpendicular to the geomagnetic field, thus the perpendicular electric field intensity drops to minimum. When the pump frequency approaches the critical frequency, the density gradient in the pump reflection region decreases. The swelling now decreases but the vertical extent of the pump–plasma interaction region increases, which affects the pump-induced perturbations. The condition when the pump wave interacts strongly with the region containing the highest plasma density in the ionosphere is here referred to as the "matching condition". It is important to discriminate between the plasma and UH matching condition at which the pump frequency equals the maximum ionospheric plasma frequency and the maximum UH frequency equals the pump frequency respectively.

1.4 Mode Conversion and Formation of Caviton

In heating of the F-region ionosphere, the high power EM wave modifies the interaction region near the reflection height by increasing both the local electron temperature and reducing the local plasma density. Due to the anisotropic transport rates along and across the ambient magnetic field, elongated field-aligned density striations (FAS) can form. Heating the ionosphere can excite new plasma oscillations and enhance those already present. This strongly influences the propagation of the EM pump wave in the perturbed region and causes large antennuation in the reflected wave, refer as anomalous absorption, [55] and scattering.

Consider an EM wave with frequency ω, propagating toward the reflection level with its wave vector $\vec{k}$ inclined at an angle θ with the density gradient. The wave is partially reflected as it first reaches its cut-off frequency at $\omega_{pe}(z) = \omega\cos\theta$. The remainder of the wave energy will then tunnel to the resonance layer, $\omega_{pe}(z) = \omega$, where it is transformed into an electrostatic (ES) wave via linear or

resonant mode conversion [33, 100, 54, 70, 47, 97, 67], and the vertical component of the E field can be resonantly enhanced. Moreover, the combination of large field enhancement, long density scale length, and large interaction region facilitates the conversion of pump EM waves to ES waves either via direct conversion [104] or parametric instability [106].

The ensuing nonlinear evolution of the ES waves leads to a strong Langmuir turbulence [11] and a density depression or caviton at the resonance layer. This resonance enhanced caviton can be generated even for a weak incident field, for values as small as $\frac{E^2}{4\pi nT} \approx 10^{-6}$. Once a caviton is created, it can decay into several cavitons [105]. This will affect a larger area around the resonance layer. Both laboratory plasma experiments [80, 2] and computer models [14] have confirmed the conversion of long wavelength EM waves into shorter ES waves at the resonance layer. Satellite data [103] also reveal a large depletion in the total electron content above the heated region at the unique condition of matching.

1.5 Stimulated Electromagnetic Emissions

When a powerful EM wave is transmitted into the ionosphere from the ground, it can excite a wide range of plasma processes. Most of these processes are plasma turbulence excited by the EM wave through parametric instabilities [79, 17, 25, 71, 20, 82]. Parametric instabilities play the dominant role near the reflection height of the EM wave. The decay modes of the parametric instabilities at this height are Langmuir wave and ion acoustic wave/field-aligned density irregularities. However, in the high latitude region, the UH resonance layer becomes important. Perpendicularly propagating modes such as the UH wave/electron Bernstein (EB) wave and the lower-hybrid (LH) wave/ion Bernstein wave/field-aligned density irregularity are involved in the parametric instabilities. These

processes can be studied using different diagnostic techniques such as ground-based incoherent and coherent scatter radar, direct spectral measurement, low power diagnostic waves, VHF satellite scintillation measurements, airglow measurements during nighttime, and in situ measurements by sounding rockets and satellites. The monostatic incoherent scatter diagnostic technique is sensitive to the longitudinal electrostatic fluctuations whose wave vector $\vec{k}$ in space satisfies the Bragg condition, $\vec{k} = 2\vec{k}_r$, where $\vec{k}_r$ is the radar wave vector. The direct spectral measurement of the weak non-thermal electromagnetic radiation stimulated by the EM wave in the interaction region is a powerful tool for observing wave-wave interactions (Figure 1.6). This pump-induced radiation is called the "Stimulated Electromagnetic Emissions" (or SEE) or in the Russian literature, the "ionospheric radiation" or "radio emission".

Since the discovery of the SEE in ionospheric modification experiments at the heating facility near Tromsø in Norway in 1981 [90, 85], extensive studies in SEE have been performed continuously [7, 6, 27, 58, 57, 59, 60, 83, 82, 86, 89, 87, 90] and the United States [1, 12, 13, 88]. The excitation of the SEE depends on the transmitted pump frequency, polarization, power, and duty cycle, and on the ionospheric conditions. In general, the SEE sidebands are asymmetric about the pump frequency. Some commonly observed spectral features [82] include the downshifted maximum (DM), the broad continuum (BC), the narrow continuum (NC), and the broad upshifted maximum (BUM) (Figure 1.7). The DM is a prominent spectral maximum downshifted by 10–20 kHz from the pump frequency and is usually several tens of dB above the noise level [82, 60]. The BC is a wide skewed feature which may extend more than 100 kHz below the pump frequency [56]. The NC is similar but much narrower which only extends 10–20 kHz below [27, 31]. The BUM consists of relatively broad upshifted sidebands which extend up from 15–200 kHz [87, 82]. It is a spectral feature that strongly

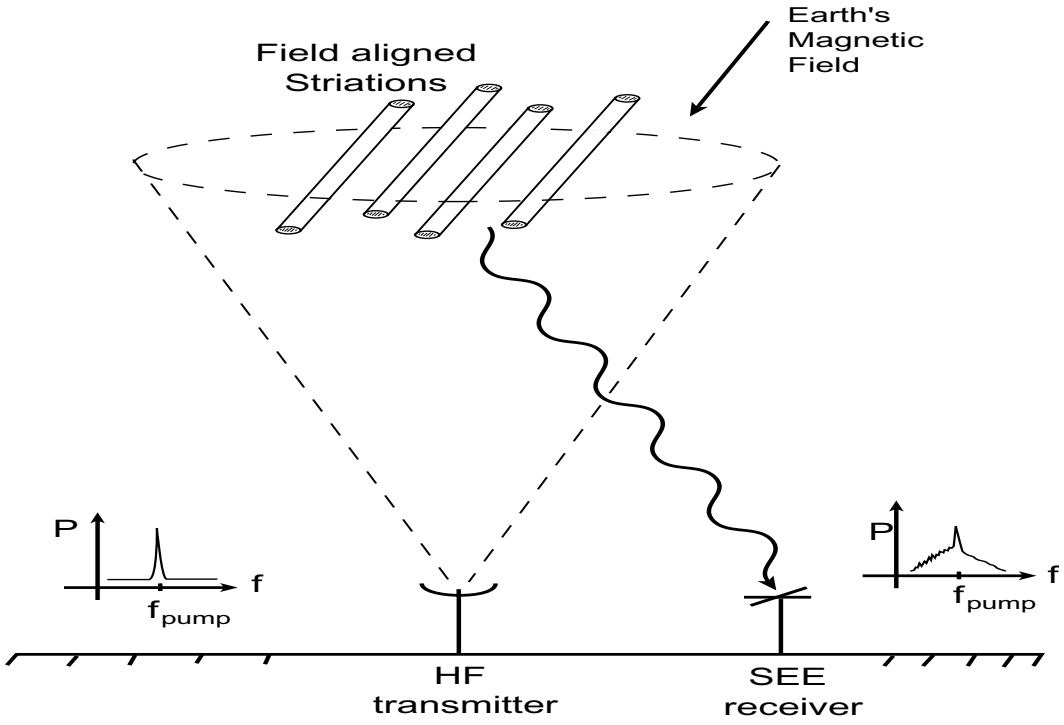

Figure 1.6: Cartoon of direct spectral measurement setup.

depends on the pump frequency being slightly above a harmonic of the electron cyclotron frequency [57, 32]. The generation of density perturbation or FAS caused by high power EM wave was clearly demonstrated by radar backscatter experiments from the resonance volume [26, 65, 22, 31]. Anomalous absorption of O-mode EM waves have been extensively studied [15, 94, 53, 98, 81]. It is generally agreed that the connection between FAS and anomalous absorption involved the scattering of the EM waves at striations [37]. Two components of anomalous absorption was reported by Frolov [27, 31]. These two components are a fast component related to the development of meter scale irregularities, and

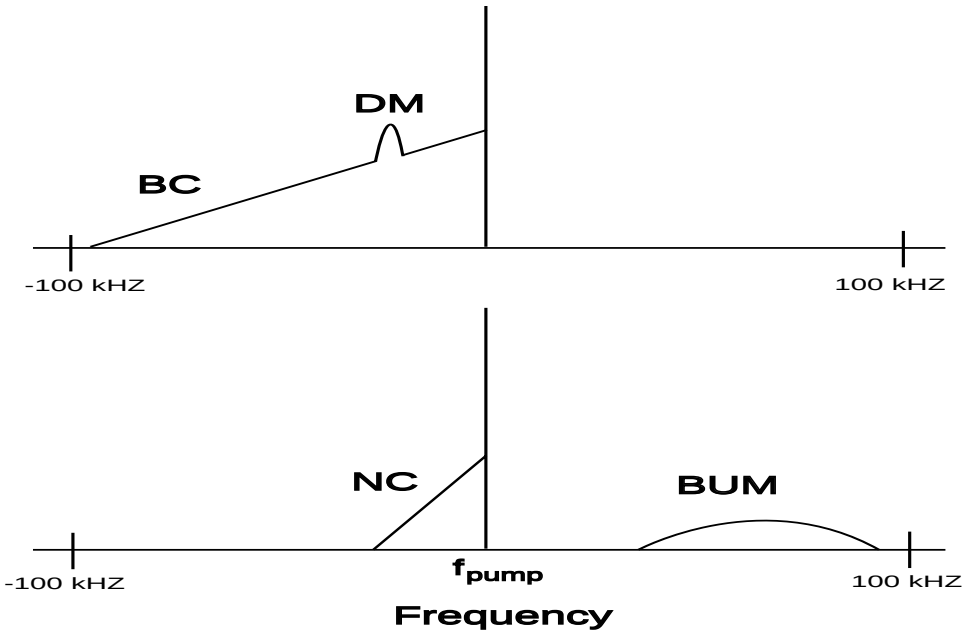

Figure 1.7: Diagrams showing the four basic SEE features.

a slower component related to the development of decameter scale irregularities. A close relationship between the FAS and the SEE is studied by simultaneous measurements of anomalous absorption to indicate the presence of striations and SEE [86].

The DM is attributed to the trapped UH oscillation decay instability in a pre-formed density depletion [39, 68, 69], and the self-localized UH oscillation decay in quantized density irregularities [51, 52]. The BC is interpreted in terms of induced scattering of UH waves on thermal ions, which gives a broad spectrum of UH waves followed by the scattering of the UH waves from small scale striations into electromagnetic radiation [35, 77, 78, 36].

The SEE also exhibits a wide range of time scale from less than a millisecond up to tens of seconds. On the short time scale, the SEE is related to the ponderomotive processes and the Langmuir turbulence. On the long time scale, the SEE is closely related to the presence of small-scale geomagnetic FAS with transverse dimensions ranging from 1 to 10 m. The small-scale FAS are typically attributed to the driven UH turbulence [42, 40, 50] while the large-scale FAS are attributed to the thermal self-focusing instability of the pump wave [43, 44].

1.6 Previous Work

Ionospheric modifications by high power radio waves, refer as pump waves in the rest of the thesis, and interactions among various types of ionospheric waves are essentially nonlinear phenomena. High frequency (HF) radio waves have been used to study these nonlinear phenomena since the early 1970's with the completion of the first American ionospheric modification facility in Platteville (near Boulder), Colorado, USA [10]. Among the expected results from ionospheric modifications is an increase of electron temperature, hence the term "heating facility" is adopted. Although a number of experiments have been performed to study the D-region modification effects, most interest is focused on the F-region modification phenomena in which plasma instabilities play a dominant role. Early experiments focused primarily on the driven Langmuir turbulence using the incoherent scatter radars [34, 106, 9, 45] and later the SEE [90], giving access to both the Langmuir and UH/EB turbulences [57, 83] and optical emission [99]. Surprising results revealed the anomalous absorption on a time scale of tens of seconds, of the radio waves incident on the heated volume [93, 15] and the generation of different sizes of field-aligned irregularities [23, 91, 26, 65, 94].

Usually the driven HF plasma turbulence experiments are performed with

overdense pumping or at a frequency well below the maximum ionospheric plasma frequency (the critical frequency, f_oF_2). Only a few experiments performed at or near f_oF_2 have been reported [64, 26, 46, 103, 58, 5]. Early experiments at Arecibo, Puerto Rico, found that large scale modification of the ionospheric plasma profile occurred, particularly when the ionospheric critical frequency was at or near the pump frequency as suggested by ionograms that showed thickened or split traces and/or hooks in the traces [34]. Furthermore, experiments at the UCLA-High Power Auroral Stimulation (HIPAS) Observatory, Alaska, using O-mode pumping at 3.349 MHz and an effective radiated power of 80 MW was conducted. Large scale electron density reductions were observed in ionograms and in the total electron content from a satellite beacon measurement at 413 MHz traversing at 1000 km altitude above HIPAS under matching conditions during sunrise [103]. In particular, observations showed that the maximum ionospheric plasma frequency was clamped to the pump frequency in the region above HIPAS while the plasma density in the neighboring region continued to increase normally because of the solar radiation in the morning. The SEE measurements at the Tromsø facility, Norway, using a pump frequency of 4.04 MHz showed that DM emission could be excited even when the pump frequency was a few hundred kilohertz above the maximum plasma frequency. This is consistent with the excitation of the DM under the UH frequency matching [58]. The SEE measurements between electron cyclotron harmonics (n = 3 to 7) have been studied extensively at the Tromsø facility and the Sura facility [57, 58, 59, 56, 31, 28, 29, 86]. To summarize their results, the commonly observed DM feature is absent, and the BUM feature appears only when the pump is slightly above the gyroharmonics in the SEE spectrum. Experiments at the Sura facility in Russia, of a pump frequency of 5.8288 MHz observed that pump-enhanced airglow at 630 nm is most intense when the pump frequency is near the critical frequency, which was

attributed to increased interaction distances for electron acceleration during the matching condition [5].

1.7 Outline of Thesis

The topics in this thesis pertain to an experimental study of the ionospheric auroral plasma using high power radio frequency EM waves. Specifically, we examine the non-linear process at the resonance layer, a phenomenon which depends on not only ionospheric parameters such as the density scale length, collision frequency, and geomagnetic field strength, but also EM wave parameters such as the frequency, power, and polarization. Interactions with the EM waves below the peak of the ionospheric electron density profile or in the overdense region have been studied most while those in the region near the peak of the density profile (f_oF_2) remain unknown. We are interested in understanding the "matching" condition by characteristics of EM wave reflections near the peak of the density profile. Most ionospheric modification facilities are limited technologically to frequencies higher than the second harmonics of the ionospheric electron cyclotron frequency. The second part of this thesis examines interactions at the second gyroharmonics.

The outline of this thesis is as follows: Chapter 2 includes descriptions of both the transmitter and receiver hardware used in this thesis. Background diagnostics to determine the ionospheric conditions and the conditions for the experiments.

Chapter 3 discusses the large density perturbation created under the matching condition via a series of short pulses within a range of frequency and experimental results from the X- and O-mode polarizations under the matching and the overdense condition.

Chapter 4 examines the density perturbation and the field-aligned striations in terms of the SEE spectral features, their enhancement of the non-linear process under the matching conditions, and influences on them from pre-conditioning the ionosphere.

Chapter 5 presents the experimental results and discussions on the second gyroharmonics. A simple model is included to explain the generation mechanism of the SEE feature excited at the second gyroharmonics.

Chapter 6 provides a summary and suggestions for further studies.

CHAPTER 2

Experimental Setup

2.1 Experimental Facilities

All of the ionospheric heating facilities have high-gain antenna arrays operating at frequencies between 3 and 10 MHz with approximately 50 to 100 MW effective radiated power (ERP). The experimental results discussed in this document are from research conducted in Alaska, specifically at the University of California, Los Angeles's (UCLA's) - High Power Auroral Stimulation (UCLA-HIPAS) Observatory near Fairbanks, Alaska, and at the High Frequency Active Auroral Research Program (HAARP) facility at Gakona, Alaska, 285 km south of HIPAS. Figure 2.1 shows the two heating facilities together with other nearby research sites in Alaska.

The HIPAS Observatory is located at Two Rivers, Alaska, 25 miles east of Fairbanks. It has geographic coordinates of $64°52'N$ and $146°50'W$. It lies within the auroral oval. The local magnetic field has a dip angle of $76°30'$ ($13°30'$ from vertical) and a declination of $28°02'E$. The magnetic field strength of approximately 0.515 Gauss giving in an electron cyclotron frequency (f_{ce}) of 1.44 MHz at 250 km.

HIPAS has a total output power of 800 kW. The antenna array (Figure 2.2), which consists of eight crossed dipoles 14 m (47') above the ground, is tuned to radiate at either 2.85 MHz or 4.53 MHz. The antennas together have a gain

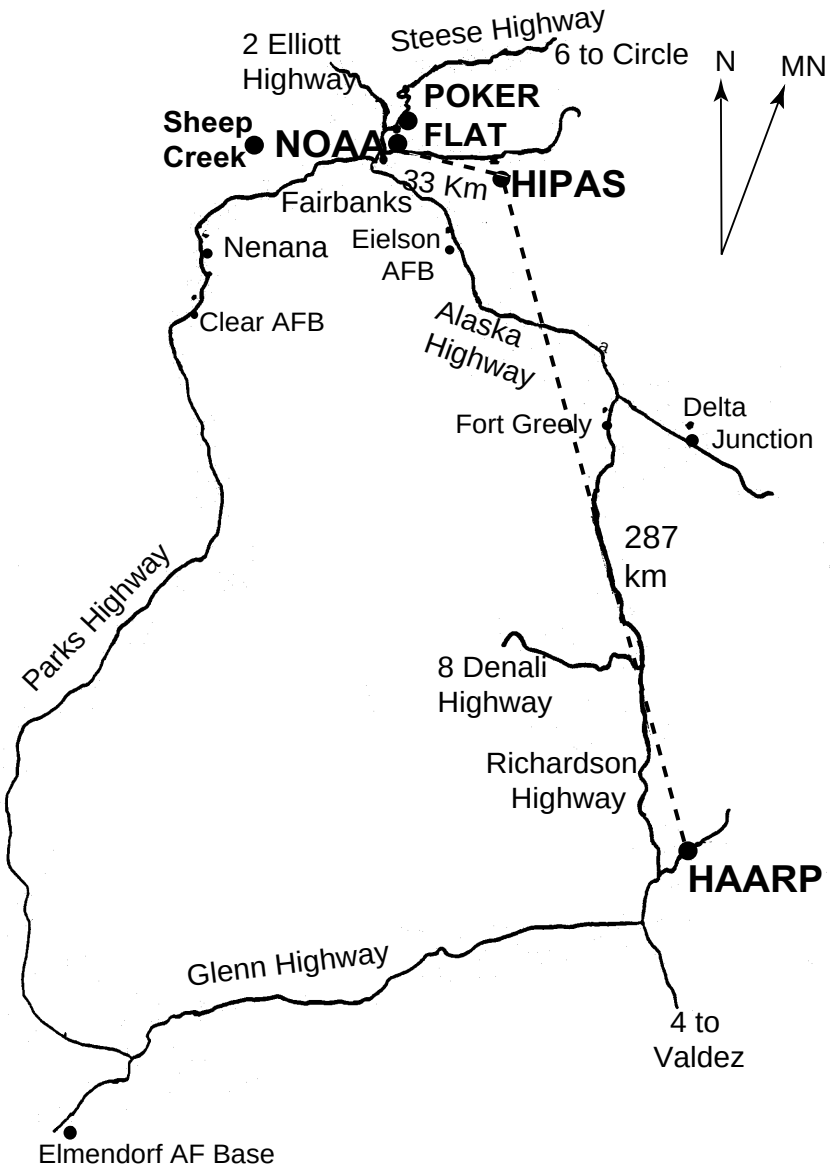

Figure 2.1: Ionospheric Research Site Map.

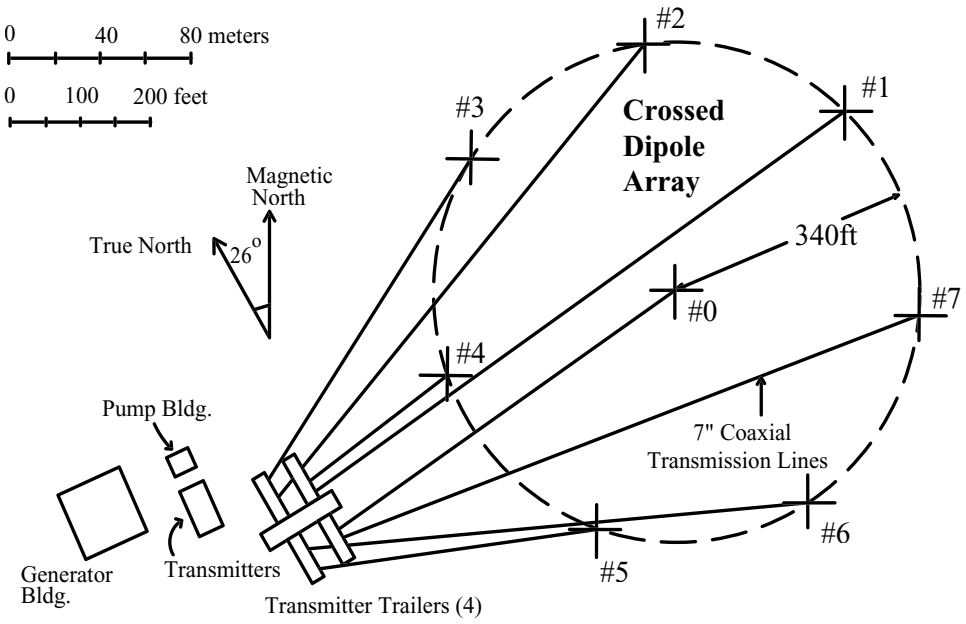

Figure 2.2: (Top) The layout of the HIPAS array with eight crossed dipole antennas field. Each antenna is connected to a transmitter with a total maximum output power of 800 kW.

approximately 18.4 dB intensity (dBi) (17.5 dBi) for frequency at 2.85 MHz (4.53 MHz), corresponding to a full beam width at half power angle of 22°. The characteristics of the transmitter are listed in table 2.1.

Each dipole antenna is connected to its own transmitter, originated from the Platteville facility, which consists of one 4CV100,000 (class C) final and one 3-1000Z (class B) intermediate amplifiers. This transmitter system allows control of the phase of each radiating antenna at the low-level (milliwatt) input to each transmitter. By adjusting the phases of the antennas relative to one another, the EM wave can be pointed towards any desired direction (Figure 2.3). All eight

	Full Power		1 Tx
Frequency (MHz)	2.85	4.53	both
Antenna Gain (dB)	18.4	17.5	3
Power (kW)	800	800	45
Effective radiated power (MW)	55.3	40	0.09
Electric field strength at 250 km altitude (V/m)	0.24	0.2	$9.5e^{-3}$
Energy flux at 250 km altitude (mW/m^2)	0.07	0.05	0.0001

Table 2.1: HIPAS operating parameters (Absorption is neglected).

transmitters and their water cooling systems are powered by two 1500 horsepower (1.2 MVA each), 4800-volt 3-phase diesel electric generators. The polarization of the antenna can also be independently configured to radiate in either O-mode (right-circular) or X-mode (left-circular) by reversing the leads on one antenna. Detailed information on the HIPAS facility is available [102].

The reflected HF signals from HIPAS were monitored by a receiver at the National Oceanic and Atmospheric Administration (NOAA) Tracking Facility at Gilmore Creek, 33 km northwest of HIPAS as shown in Figure 2.1 . This receiver site is shielded from the transmitted ground wave by mountains. The calculated diameter of the heated region in the F-layer is about 100 km, which is large enough to consider the receiver as lying beneath the heated ionosphere.

The other Alaska heating facility, the High Frequency Active Auroral Research Program (HAARP) (Figure 2.1), is located at Gakona. It has the geographic coordinates $62°23.5'N$ and $145°3.3'W$. HAARP is managed jointly by the Air Force Research Laboratory and the Office of Naval Research. It is devoted to

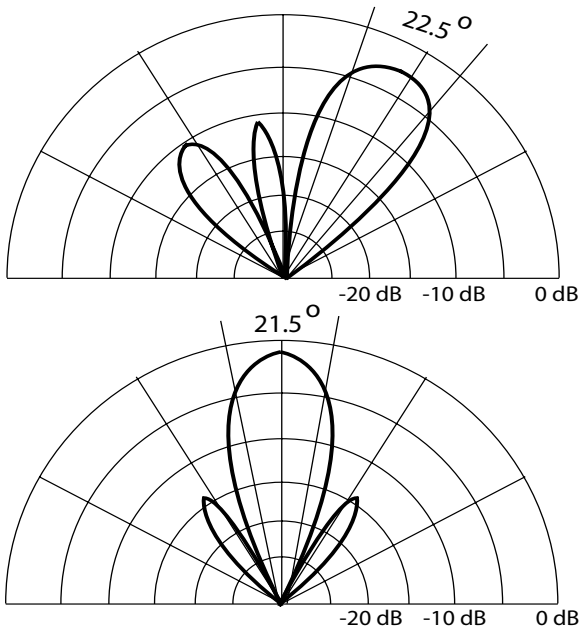

Figure 2.3: (Top) Beam pattern with antennas phased 30 deg off vertical. (Bottom) Beam pattern with all 8 antennas in phase.

the study of upper atmospheric physics and potential applications [74, 63]. The magnetic field strength is approximately 0.504 Gauss at an altitude of 250 km, which would produce an electron gyro frequency of 1.41 MHz. Currently, this array consists of 48 antenna elements, arranged as a rectangular array of 8 columns by 6 rows. Each antenna element is driven by a separate transmitter and has a combined radiated power of 960 kW. All the transmitters are powered by one diesel generator which is rated at 3,600 horsepower and can produce 2,500 kW of electrical power. The HAARP transmitter system with the antenna matching unit can radiate over a frequency band from 2.8 MHz to 10 MHz with antenna gain as a function of operating frequency (see Table 2.2). The antenna beam can

antenna array	6 x 8	
transmitting frequency (MHz)	2.8 – 8.1	
Pointing angle	Within 30 degrees of vertical	
Reposition time	15 degree within 15 microseconds	
Polarization	Left/right Hand circular, Linear	
Frequency (MHz)	2.8	8.1
Net radiated power (kW)	720.0	936.0
Antenna gain (dB)	11.8	22.8
Half power beam widths (N-S plane)	31.9 degrees	11.0 degrees
Half power beam widths (E-W plane)	44.6 degrees	15.4 degrees
Effective radiated power at the center	70.5 dBW	82.5 dBW
Energy flux at 250 km altitude ($\mu W/cm^2$)	0.0014	0.023

Table 2.2: Parameters of the HAARP antenna array.

be pointed at any direction within $\pm 30^{\circ}$ from the zenith in either circular or linear polarization. In addition, it has the capability of simultaneous transmission at two different operating frequencies.

The HAARP antenna system consists of multiple independently driven horizontal cross dipole elements. Each antenna consists of two upper and two lower cross dipole antennas for operation at the low frequency (2.8 – 7 MHz) and the high frequency (7 – 10 MHz), respectively. The dipoles are mounted to an aluminum tower 72 feet high which is supported at the base by a thermopile for reliable and long-lasting stability. A wire mesh ground screen is attached mechanically and electrically to the tower at a height of 15 feet above the ground.

2.2 Diagnostics Techniques

2.2.1 HF Receiver

Two types of HF receivers were used at different stages in this project, a narrow band (8 kHz) HF receiver (Figure 2.4) for monitoring the skywave and a wide band (125 kHz) HF receiver (Figure 2.5) for monitoring the SEE. The receiver was set up at the NOAA Tracking Station at Gilmore Creek, Alaska, approximately 34 km northwest of the HIPAS Observatory (see Figure 2.1). The receiving antenna was an efficient T-shaped broadband double Bazooka antenna (Figure 2.4b) built along the hillside and did not require a balun. This antenna consists of a coax (RG58) cable with its shield removed at the center. The feedline was attached directly to the two open ends and acted as a half-wave dipole along with the open wire end sections. Since the antenna had no exposed metal wire, static charges could not accumulate. Noise is reduced by $\sim 6\ dB$ in comparison to antennas constructed of exposed wire.

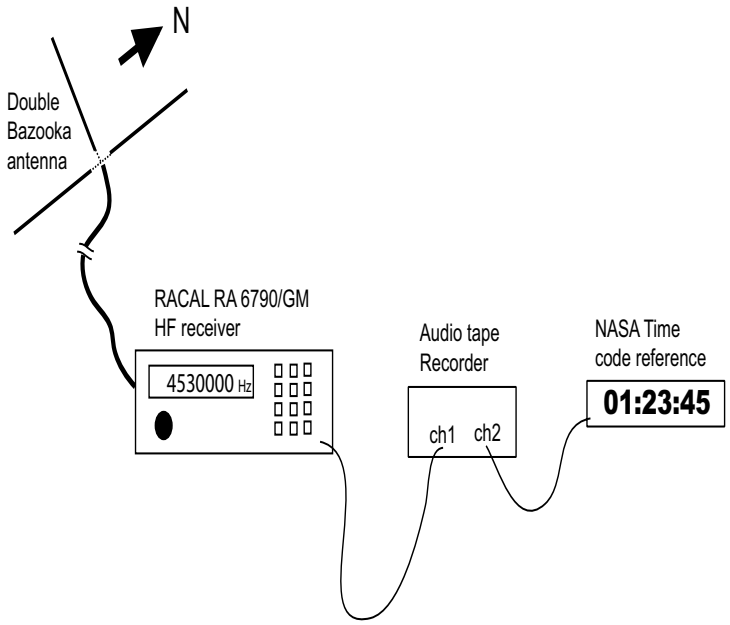

Figure 2.4: Setup of the narrow band (8 kHz) HF receiver for monitoring the skywave.

The double Bazooka antenna was connected to an indoor receiver via an RG-8 cable to minimize loss. The input was then connected directly to a RACAL HF radio receiver, model RA6790/GM, a solid-state receiver fully synthesized, microcomputer-based, tunable, and designed for a frequency range of 0.5 MHz to 30 MHz. It was capable of either automatic RF gain control (AGC) or manual control of the AGC threshold within the range of 0 to 110 dB above the preset. Manual mode was chosen for our work to detect the amplitude fluctuation of the reflected skywave with a frequency tuning resolution of 1 Hz. The receiver had seven built-in IF filters; we used an 8 kHz bandwidth filter to eliminate aliasing signals. The audio output was recorded on a digital audio tape through a phone

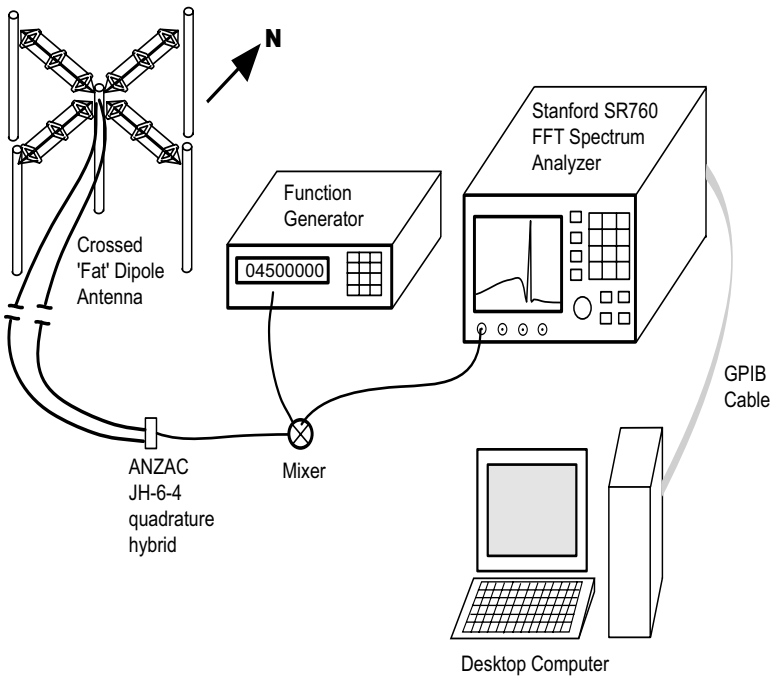

Figure 2.5: SEE receiver setup.

jack connector. An external 1 MHz reference signal was fed into the RACAL for timing accuracy. The second channel simultaneously recorded the NASA time code reference.

2.2.2 SEE Receiver

A wideband (125 kHz) receiver was used to monitor the SEE signals from the heated region. The whole receiver system (Figure 2.5) included a cross "fat" dipole antenna (see Figure 2.6), a frequency generator, a Stanford SR760 FFT spectrum analyzer, and a Pentium II desktop computer. The "fat" dipole antenna

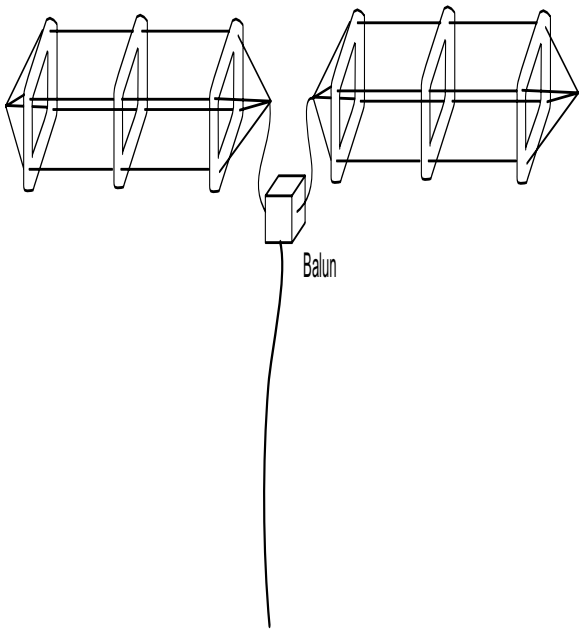

Figure 2.6: Fat dipole antenna.

was 19 m long and consisted of a 'bundle' of 4 wires, spaced approximately 30 cm apart, was easy to assemble and thus portable. The center of each dipole was fed to a 4:1 impedance ratio voltage falun. The cross dipole was aligned along the magnetic north-south and east-west directions. Signals from the two baluns were combined through an Anzac JH-6-4 quadrature hybrid and then mixed with an IF signal from the HP3253A function generator. At a frequency either 50 kHz or 60 kHz below the pump frequency and an amplitude of -10 dBm. The mixer output was connected to the SR760 spectrum analyzer.

For our work, the SR760 spectrum analyzer was set to have a frequency span of 100 kHz with a resolution of 250 Hz. The SR760 has a dynamic range of 90 dB and a digitizing rate of 256 kHz for its 16 bits A/D. The analyzer has a

built-in digital filter which filters and heterodynes the input in real time. The SR760 offers four types of windowing functions. The Hanning window which is the most commonly used window with amplitude variation of about 1.5 dB was used throughout the project. The SEE spectra shown in the following chapters are averages over 10 spectra with equal weighting in RMS to reduce fluctuations. The SR760 was automated by a personal computer via GPIB. The processed data was saved in the same computer.

2.2.3 Background Diagnostics

An ionosonde is a basic device used to measure the ionospheric electron density distribution. A series of short pulses are transmitted upward to the ionosphere, and then reflected from a layer whose local plasma frequency, $\omega_{\mathsf{p}} = (4\pi n_{\mathsf{e}} e^2/m_{\mathsf{e}})^{1/2}$, equals the incident wave frequency. The reflected pulse is recorded by a receiver after a time delay equal to the total time of flight of the pulse, t. Giving the pulse propagation at the speed of light, the virtual height, h', can be obtained by $h'(f) = 1/2ct$. Since the pulse is traveling in a plasma media, the speed of the pulse is smaller than the speed of light. The value of the virtual height obtained from the above equation is thus greater than the true height. A plot of the virtual heights versus the corresponding frequencies is called an ionogram [49].

A vertical-incidence ionosonde, the Lowell Digital Ionospheric Sounding System (DISS), operated by the Air Force Space Forecast Center at Sheep Creek, about 50 km west of HIPAS is available through a 1200/2400 baud modem connection. It has a fixed probing time interval and frequency range, which provide the general information on the density profile and the peak frequencies of the ionospheric F1, F2, and E layers every 30 min. Another digital sounder, the Lowell Digisonde model DPS-4, located at the HAARP facility, is accessible via

internet connection. The ionogram at the HAARP facility is updated every 15 min.

A Stanford Research Institute (SRI) digital ionosonde located at the NOAA facility can be accessed and initialized through an internet connection. When performing experiments at the HIPAS facility, the SRI ionosonde is set to sound every 10 minutes to provide the ionospheric background condition at the receiving site.

The critical frequencies of the ionospheric E and F layers are influenced by the solar activities. When sunspots appear on the surface of the sun, strong magnetic fields may be detected on earth. During a magnetic disturbance, additional currents circulate in the ionosphere, especially at high latitudes, and concentrate along the auroral field lines. Enhanced ionization in the ionosphere causes stronger absorption in the E and D-regions. Both sunspots and solar flares can greatly enhance ionospheric ionization [16]. Hence, both magnetic and solar information is needed to predict the ionospheric conditions and to determine the parameters in the experiments.

A magnetometer is an instrument for measuring the strength and direction of magnetic fields on or near the Earth surface and in space. Using magnetometer data, one can track the current state of the geomagnetic conditions including the magnetic fluctuations due to auroral substorms and magnetospheric storms. A riometer is a device using cosmic radio noise to measure ionospheric absorption. This cosmic noise absorption has a sidereal variation from the changes in the ionization and the condition of the upper atmosphere. Thus by monitoring the background cosmic noise intensity on the ground, we can observe disturbances in the ionosphere, which often reflect auroral events at higher latitudes. The magnetometer and riometer data are collected at both the High Latitude Monitoring

Station (HLMS) at Elmendorf Air Force base near Anchorage and at the United States Geological Survey (USGS) College station as a part of the Space Environment Laboratory Data Acquisition and Display System (SELDADS) database. The daily summaries of ionosphere and solar geophysical activities are available on the internet (http://www.sec.noaa.gov/forecast.html). In addition, the HLMS has a 50 MHz single beam radar that measures reflections from the auroral structures in the E-region. It covers the distance from the Anchorage station to approximately 100 miles north of HIPAS, $\sim$ 1200 km from the radar (Figure 2.7) .

The Super Dual Auroral Radar Network (SuperDARN) is an international collaborative program for scientific investigation of the upper atmosphere, ionosphere, and magnetosphere. It is a network of high-frequency radars for studying the Earth's ionosphere. The SuperDARN consists of HF radars in the northern and southern hemispheres. Three radars within this network observe the Alaska sector, Kodiak and King Salmon in Alaska, and Prince George in British Columbia. The HAARP facility is centered in the Kodiak field of view at about 650 km range. Each radar's azimuthal scan is done in 16 sequential beams within 1 to 2 minutes. There are several scan modes for different temporal and spatial resolutions. The primary product of the radars is line-of-sight plasma drift velocity in the F-region. Combining all the velocity data from the entire northern hemisphere network produces convection maps. The SuperDarn radars can also determine the evolution of density irregularities generated by the HF heating in the F-region.

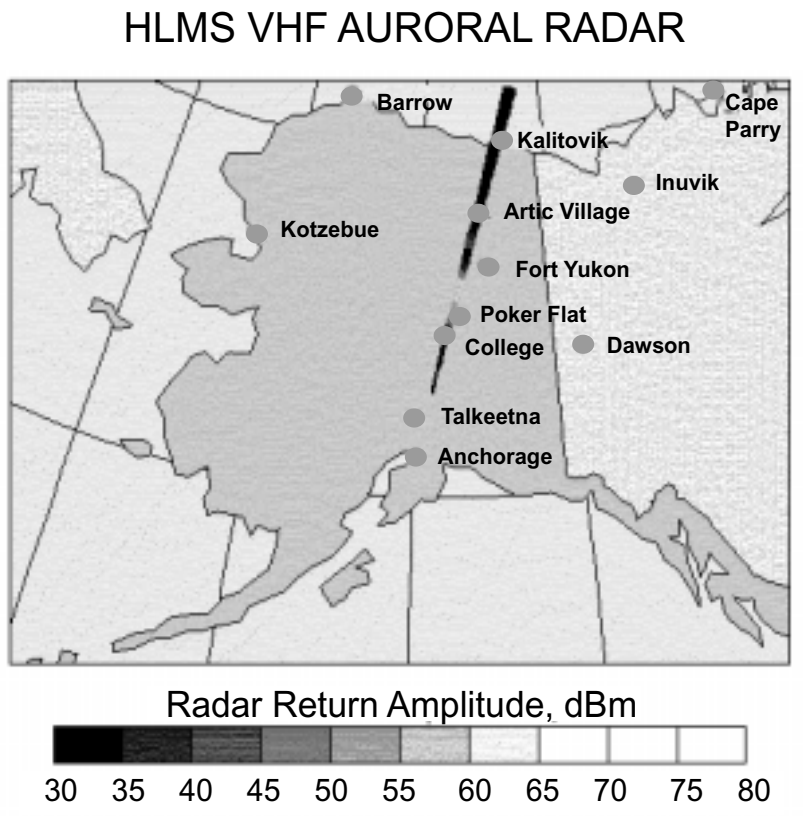

Figure 2.7: Radar coverage area of the HLMS auroral radar.

2.3 Conditions for the Experiment

The effect of matching at the peak frequency in the F layer is optimized under quiet ionospheric conditions. These quiet conditions allow an unambiguous determination of the peak ionospheric plasma frequency f_0F_2, a better determination of the time window for the matching conditions, and reproducible experiments. Normal absorption in the collisional D-region (70 – 90 km) is a prerequisite to efficient coupling to the higher altitude. An ionosonde records the range of frequency for observable return pulses and thereby determines the absorption in the ionosphere. As a collisional absorption is inversely proportional to the HF frequency, clear echo returns at low frequencies indicate low absorption and no field-aligned precipitation. Magnetometer readings also help determine the conditions in the ionosphere. A magnetic fluctuation of more than 300 nT implies a very absorptive condition whereas a fluctuation of 100 to 200 nT suggests a high electron density in the E-layer. The latter will cause an EM wave reflection at a lower altitude. Thus, a minimal magnetic fluctuation is preferred for coupling the EM wave to the F-layer. The process of ultraviolet (UV) ionization and molecular recombination changes the ionospheric density profile. As a result, the electron density is higher and more variant during daytime and in summer at high latitude. For these reasons, the matching experiments are conducted between late September and early April either in the morning or late in the afternoon.

CHAPTER 3

Reflected EM Wave under Matching Condition

This Chapter will present the experimental results on the density profile modifications under the matching condition or when the heater frequency is equal to the peak ionospheric plasma frequency, f_oF_2 at the HIPAS facility.

3.1 Spreading of the Ionosonde Echo Returns

3.1.1 Setup of the Dynasonde

A joint campaign to measure the ionospheric modification was conducted in the Fall of 1992, with the Utah State University (USU) Dynasonde group. The ionosphere was modified using the HIPAS heater at a frequency of 2.85 MHz. The digital USU Dynasonde was deployed at the NOAA facility during the campaign. The receiving antenna array of the Utah Dynasonde had an L-shape with a cross dipole at the corner as is shown in Figure 3.1. The reference point "O" was at the center of the cross dipole pair. Each dipole was aligned along a side of the "L" in the north-south and east-west directions. This set up was an improved configuration by which the Dynasonde data could be processed with minimal phase aliasing [92] . The Dynasonde transmitter was located approximately 200 m away from the receiver. The dynasonde used a TMS32010 DSP processor and an echo detection scheme to eliminate interference and atmospheric noise

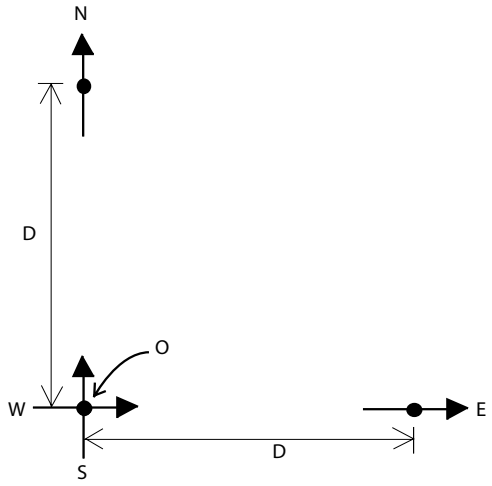

Figure 3.1: The USU dynasonde receiving antenna array configuration. D is typically 30 meters.

from the ionogram. The Dynasonde transmitted a group of four pulses at each of the specified frequencies. Within the group, a small frequency increment of 8 kHz was used for additional group height accuracy and tests of pulse dispersion. The reflected echoes were received by the two dipole antennas for each pulse. A total of eight echoes were received from one pulse set. The built-in software program then converted these eight echoes into the echolocation, wave polarization, and Doppler shift. More details on the Dynasonde can be found in the paper [92, 19, 18, 107, 108].

3.1.2 Experimental Results

During the Fall 92 campaign, the USU Dynasonde transmitted every three to six minutes. Figures 3.2 and 3.3 show the Dynasonde results observed on October

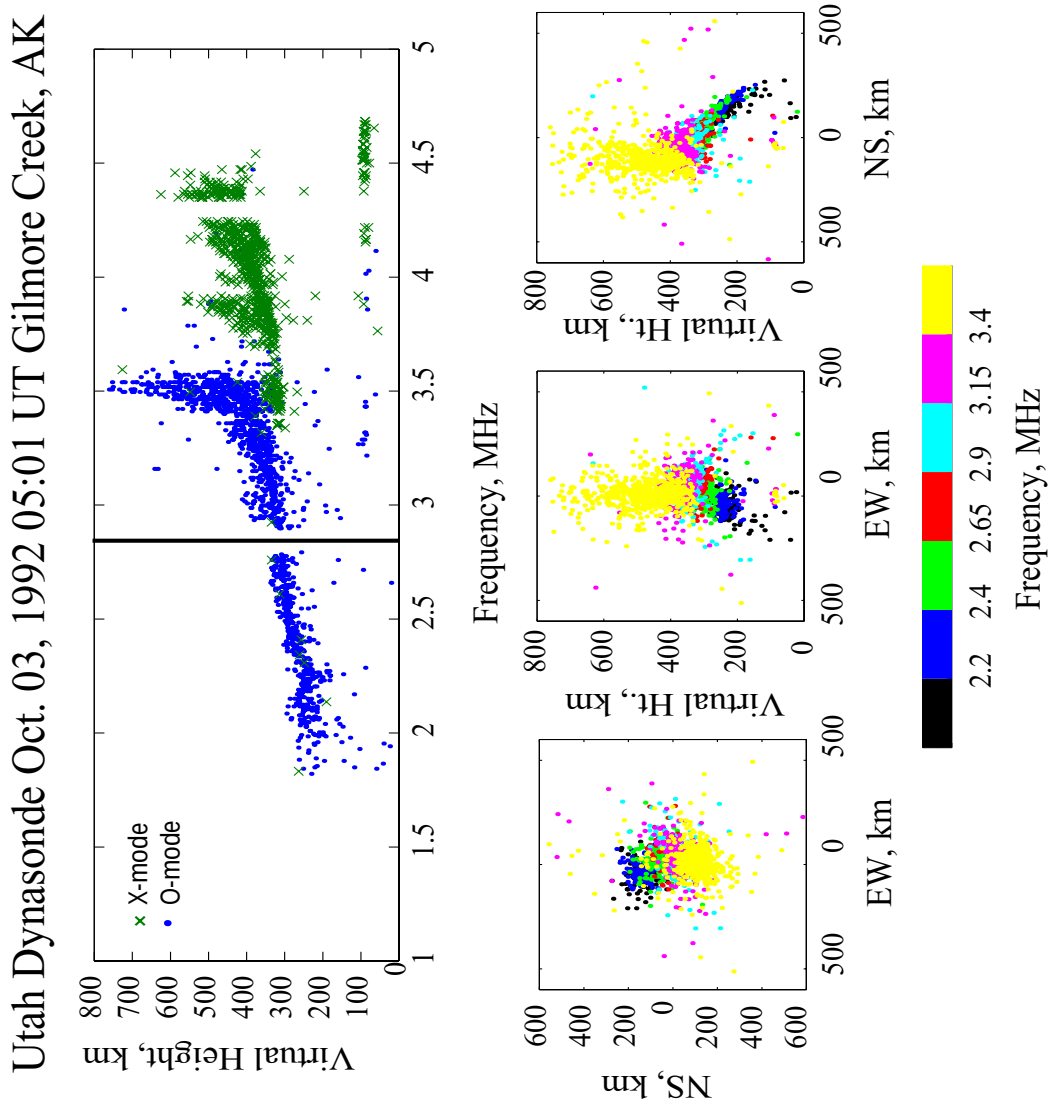

Figure 3.2: Ionogram obtained on October 3, 1992 at 05:01 UT (before matching) by the Utah Dynasonde. (Top panel) The ionogram shows a smooth F-layer return at a peak frequency 3.5 MHz. The solid line indicates the pump frequency. (Bottom panel) Skymaps show the scattering pattern of the O wave echo return. Geomagnetic coordinate is used.

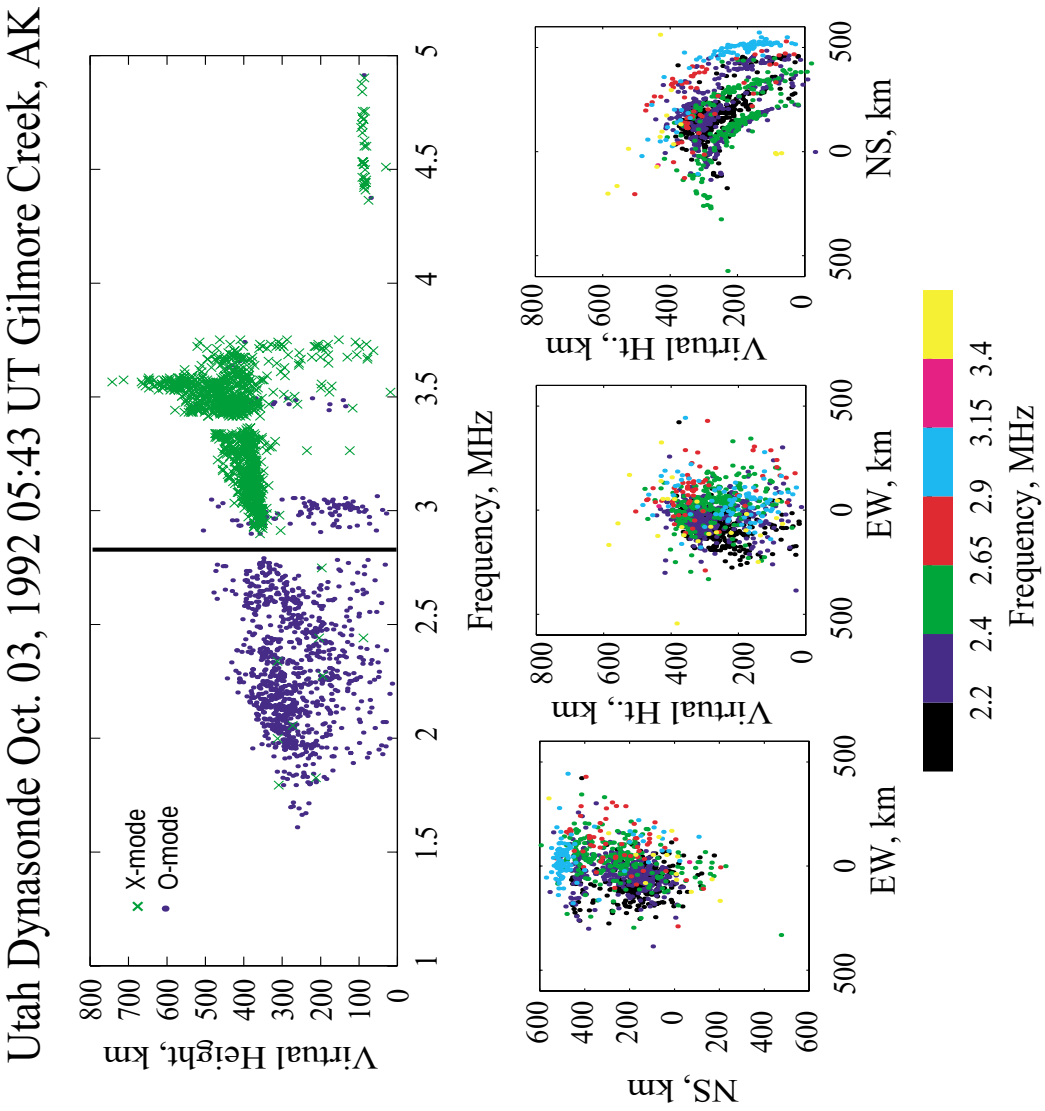

Figure 3.3: Ionogram taken at 05:43 UT when the pump frequency matched the f_oF_2 at 2.85 MHz. (Top panel) The ionogram shows a spreading of the echoes with a frequency span of approximately 0.8 MHz and the spatial disturbance extends over a distance of 250 km. The solid line indicates the pump frequency. (Bottom panel) Skymap during matching shows the O wave echoes spread more towards the northeast direction and are closely aligned with the magnetic field lines. Geomagnetic coordinate is used.

3, 1992. The HIPAS pump frequency was within the f_oF_2 range, 2.75 – 2.95 MHz (or 2.85 ± 0.1 MHz), from 0532 to 0558 Universal Time (UT). The heater caused a sudden increase in the signal to signal ratio at a frequency around 2.85 MHz. Hence, the echo recognition process rejected all the data around 2.85 MHz and leaves a gap in the O wave trace of the ionogram.

The USU ionograms showed clear non-spread echo returns from the F layer before the heater frequency matched f_oF_2 (Figure 3.2 top panel). As f_oF_2 decreased towards the pump frequency at 2.85 MHz, the ionograms showed apparent spreading around 2.85 MHz (Figure 3.3 top panel). The spread of the echoes extended over a broad frequency range and a large spatial extent. The spread had a frequency span of approximately 0.8 MHz, and the disturbance appeared to extend over a distance of 250 km. The affected region corresponded to an absolute density change of $\Delta n = 4.8 \times 10^2$ cm^{-3} in the density profile.

The skymaps in Figure 3.2 and 3.3 display the O wave echo scatter locations in the ionosphere before and during the matching, respectively. The (0,0) coordinate refers to the zenith at NOAA using the geomagnetic coordinate system. The (x,y) coordinates correspond to the virtual reflection location of the echo derived from the angles of arrival. During the period of matching, the echoes spreaded more towards the northeast direction and were closely aligned with the magnetic field lines. This indicates that large-scale, field-aligned density striations are created, giving rise to enhanced scattering of HF waves over an extended frequency range.

3.1.3 Discussions

During the matching conditions, ionosonde echoes spreads more towards the northeast direction, i.e., towards the geomagnetic pole (the magnetic declina-

tion at HIPAS is $\sim 26°$). As shown in Figure 3.4 , the O-mode shape spot is asymmetric, leaning towards the northeast due to ray bending near the reflection layer. Near the matching conditions, the resonance layer can extend as far as 60 km. Thus the strongest heating should result in an extended region northeast of HIPAS where most of the echo locations are observed. The echo locations also appear to align more or less along the magnetic field (Figure 3.3 bottom panel). This is consistent with the model in which large spread of ionosonde echo returns can be attributed to anomalous and multiple scattering of the echoes by FAS, first initiated near the reflection region and then extended to align along the field [26]. During the matching condition, only spreads at lower heights are observed. Fewer data points are recorded in the matching case (Figure 3.3 bottom panel) in comparison to the overdense case (Figure 3.2 bottom panel) since the ionosphere is transparent to EM waves at frequencies greater than f_oF_2. As f_oF_2 decreases, less echo returns are recorded on the ground within the same sounding frequency range.

In conclusion, the USU ionograms show significant density perturbation during the critical frequency match. Large density perturbation indicates the collapse of caviton into smaller ones. The amount of turbulence can be estimated from the variation in the wavenumber distribution. Individual caviton cannot be resolved using an ionosonde alone, more diagnostics need to be introduced in the future.

3.2 Comparison Between X- and O-Mode Heating

X- and O-mode heating has been conducted several times. Every attempt was made to ensure that the experiments were conducted under quiescent and reproducible ionospheric conditions. Nevertheless, conditions did vary, and the data presented here were recorded under different ionospheric conditions ranging from

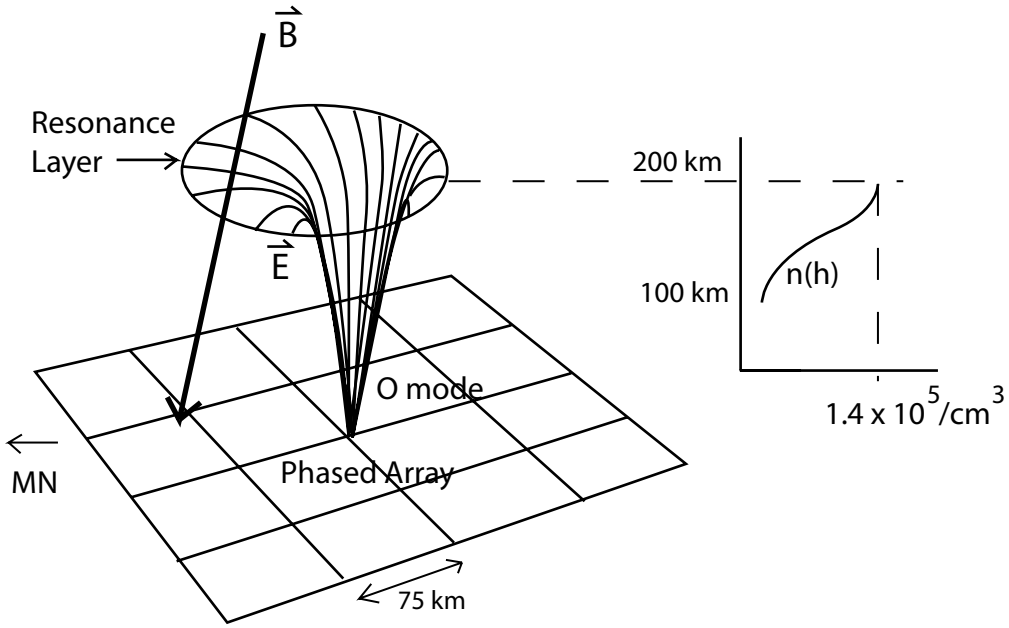

Figure 3.4: The ray paths computed from a cold-plasma theory. The Earth's magnetic field makes an angle of 13° with the density gradient at HIPAS.

being quiet to moderate magnetic activity. Experiments were usually performed late in the afternoon or during the evening. During these periods of time, the peak frequency in the F layer decreased from a value well above to below the HIPAS operating frequency at 2.85 MHz or 4.53 MHz. Continuous wave (CW) was used with continuous switching between O- and X-mode. The reflected signals from the pump were monitored using the HF narrow band receiver at the NOAA facility.

3.2.1 Experimental Results

Figures 3.5 to 3.10 show the comparison between X- and O-mode CW heating at 2.85 and 4.53 MHz. The ionospheric conditions were similar on these two days with no presence of any E layer throughout the experiments.

A difference of 3 – 6 dB in the reflected amplitude is observed between X- and O-mode heating until near the matching condition. Near the matching condition, the signal strength of the O-mode skywave return decreases dramatically so that the difference between the two modes becomes 10 – 15 dB (Figures 3.5 and 3.6). This appears to be a rather robust and reproducible phenomenon under the matching condition for O-mode heating and indicates an anomalous or enhanced absorption of the pump wave. Long density scale length, a large interaction region, efficient mode conversion, and long interaction time (due to slow convective loss as a result of long scale length) of the converted ES waves all contribute to this effect and will be discussed in more details later.

The Doppler frequency shifts of the skywave return also show a significant difference between X- and O-mode heating. Factoring the effects of statistical noise and background fluctuations of the ionosphere, a net positive frequency shift is observed from the O-mode heating and a smaller negative shift from

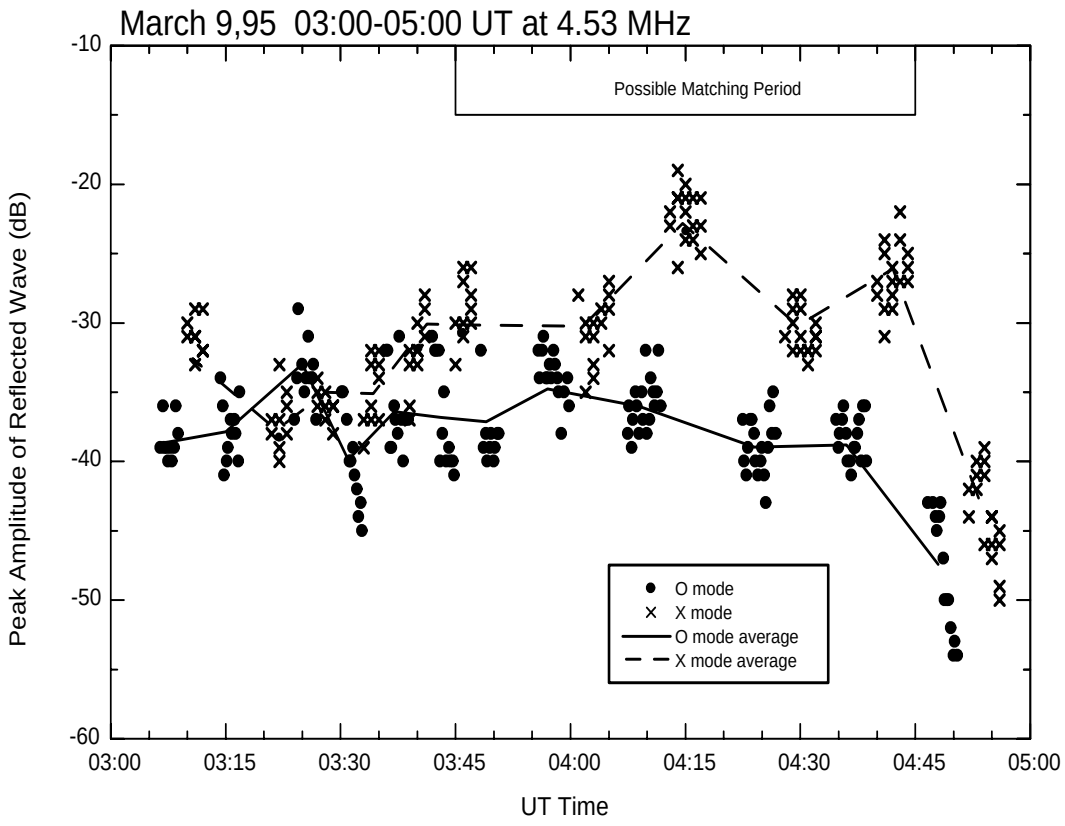

Figure 3.5: Data obtained on March 9, 1995 showing the amplitude of the reflected wave and the interpolated density profile generated from the DISS during the experiments. The pump frequency was set at 2.85 MHz.

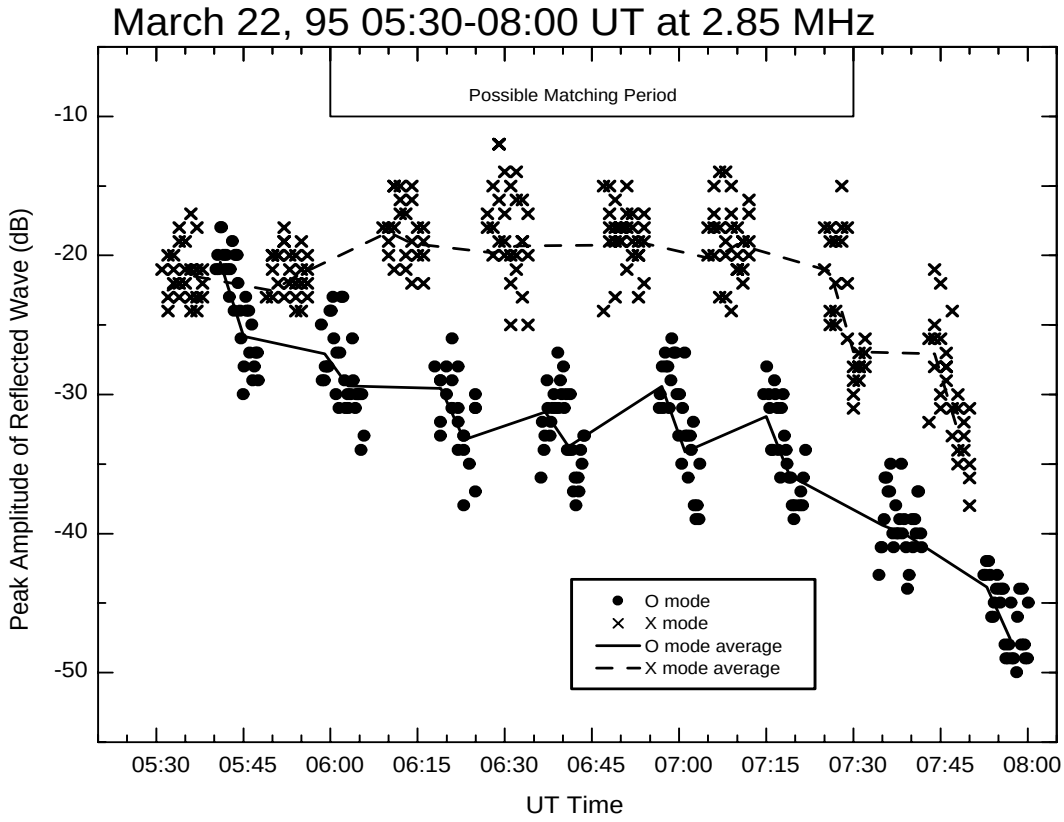

Figure 3.6: Data obtained on March 22, 1995 showing the amplitude of the reflected wave and the interpolated density profile generated from the DISS during the experiments. Ionograms were taken only before and after possible matching condition. The pump frequency was set at 4.53 MHz.

the X-mode heating. Figure 3.7 illustrates how frequency shifts become more significant when the heater frequency is close to f_oF_2. Since Doppler shifts of HF waves in general indicate motion of the reflecting layers or density changes along the ray path, the results appear to indicate that X- and O-mode heating produce opposite layer motions or density changes. It should be emphasized that the ray paths for the X- and O-modes are very distinct and quite far apart laterally for high latitude launch as is the case at HIPAS and that the X-mode cutoff occurs at a much lower height than that of the O-mode [8]. These observations have also been reported [95, 96, 3, 4] at other HF heating facilities under non-matching condition.

In addition, a spectral analysis of the skywave return shows dramatic broadening in the skywave spectra during the matching condition. Figure 3.8, 3.9 and 3.10 show different degrees of broadening widths in the frequency spectra during the matching period. An increase of more than 15 Hz in halfwidth (Δf) was recorded on February 17 and September 20, 1995 (Figures 3.8 and 3.9) and 4 – 10 Hz on March 9 (Figure 3.10). The halfwidth of the frequency spectrum is defined here as the full width at half maximum (FWHM), or the difference between each of the two frequencies at which the amplitude is equal to half the peak amplitude (in dB) above the noise level. This dramatic increase in the halfwidth of the spectrum during the matching condition indicates anomalous scattering of the pump wave with enhanced low frequency fluctuations, parametric decay, and mode coupling processes. As mentioned earlier, this is facilitated by the large interaction region of enhanced ES wave turbulence. Again, this frequency broadening phenomenon appears to be quite robust near the matching condition.

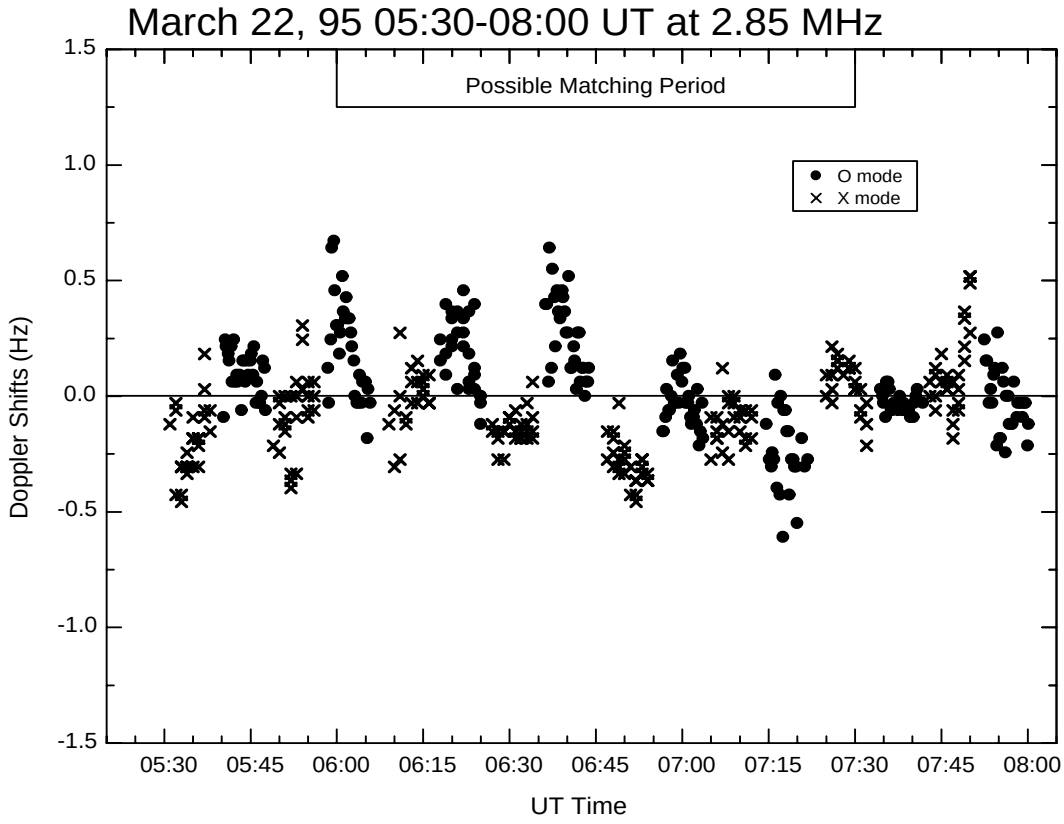

Figure 3.7: A plot of the Doppler frequency shifts of the skywave return taken on March 22, 1995. A net positive frequency shift is observed from the O-mode heating and a negative shift from the X-mode heating. The frequency shifts become more significant when the heater frequency is close to f_0F_2 between 6:00 and 7:00 UT. The pump frequency was set at 4.53 MHz.

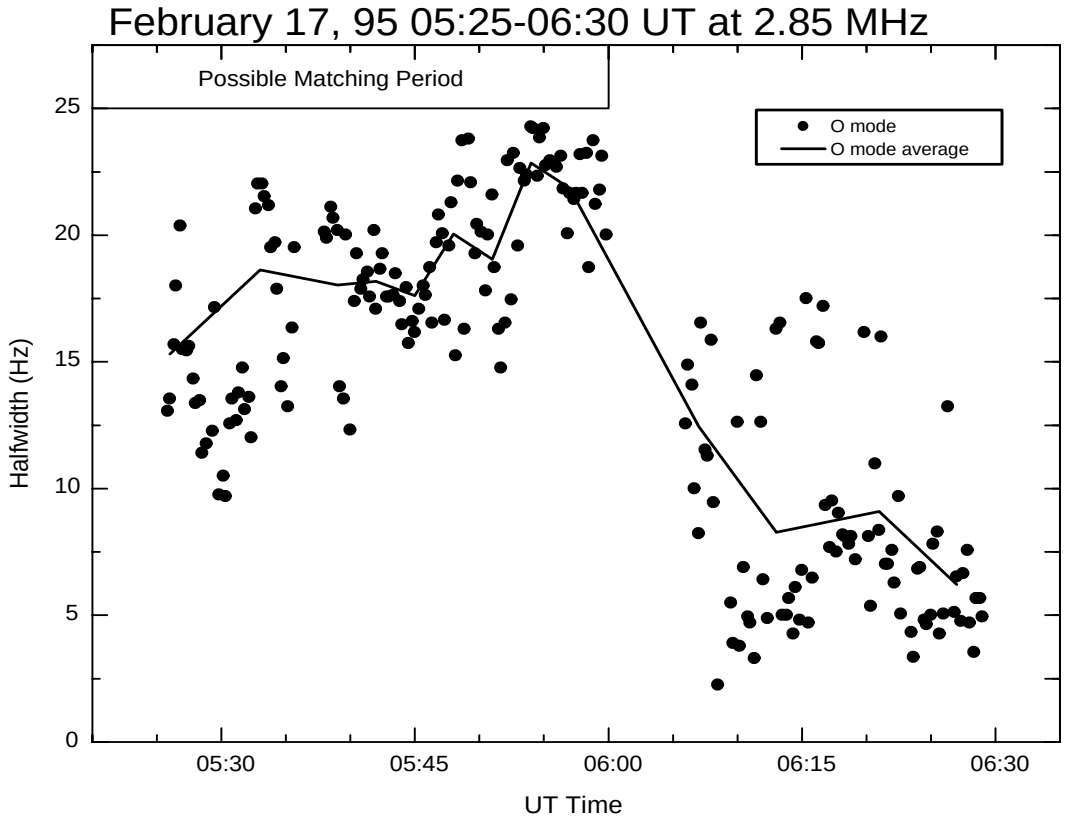

Figure 3.8: A plot of FWHM of the reflected pump signals as function of time for the data taken on February 17, 1995. CW O-mode heating was used. The solid line shows the average halfwidth for every five-minute interval. The pump frequency was set at 2.85 MHz.

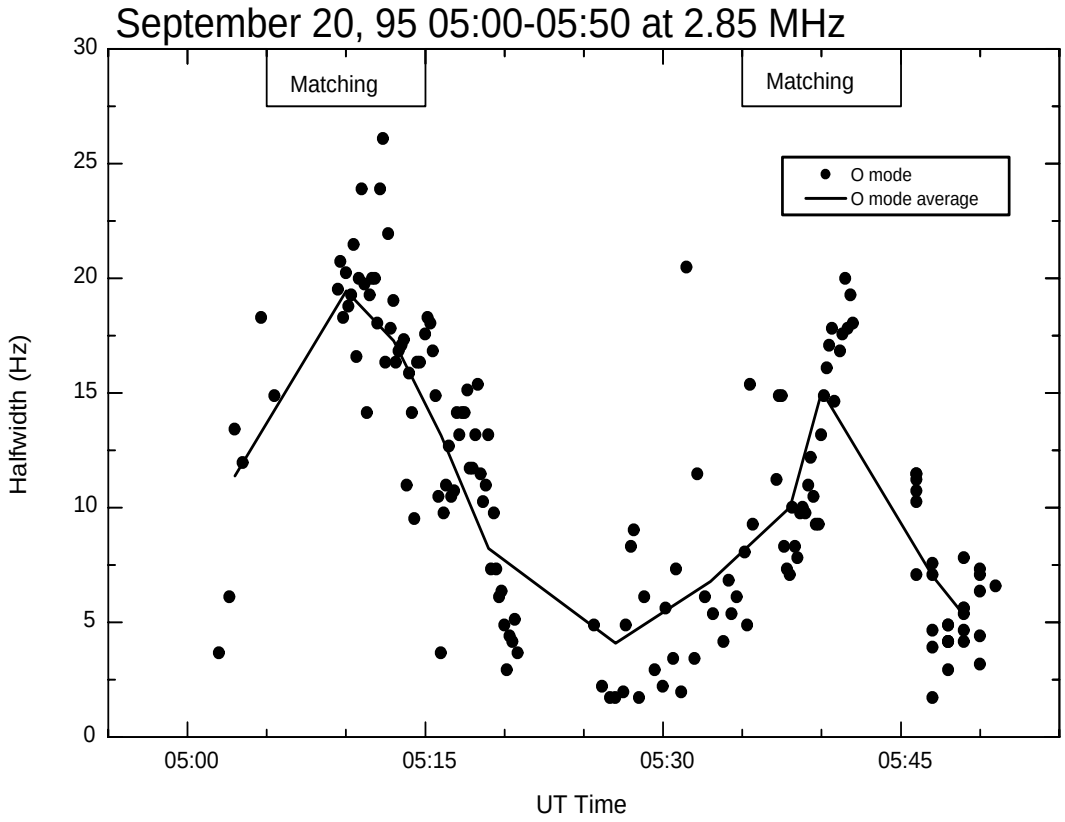

Figure 3.9: A plot of FWHM of the reflected pump signals as function of time for the data taken on September 20, 1995. CW O-mode heating was used. The solid line shows the average halfwidth for every five-minute interval. The pump frequency was set at 2.85 MHz.

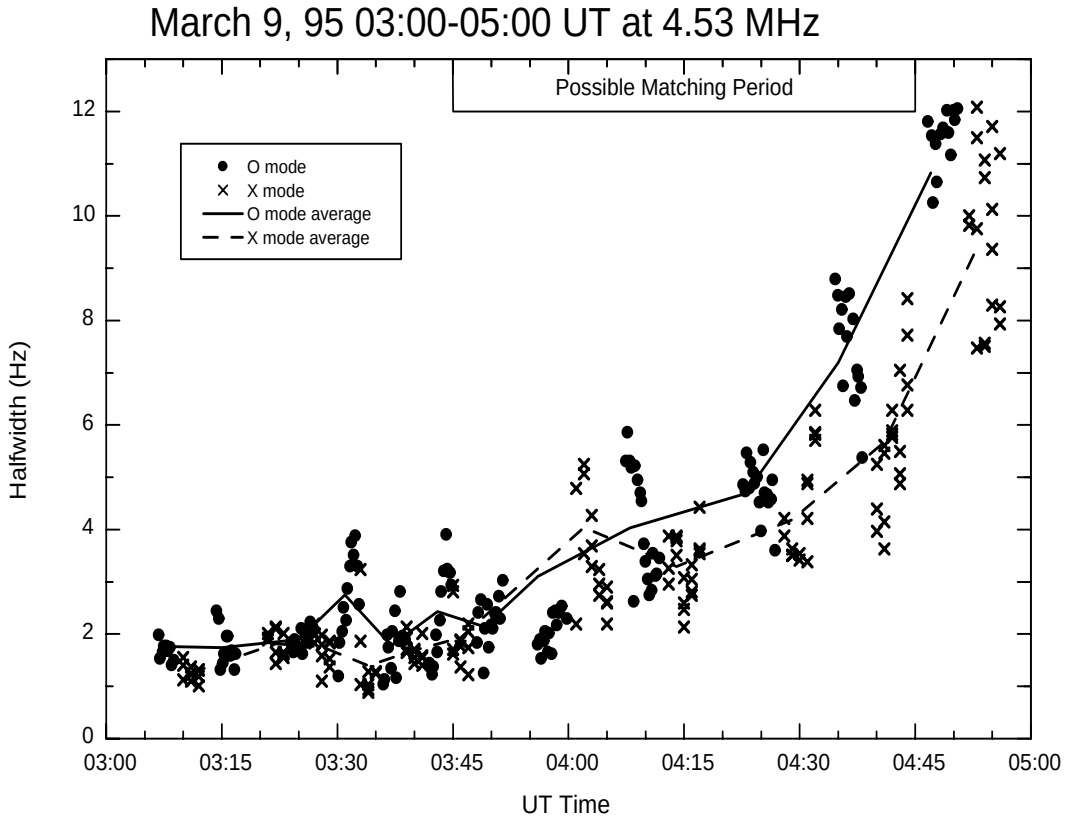

Figure 3.10: A plot of FWHM of the reflected pump signals as function of time for the data taken on March 22, 1995. A halfwidth of 4–10 Hz was observed when the heater frequency was close to f_oF_2 between 03:45 and 04:45 UT. The solid and dashed lines show the average for each O- and X-mode heating cycle, respectively. The pump frequency was set at 4.53 MHz.

3.2.2 Discussions

F layer heating effects are consistently the strongest for O-mode heating based on previous observations on HF heating [93, 15, 84, 46, 103]. For overdense heating the amplitude of the pump wave can be strongly affected by D-region absorption, difference in the reflection height, and F-region scattering of the EM waves into the Langmuir waves from small scale FAS, i.e. anomalous absorption.

A powerful wave of either polarization is capable of causing a strong increase in the D-region absorption [38, 24]. The steady amplitude from the X-mode skywave return throughout the experiments (Figures 3.5 and 3.6) provides conclusive evidence that the decrease in the O-mode skywave return signal when near matching is caused by the D-region absorption. The nondeviative absorption (Γ_D) of an EM wave transversing the D-region depends on the frequency [101, 73]

$$\Gamma_D \propto (f \mp f_l)^{-2} \tag{3.1}$$

where f is the EM wave frequency, and f_l is the longitudinal component of the electron gyrofrequency. The plus and minus signs correspond to the O- and X-modes, respectively. From equation 3.1, the X-mode absorption is expected to be larger than the O-mode absorption. However, our data show that the O-mode skywave return signal is weaker than that of the X-mode and further proves that the decrease in O-mode is not due to the D-region absorption.

We can also exclude the mechanism due to the different reflection heights for O- and X-mode. An O-mode wave was reflected at a height between 250 and 300 km during the experiments conducted on March 9 and 22, 1995. Though an X-mode wave reflects at a lower altitude than an O-mode wave, their difference in the power density, assuming $1/r^2$ dependence is less than 5 dB. Our observed values before matching lie within this range. However, this mechanism does not

explain the 10-15 dB difference in the amplitude observed during the period of matching.

As mentioned earlier, large enhanced electric field, mode conversion, and local heating near the reflection layer lead to profile modifications. Due to the anisotropy in transport rates, the parallel rate is at least 3 orders of magnitude larger than the perpendicular rate. As a result, density perturbations can elongate to form FAS and further enhance the mode conversion process leading to anomalous absorption of the pump EM wave. Once these striations are formed, parametric instabilities can occur preferentially within. One such instability is the decay or conversion of the pump EM wave to an UH wave. The electrostatic UH wave has a short wavelength and can be trapped inside the striations. Thus an efficient feedback process can result when the pump EM wave generates the striations, which then cause conversion of EM wave to an UH wave, which in turn steepens the striations that further enhance wave conversion and anomalous absorption [21, 66, 67]. Clearly this is an efficient and highly nonlinear mechanism for the absorption and damping of the pump wave. Anomalous absorption effects have been reported during the O-mode heating of the F layer ionosphere. A considerable diagnostic amplitude reduction of up to 10 dB during the O-mode heating is observed, while the X-mode heating shows less than 1 dB change [93, 15, 84]. However, such results were obtained under normal heating scenarios without the matching condition. It remains to be seen theoretically whether the efficiency of such a process can be further enhanced by the matching condition.

The difference in Doppler shifts for the X- and O-mode heating, as discussed earlier, can probably be attributed to the difference in ray paths and cutoff height for the two-modes. When the heater frequency matches f_oF_2, the X-mode cutoff height can be 50 km below that of the O-mode. Large Doppler shifts observed dur-

ing the matching condition indicate strongly induced layer motions and density changes consistent with strong wave activities and turbulence in the extended interaction region. The positive shift during the O-mode heating is consistent with the elongation of the depleted density striation towards lower height. For the observed Doppler shift values in the range of about 0.5 Hz (Figure 3.7), the calculated Doppler velocity is about 125 m/s. This is equivalent to a plasma drift from an ambipolar electric field of about 25 mV/m, a value frequently observed at high latitudes. In comparison, thermal diffusion time for the sizes of the beam spot and large interaction region is about 10 minutes, too slow to account for the observed Doppler shifts.

The negative shift during the X-mode heating, can be explained by the upward motion of the plasma at the X-mode reflection layer, back-filling the perturbed depleted region at higher heights created by the previous cycle of the O-mode heating. The observation of opposite Doppler shifts for the two polarizations, is therefore consistent with the physical picture of plasma expulsion and refilling during the nonlinear heating processes. As mentioned earlier, observations of both positive and negative Doppler shifts have been reported recently [95, 96, 3, 4]. The positive Doppler shifts have been attributed to density increases from either a reduction in recombination rates or to enhance ionization from accelerated electrons during the HF heating. The negative shifts, on the other hand, have been attributed to density depletions and striations caused by intense ES wave intensity. In these experiments, test HF waves at multiple frequencies were launched and their Doppler shifts were recorded during the O-mode heating under non-matching conditions. In our work, only the Doppler shifts of the HF pump waves were recorded. A multiple frequency HF Doppler diagnostic is currently being tested at HIPAS.

The increase in the FWHM of the skywave spectra appears to be the result of enhanced scattering of the pump wave from low frequency fluctuations or turbulence over an extended interaction region near the flat top of the density profile. One likely candidate for low frequency fluctuations is ion acoustic fluctuations which are easily excited by parametric instabilities and a strong Langmuir turbulence. The expected halfwidth of the broadening due to scattering from ion acoustic fluctuations can be easily estimated using the O-mode dispersion relation. For a pump frequency of 2.85 MHz, $T_e = T_i = 0.1$ eV and assuming that under the matching conditions, the frequency difference between f_o and f_oF_2 can be controlled to 50 – 250 kHz. The calculated broadening halfwidth of $\Delta f \approx 2k_{em}C_s$ then ranges from 5.5 to 12.4 Hz where k_{em} is the wave vector of the heating beam. This agrees well with empirical values of 4 – 10 Hz in the X- and O-mode switching experiments. For the O-mode CW heating, local electron heating can occur and the ion acoustic speed can increase. A modest increase of T_e to 0.3 eV will result in a calculated halfwidth of Δf=15 Hz, identical to the observed value. In comparison, the ion cyclotron frequencies for O^+, NO^+, and O_2^+ are 49, 26, and 24.5 Hz, respectively. Thus, the broadening in the reflected pump wave does not appear to be related to ion cyclotron wave activities.

3.3 Conclusions

Under the unique condition of matching the heater frequency to the peak plasma frequency, f_oF_2, the O-mode heating effects are strongly enhanced and amplified. This leads to strong wave activity and turbulence, profile modification, local electron heating, and Doppler motion. The resultant FAS initiates a nonlinear feedback mechanism that leads to mode conversion and anomalous absorption of the pump wave. These further lead to amplitude depletion of the skywave. The

pump wave and other EM waves (radiated by the ionosonde) are also strongly scattered by the striations leading to large broadening in the reflected pump wave and thus spread of the echo returns.

CHAPTER 4

Spectral Structure of SEE under Matching Condition

This chapter presents the SEE results from both HIPAS and HAARP facilities, obtained at both sunrise (when f_oF_2 slowly builds up and passes the pump frequency from below) and during sunset (when f_oF_2 slowly decreases).

4.1 High Power Pumping

The SEE experiments were performed using the HIPAS and HAARP heating facilities. The heater was turned on in full power for several minutes. The pump frequency was at least 200 kHz from the nearest harmonic of the ionospheric electron cyclotron frequency to minimize the gyroharmonic effects [57, 83].

4.1.1 Experimental Results

Under overdense pumping, the SEE sidebands are generally composed of a BC and DM. They are excited within 3 s from the pump turn on after a cooling period of 3 min or more, or a "cold start". Anomalous absorption [15, 84, 31] is commonly observed after the pump has been turned on for a few seconds. Figure 4.1 shows the temporal evolution of the reflected pump wave at 4.53 MHz and the SEE signal at -10 kHz from f_{pump}. After the high power pump is turned on

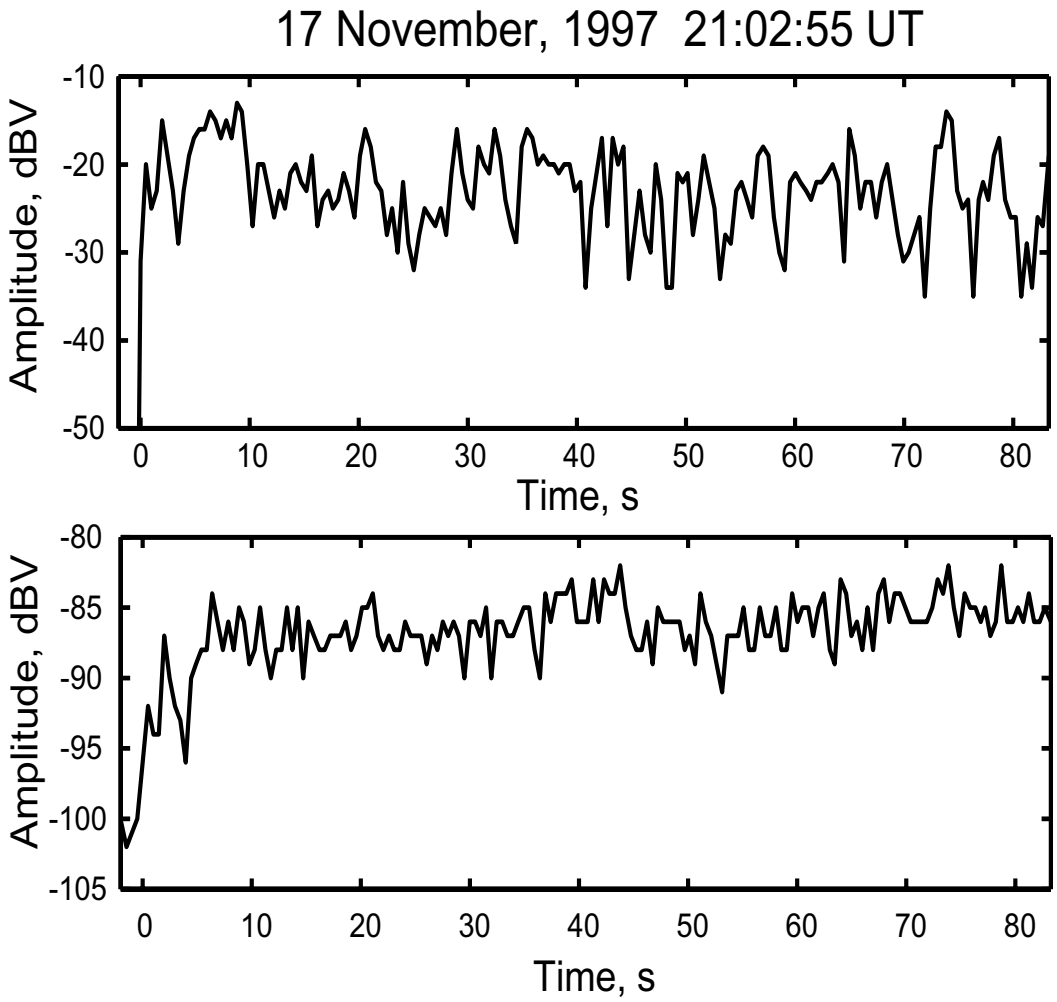

Figure 4.1: Temporal evolution of the reflected pump wave at 4.53 MHz (top panel) and the SEE signal at -10 kHz from f_{pump} (bottom panel). A gradual increase is observe in the bottom panel during the first 10 s. Data were taken at cold start.

at $t = 0$ s, the reflected pump signal (top panel) drops from a level of -15 dB to -25 dB after 10 s. This drop in the signal strength is generally attributed to the anomalous absorption of the pump signal as a result of the formation of striations. The SEE signal at -10 kHz (bottom panel) shows a gradual increase in the signal strength within the first 10 s after the pump is turned on. These two plots clearly show that the growth of SEE is correlated with the decline of pump signal and the excitation of striations.

With the presence of preexisting striations, strong overshoot at the turn on of the pump can be observed in the reflected pump signal and the SEE signal at -10 kHz (Figure 4.2). This is in contrast to those observed during cold start (Figure 4.1). The overshoot lasts for less than a second which is followed by a quick drop with the signal level settling into the same range above noise level as during cold start. Such overshoot can be easily reproduced; however, it is absent when the pump frequency is at 6.8 MHz, 7.7 MHz, and 8.05 MHz, and this is consistent with results reported in other facility [31].

A change in the SEE spectra is observed as f_oF_2 becomes close to the pump frequency. Figure 4.3 shows a sequence of spectra taken when HIPAS is transmitted at $f_{pump} = 4.53$ MHz as f_oF_2 increased. The horizontal scale of the spectra is the frequency offset from the pump. During the matching conditions, a distinct and strong DM feature is excited on top of the BC backgrounds is shown in figure 4.3. When the pump frequency is above f_oF_2, (Figure 4.3 (b) and (c)) the DM feature becomes barely observable above the BC background . Moreover, the BC has a signal strength ~ 10 dB weaker and a few kilohertz narrower than that observed during the matching condition. Figure 4.4 shows another set of spectra taken at HAARP using a higher pump frequency, $f_{pump} = 5.9$ MHz. Both the BC and DM features are distinctively excited under the overdense conditions.

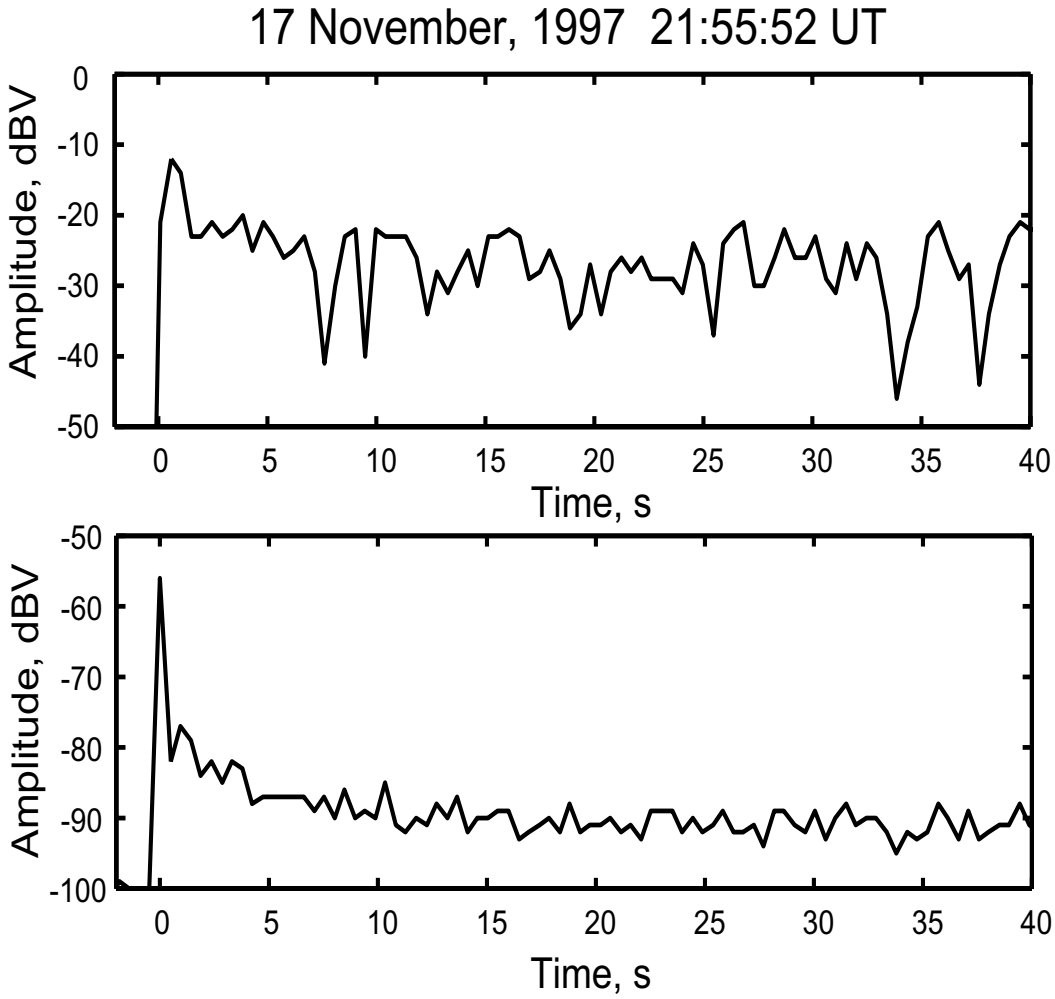

Figure 4.2: Temporal evolution of the reflected pump wave at 4.53 MHz (top panel) and the SEE signal at -10 kHz from f_{pump}. Strong overshoot is observed immediately after turn-on. Data were taken during high power heating after pre-heating the ionosphere.

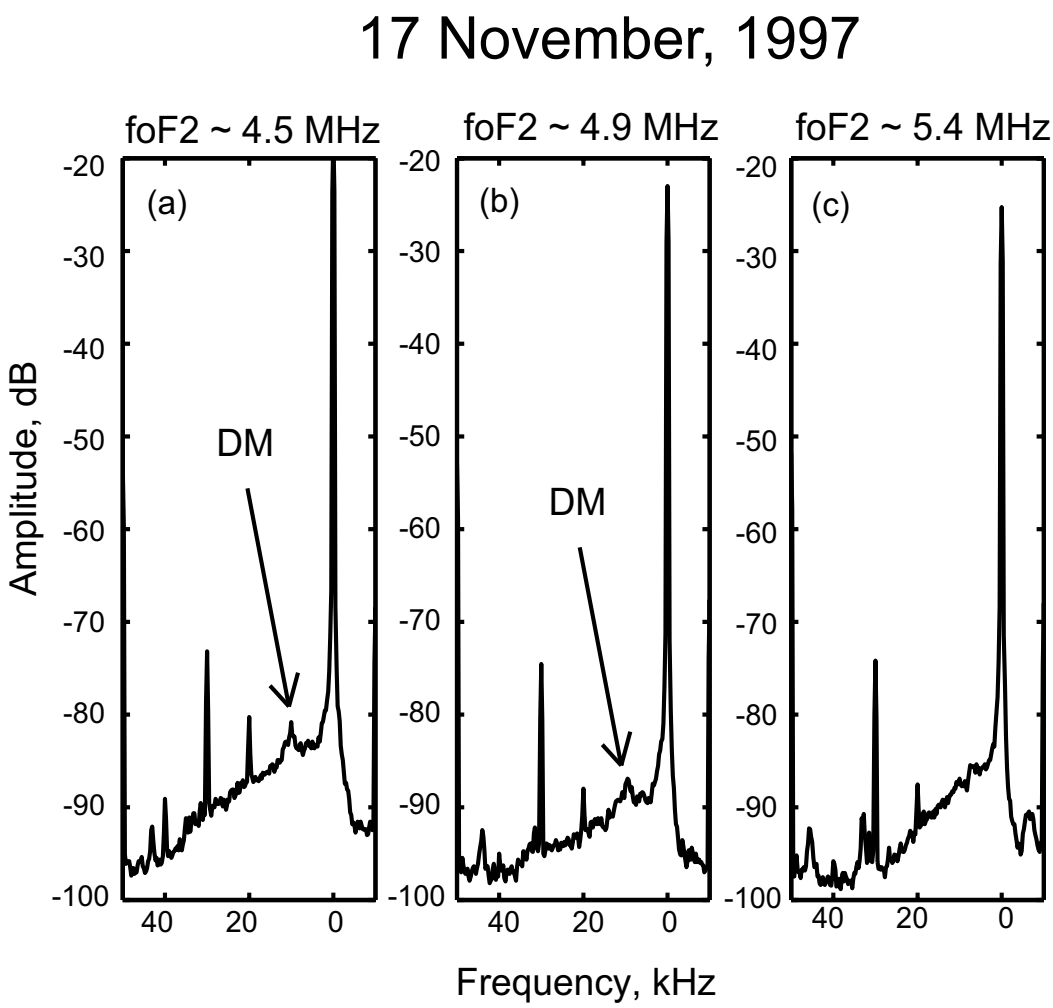

Figure 4.3: Frequency spectra taken on November 17, 1997 at HIPAS with f_{pump} = 4.53 MHz under different values of f_0F_2. The horizontal scale is the frequency offset from 4.53 MHz.

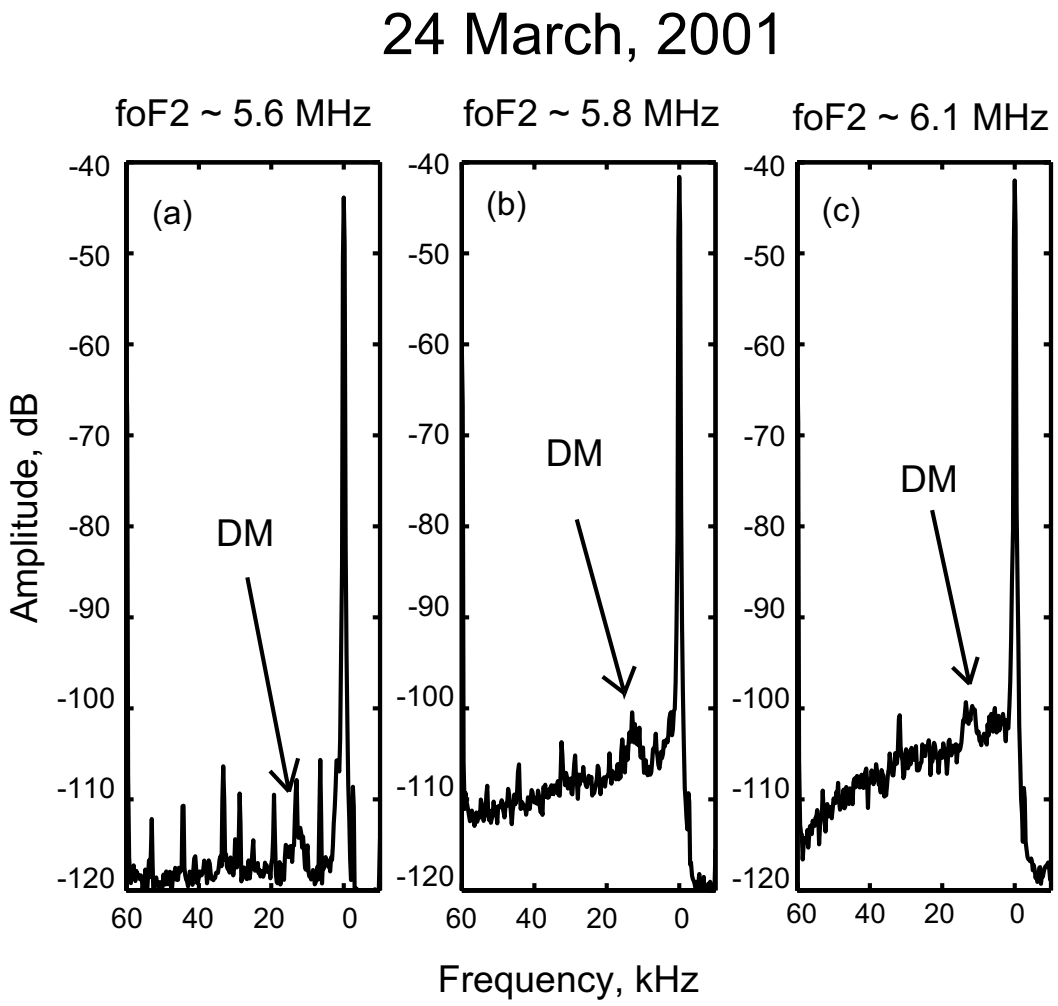

Figure 4.4: Frequency spectra taken on March 24, 2001 at HAARP with f_{pump} = 5.9 MHz under different values of f_oF_2.

The BC, however, is again much stronger and wider when f_oF_2 is near the pump frequency.

We have continuously recorded the SEE spectra when f_oF_2 was passing through the pump frequency at 7.4 MHz from above (Figure 4.5). The BC clearly continues to decrease in signal strength, but the intensity of the DM feature remains unchanged. Figure 4.6 shows spectra for f_oF_2 a few 100 kHz below the pump frequency at 4.56 MHz. The only emission observed under this condition is the DM feature, as is also observed in Tromsø [58].

4.1.2 Discussion

During high power pumping near the matching conditions when f_oF_2 decreased from the overdense to matching conditions, the strength of the DM feature as well as the width of the sidebands increase (Figure 4.3). The reason for this behavior is unknown. It may simply be a decrease in the absorption of the pump wave, such as a decrease in the excitation level of the Langmuir turbulence near the pump reflection height, because of a decreasing swelling in the pump electric field, as the background plasma density gradient decreases near matching. When f_oF_2 decreases slightly below the pump frequency the excitation of Langmuir turbulence is suppressed by the absence of plasma resonance. As a result, the reflected pump wave decreases in the signal strength. This makes it difficult to estimate the influence on the excitation of the UH turbulence without more detailed modeling.

The strong SEE features during the matching condition may be explained by the increase in the interaction lengths in the more homogeneous background plasma density profile. This is similar to what has been suggested for the intensification of 630-nm airglow during matching [5].

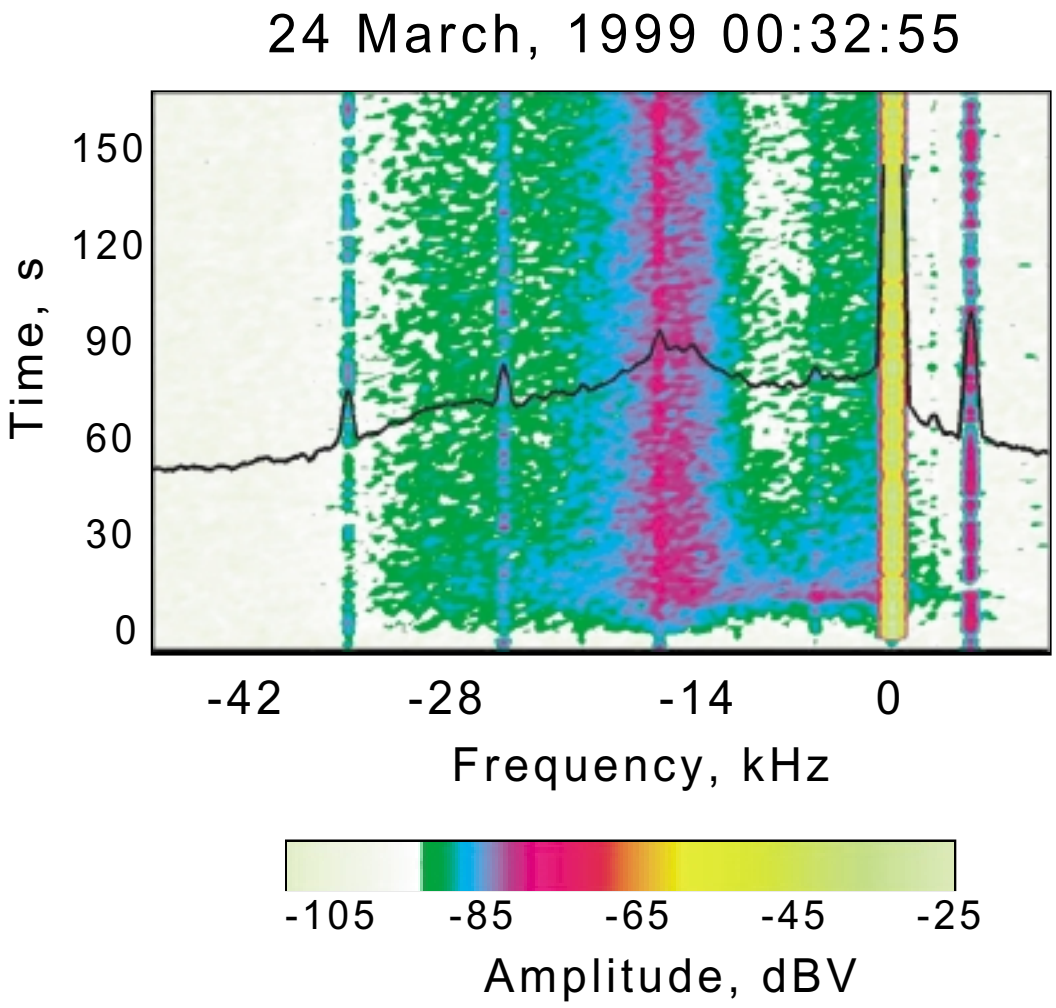

Figure 4.5: Frequency spectra taken on March 24, 1999 at HAARP when f_oF_2 was passing through $f_{pump} = 7.4$ MHz from above. The vertical scale is the offset from the start of the transmission.

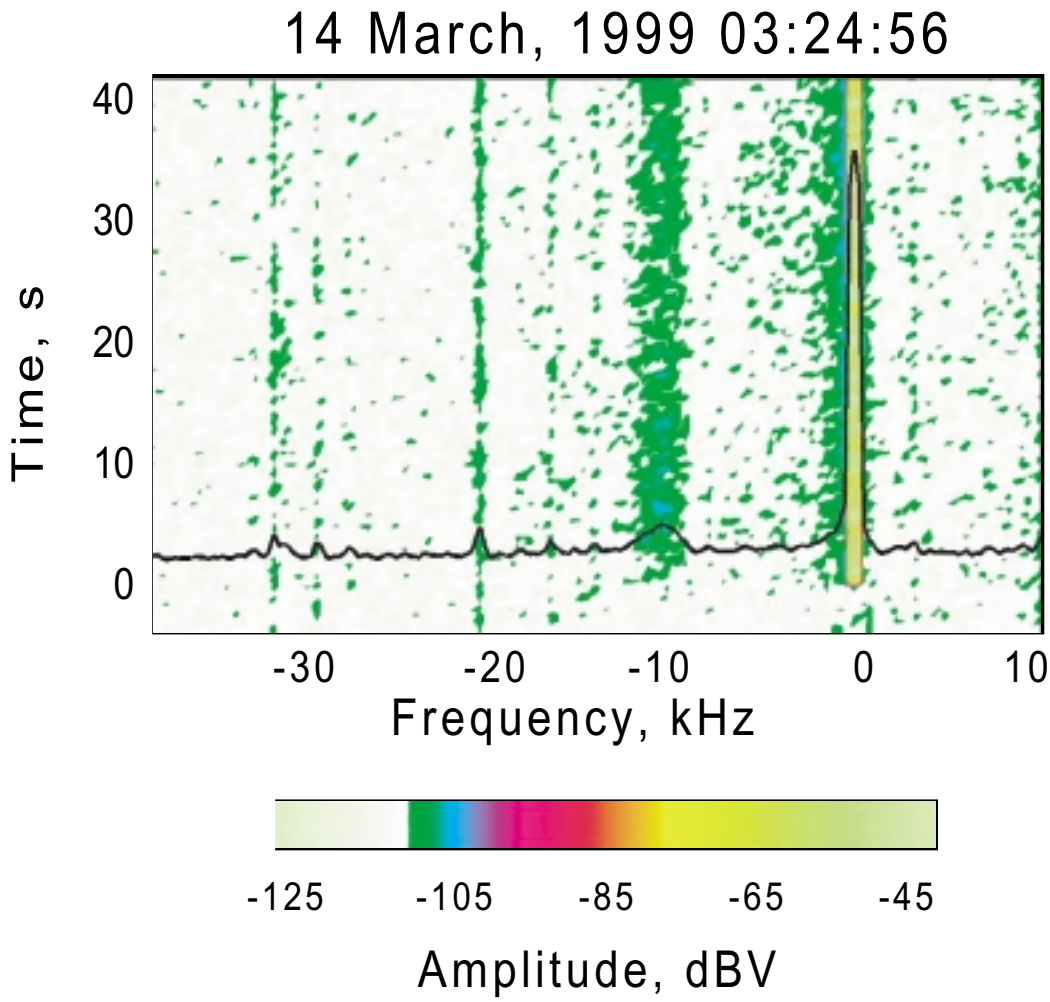

Figure 4.6: Frequency spectra taken on March 14, 1997 at HIPAS when $f_o F_2$ was a few 100 kHz below $f_{pump} = 4.56$ MHz.

As f_oF_2 passed through the pump frequency from above, the BC eventually decreased in strength without a corresponding decrease in the DM (Figure 4.5). When f_oF_2 was a few 100 kHz below the pump frequency, the only SEE feature observed was a weak DM (Figure 4.6). These experimental results seem inconsistent with theoretical interpretations of the DM for trapped upper-hybrid oscillations in striations [39, 68, 51] and the BC for freely propagating UH waves [35, 78, 36]. In order to trap upper-hybrid oscillations a higher plasma density is required than freely propagating waves at the same frequency. Given that the BC depends on the electron gyroharmonics and the excitation of UH waves as is suggested by its slow evolution on the thermal time scales after a cold start [56], the experimental results suggest that the BC also depends on the trapping of upper-hybrid oscillations. Excitation of trapped upper-hybrid oscillations leads to high oscillation amplitudes. We therefore conjecture that the BC depends on escape of the trapped oscillations by scattering of the initial trapped oscillations from nearly perpendicular to the geomagnetic field toward smaller angles where they can escape from the trapping density depletion. The wide spectrum of the BC can then be generated by the oblique UH waves, by induced scattering of ions along the lines previously suggested without considering initial trapping [35, 78, 36]. As f_oF_2 decreases and passes through the pump frequency from above, electron plasma waves exist at successively smaller angles to the geomagnetic field for the successively lower f_oF_2 because of linear dispersion. The excitation of oblique waves will therefore cease before the excitation of perpendicular trapped oscillations, and the BC would be suppressed before the DM, consistent with the experimental results. The dependence of the DM on the interaction of upper and lower-hybrid oscillations requires the oscillations to be highly perpendicular to the geomagnetic field. In addition, the weak residual DM seen near the upper-hybrid matching condition (Figure 4.6) may also have contributions from freely

propagating UH waves [109, 76].

Measurements on the anomalous absorption in future experiments are highly recommended to compare the overdense and matching cases. Anomalous absorption is caused by the excitation of small scale density striations which, in turn, is an aspect of the driven upper-hybrid turbulence [41]. To measure the anomalous absorption therefore gives an indication of the intensity of upper-hybrid phenomena. However, more diagnostics will be necessary in future experiments to include the measurement of the anomalous absorption.

4.2 The Effect of Preconditioning on Low Power Pumping

The effect of preconditioning was investigated by transmitting a sequence of low power pulses alternating with high power pump pulses. By using this pump sequence it was previously found that the DM could be excited at a low pump power of $\sim$ 80 kW during the overdense conditions, if the ionosphere had been preconditioned, in this case, with $\sim$ 20 MW effective radiated power [13]. These experimental results agree well with theoretical predictions [39, 68, 69]. The DM is excited via the decay of the trapped upper-hybrid oscillations in pre-formed density depletion regions during the low power pulsing.

4.2.1 Experimental Procedure

A special heating sequence is used to perturb the ionosphere which is then probed by a sequence of low power short duration transmissions (Figure 4.7). The cycle starts with a sequence of low power test waves, T1, to ensure the ionosphere is in the unperturbed state. It is followed by a 120 – 140 s high power CW transmission, H1, to heat the ionosphere. The following T2 (H2) serves as the

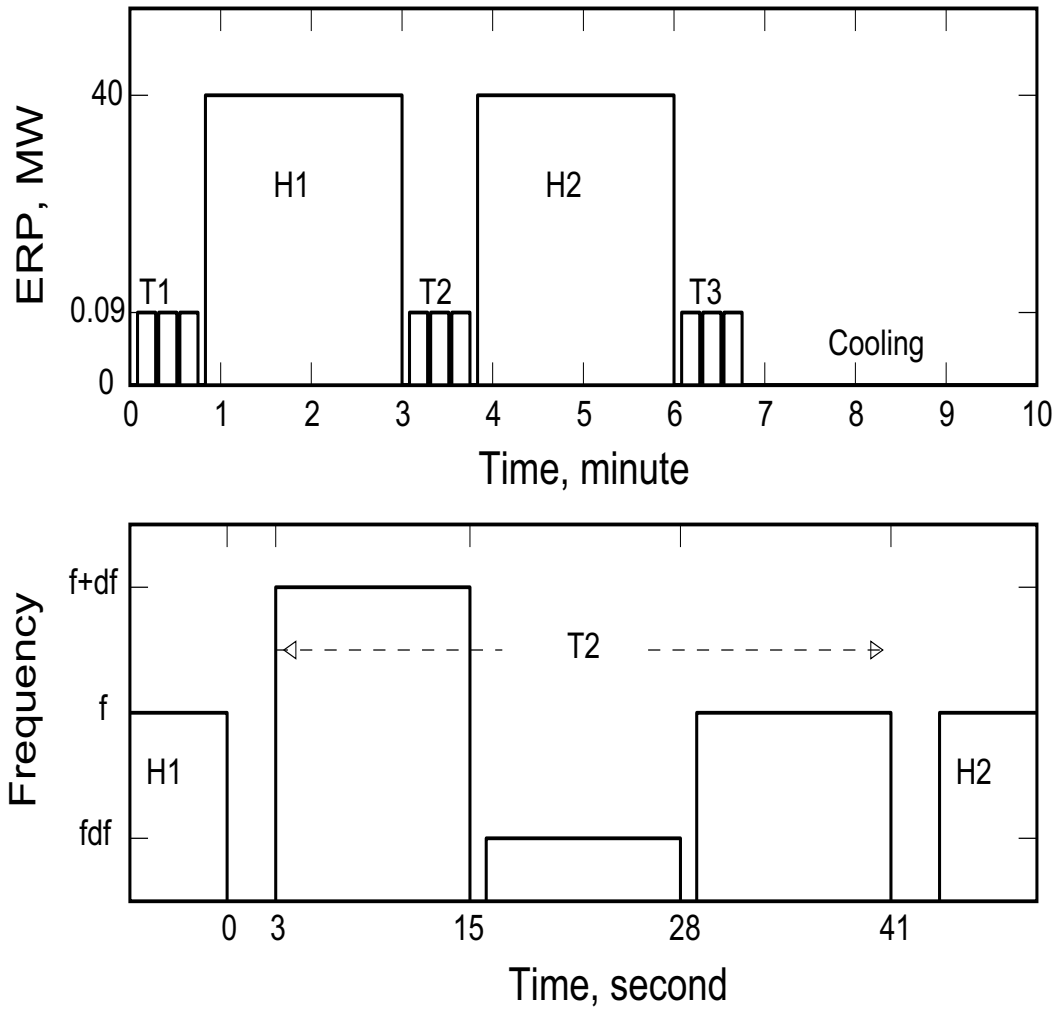

Figure 4.7: (a) Heating schemes used during the pre-conditioning experiments and (b) detailed procedure for the low power heating sequence.

low (high) power probe in the pre-heated region. H2, meanwhile, further modifies the ionosphere for another 120 – 140 s. The last sequence T3, is used to diagnose the ionosphere after prolonged heating (H1 and H2). The cycle ends with a cooling period of 200 – 230 s to allow the ionosphere to return to its unperturbed state. A 3 sec off period is added in between each sequence for the transmitter frequency change and as a time marker for the data acquisition. Each full cycle is 10 minutes in duration.

Three different test frequencies are transmitted consecutively in each of the 40 s low power (ERP of $\sim$ 0.1 MW) transmissions (T1, T2, and T3) (Figure 4.7b). The test frequencies are set in the order of $f_{\mathsf{pump}} + \delta f$, $f_{\mathsf{pump}} - \delta f$, and f_{pump} where $\delta f \leq 30$ kHz. As soon as the test frequency becomes greater than f_0F_2, the corresponding test wave will pass through the ionosphere and only a small portion of its power will be reflected back. As a result, the low power transmissions determine the matching period and at the same time probe the heated region.

4.2.2 Experimental Results

The following results were obtained during the low power pumping using the aforementioned heating scheme. No SEE was observed during the first low power sequence (T1) under both the overdense and near matching conditions. This indicates an unperturbed ionosphere state. However, once the ionosphere was preconditioned by the high power sequence (H1 and H2), the SEE features were excited during the following T2 and T3 low power sequence.

Figures 4.8 and 4.9 show the spectrograms of the T2 sequence data taken on November 17, 1997 using the HIPAS facility with $f_{\mathsf{pump}} = 4.53$ MHz and $\delta f = 25$ kHz. The horizontal axis is the frequency offset from 4.53 MHz and

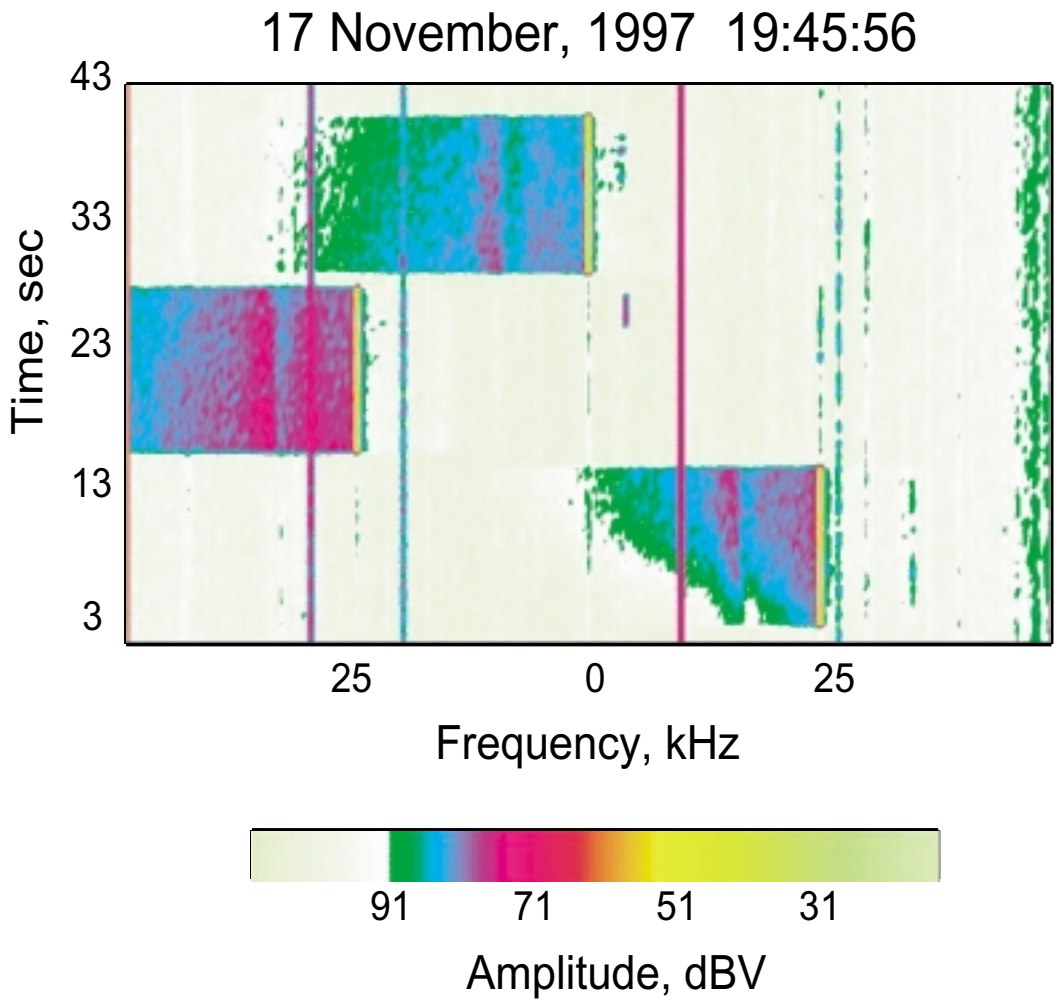

Figure 4.8: Frequency spectra taken on November 17, 1997 at HIPAS during the T2 sequence under matching condition. The axes are the frequency offset from 4.53 MHz and the time offset from the time the H1 sequence is off.

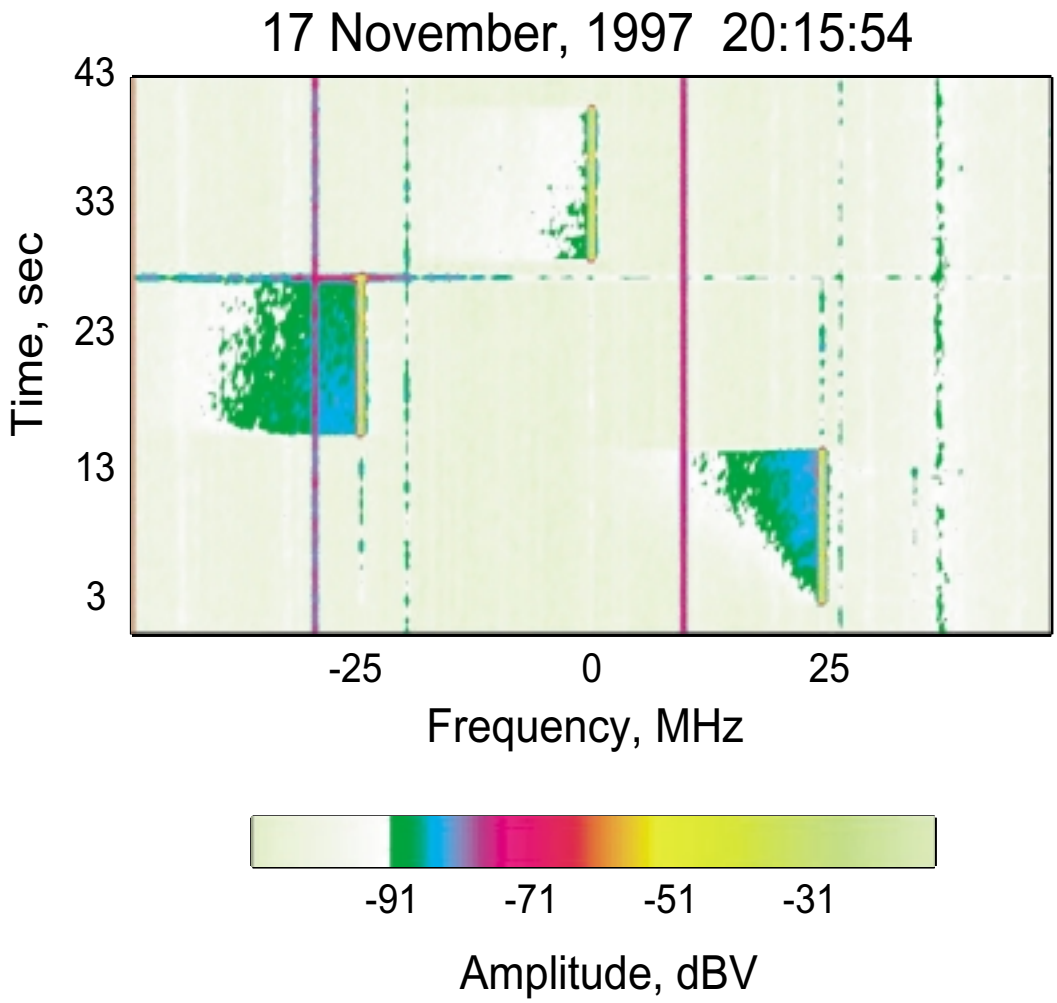

Figure 4.9: Frequency spectra taken on November 17, 1997 at HIPAS during the T2 sequence under overdense condition. The axes are the frequency offset from 4.53 MHz and the time offset from the time the H1 sequence is off.

the vertical, the time offset from the time when the high power pumping (H1) was turned off. Under matching conditions (Figure 4.8), the sidebands of all three test waves were at least 10 kHz wider. The DM feature was distinctively observable with an amplitude of a few dB above the continuum.

Under both the matching (Figure 4.8) and overdense conditions (Figure 4.9), the continuum developed during the first test wave transmission at $f_{\mathsf{pump}} + \delta f$. At the second test wave ($f_{\mathsf{pump}} - \delta f$) transmission, the sideband was already fully developed at the turn on of the transmitter in both conditions. The continuum extends to a frequency range of $\sim$ 18 kHz when it was fully developed during the overdense condition, but more than 25 kHz during the matching condition. This is referred to as low power continuum (LPC). Since the receiving system had only 100 kHz bandwidth, it was not possible to record the full SEE spectra when transmitting the second test wave. At the last test wave (f_{pump}) transmission, the overdense continuum had a frequency extent of $\sim$ 18 kHz with a signal strength of a few dB above the noise level and was weaker than those observed during the previous second test wave transmission. The continuum excited under the matching condition was much wider and stronger with a frequency extent of $\sim$ 40 kHz and a signal 10–15 dB stronger than those excited under the overdense condition.

During the T2 and T3 low power transmissions, the DM feature was immediately observed under the matching condition and the continuum feature took $\sim$ 10 *sec* to fully developed. The temporal evolution of the SEE signal at -10 kHz with respect to each test frequency as shown in (Figure 4.10) suggested that there was a growth period of $\sim$ 6 *sec* in both conditions. Data was taken on November 17, 1997 using the HIPAS facility with $f_{\mathsf{pump}} = 4.53$ MHz and $\delta f = 25$ kHz. When the maximum intensity level was reached, the signal became steady and

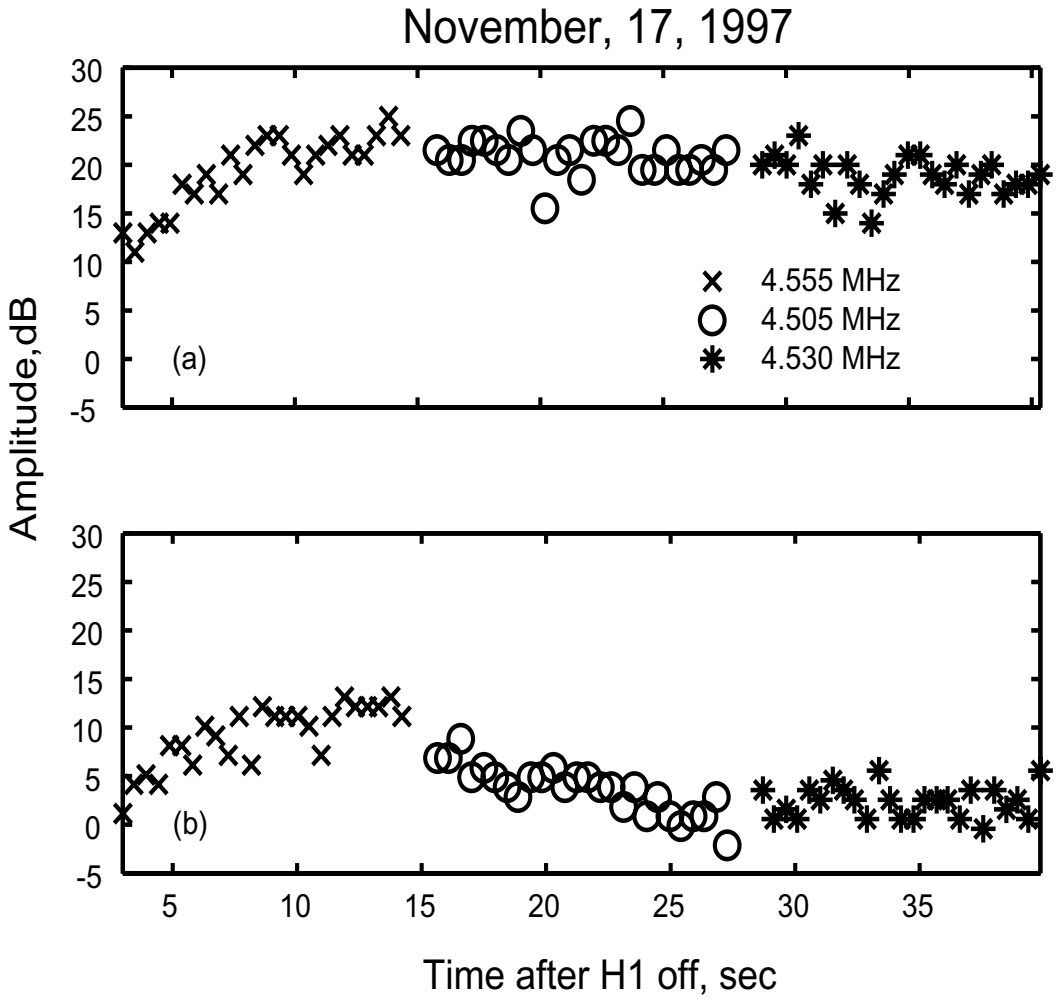

Figure 4.10: Temporal variation in intensity of SEE signal at 10 kHz below each test frequency during *T2* transmission at (a) matching and (b) overdense condition. The signal is more steady and stronger when matched and gradually decreased to noise level when overdense. The average noise level is set to 0 dB.

independent of the transmitting frequency during matching, whereas it became unstable and decreased gradually to noise level under the overdense condition. From the difference in steadiness of the signal, we conclude that heating effects are enhanced and sustained during a matching condition. Similar results were also observed during T3 transmission.

Figure 4.11 shows spectra taken within 0.5 s after the turn on of the T2 sequence with the test frequency at $f_{\mathsf{pump}} + \delta f$. A distinct DM peak $\sim$ 5 dB above a narrow LPC was immediately excited near the matching condition (solid line). During the overdense heating, only a very narrow continuum of width $\sim$ 10 kHz was excited (dotted line), whose signal strength was 10 dB weaker than that excited under the matching condition. However, the amplitude of the reflected pump wave was also 10 dB stronger in the overdense case.

Figures 4.12, 4.13, and 4.14 show another set of T2 data taken at the HAARP facility on March 24, 2001 with a higher pump frequency, $f_{\mathsf{pump}} = 5.9$ MHz. Only the first 32 s of the T2 sequence was recorded. After the ionosphere was preconditioned for 120 s, 18 s less than the previous case, the low power sequence (T2) was turned on after a 5 s off period. Furthermore, only one test frequency ($f_{\mathsf{pump}} + \delta f$) was used throughout the T2 sequence. The spectra were taken when f_0F_2 was about 6.1 MHz, 6 MHz, and 5.8 MHz from the panel top to bottom, respectively. As f_0F_2 approached the test frequency (Figure 4.13), the SEE sidebands appeared for a longer period of time while the signal strength of the DM feature was stronger than those observed during overdense condition. When f_0F_2 was slightly below the test frequency (Figure 4.14), the DM feature became distinct on top of a narrow LPC that continued to exist throughout the recorded 32 s.

Previous experiments have observed large scale modifications of the ionospheric

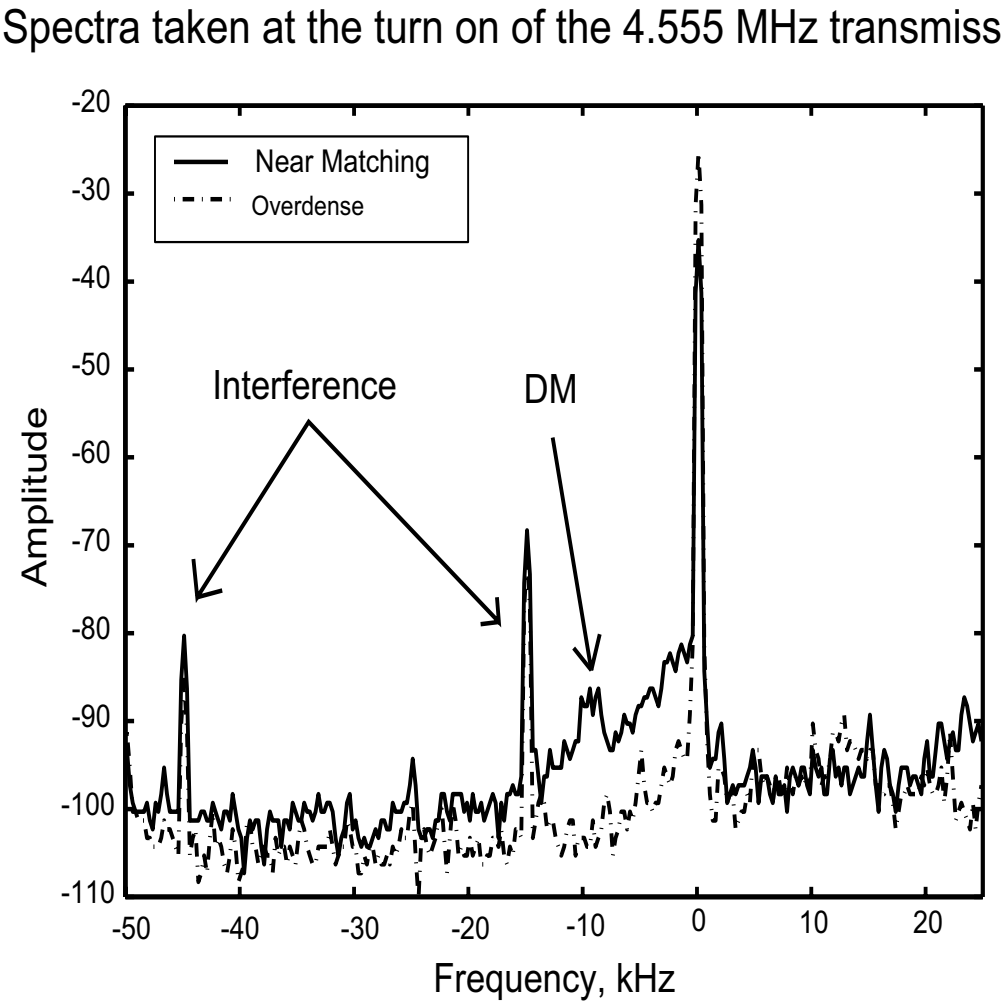

Figure 4.11: Frequency spectra taken at 0.5 s after the turn on of the T2 sequence at 4.555 MHz under the matching (solid line) and overdense condition (dotted line).

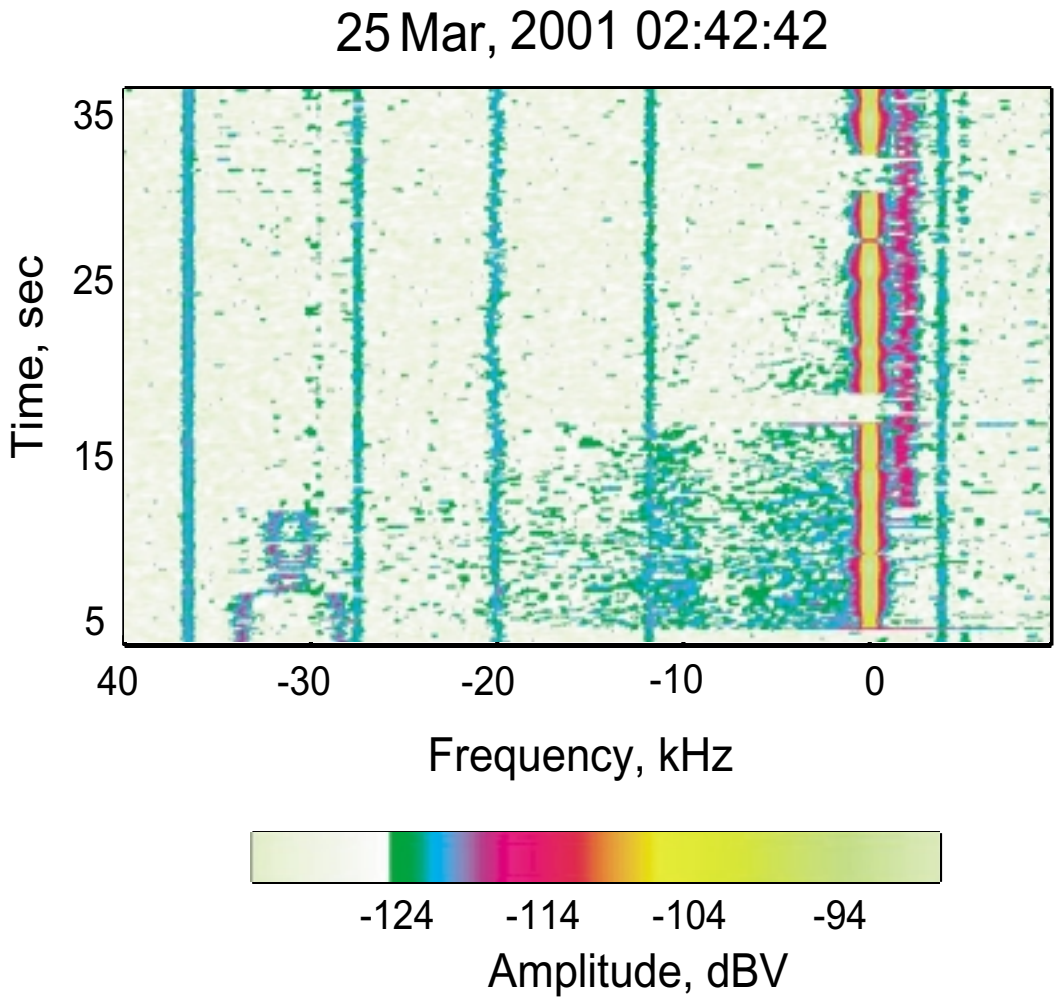

Figure 4.12: Frequency spectra taken on March 24, 2001 at HAARP during the T2 sequence at 5.93 MHz. Data was taken when f_0F_2 was about 6.1 MHz under the overdense condition.

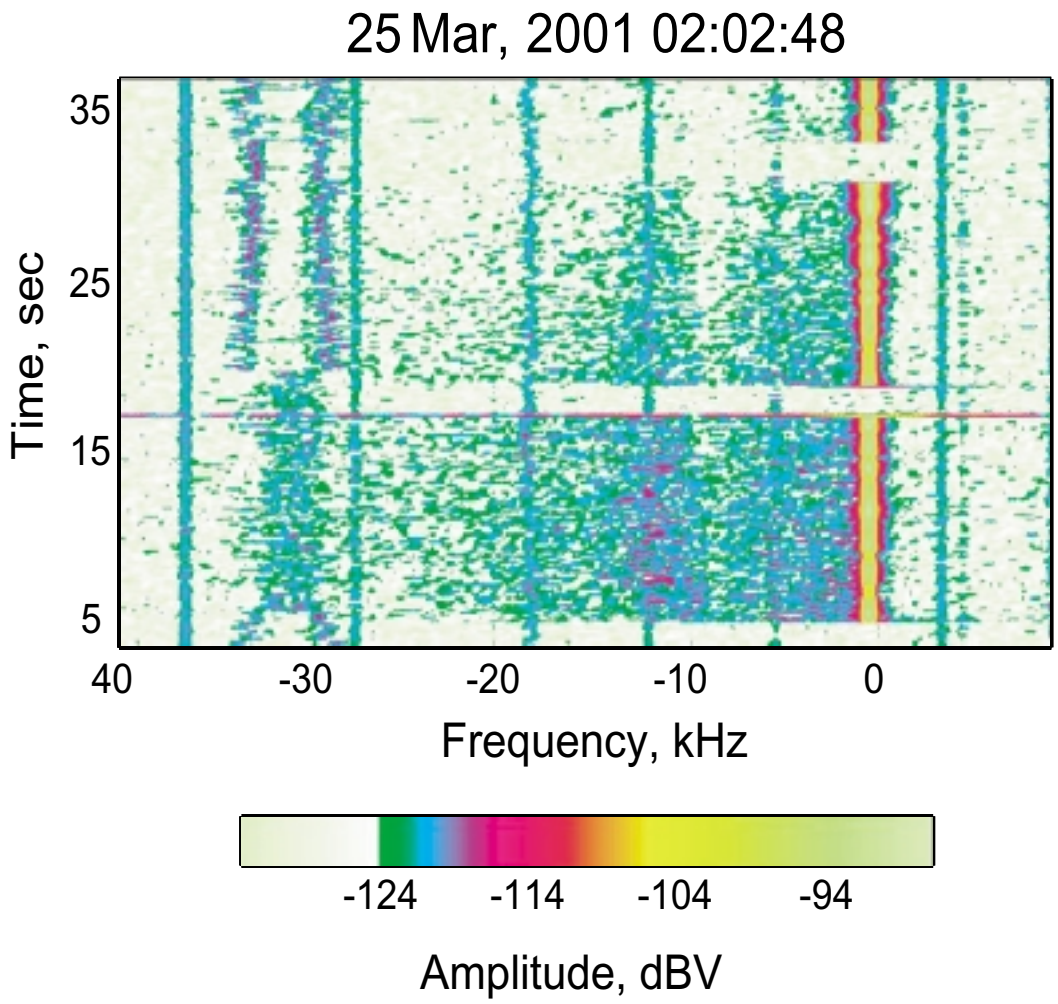

Figure 4.13: Frequency spectra taken on March 24, 2001 at HAARP during the T2 sequence at 5.93 MHz. Data was taken when f_0F_2 was about 6 MHz near the matching condition.

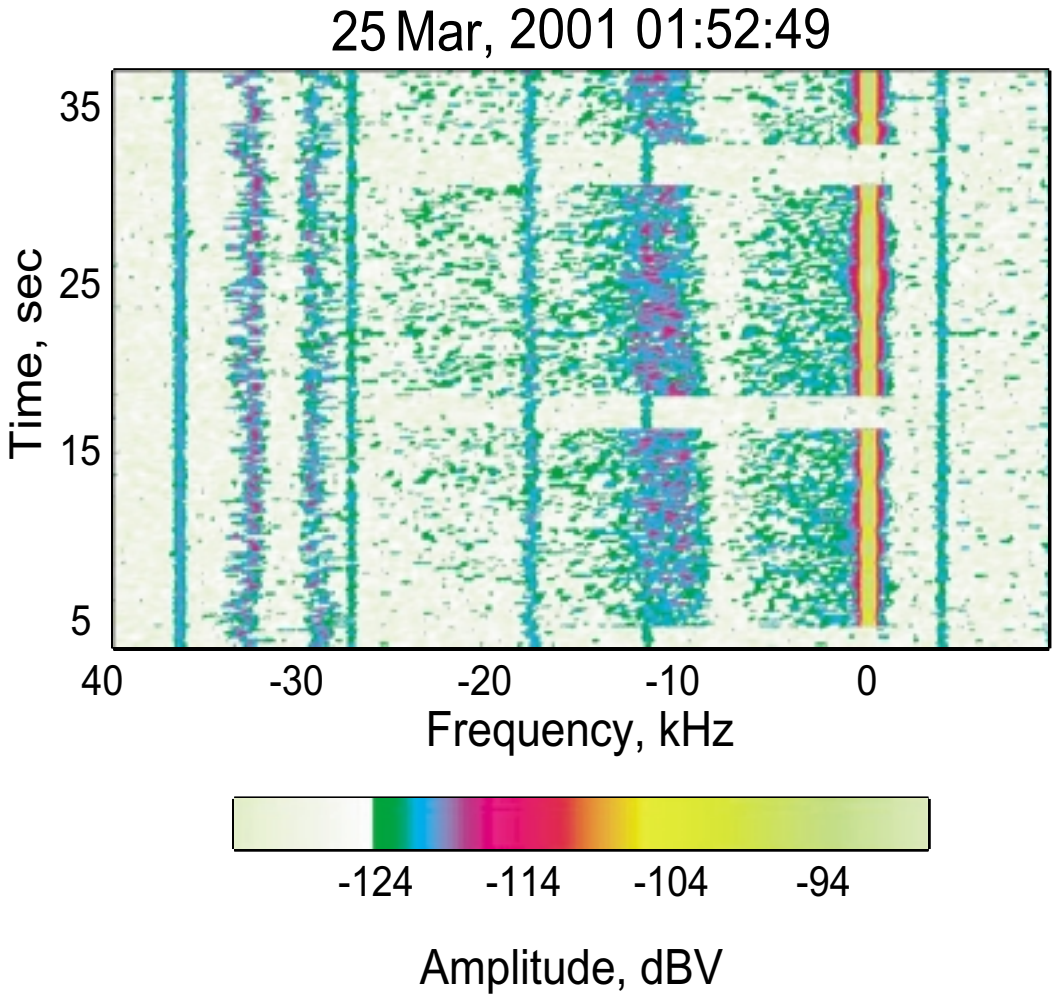

Figure 4.14: Frequency spectra taken on March 24, 2001 at HAARP during the T2 sequence at 5.93 MHz. Data was taken when f_0F_2 was about 5.8 MHz under the slightly underdense condition.

density profile when the pump frequency was near the critical frequency [34, 103]. However, the ionograms from our experiments do not indicate any large scale perturbations in the density profile.

4.2.3 Discussion

The experimental results from preconditioning with low power pumping for the matching and overdense conditions are similar to those from high power pumping. The SEE is stronger under the matching conditions (Figure 4.8 and 4.9). This again can be attributed to decreased absorption by suppression of the Langmuir turbulence excitation and/or increased pump–plasma interaction lengths in the more homogeneous background plasma near the peak of the ionospheric density profile. The slow growth of the SEE in the first low power pulse within T2 after the preconditioning appears similar to the increase in the SEE intensity during the low duty cycle pumping with short pulses (so called diagnostic SEE) followed by the high duty cycle pumping. This has also been observed in experiments at the Sura facility in Russia [27] and in computer simulations [78, 36]. The increase in SEE intensity is attributed to the decrease in the anomalous absorption of the pump and the decay of the short scale striations after the high duty cycle pumping (i.e., the preconditioning) is turned off [36]. The following decrease in intensity in the last pulse during T2, is due to the longer decay of larger scale striations that are sources for the SEE. Consequently, the source of the SEE is not associated with only the smallest scale irregularities. Furthermore, the present low power spectra (T2) show both a DM and LPC. The experimental results reported by [58] on the low power transmission of approximately 86 kW ERP after 30-s preconditioning at 270 MW ERP only have observed continuum feature and not a DM. The low power continuum appears to have an even lower

threshold than the DM from the low power pumping after preconditioning.

4.3 Conclusion

In this chapter, SEE spectra from the overdense to underdense conditions are compared. The strength of the DM and the width of the BC and LPC increase when the pump frequency is near the matching condition for both the high and low pump powers after preconditioning. These may be caused by the decrease in absorption of the pump wave and/or the increase in the interaction lengths near the peak of the profile. To further understand the mechanisms of these changes, we need to include measurements on the anomalous absorption in future experiments.

The experimental results of preconditioning on the low power pumping are similar to the diagnostic SEE observed by [27]. According to Frolov [27] and computer simulations [78, 36], the increase in the SEE intensity observed during the beginning of the low power pumping sequence (T2 and T3) is a result of the short scale striations decay after the high duty cycle pumping. The decrease in the SEE intensity later in the sequence is attributed to the decay of larger scale striations also on a longer time scale. However, no actual measurement of the irregularities are taken together with the presented data, but this should be included in future experiments when an incoherent backscatter radar is installed in Alaska.

CHAPTER 5

Spectral Structure of SEE at $2f_{ce}$

This chapter presents observations of SEE excited at a pump frequency near the second harmonics of the ionospheric electron cyclotron frequency, i.e. $f_{pump} \approx 2f_{ce}$, in the ordinary mode. A new type of the SEE feature is observed. The new feature, referred to as the "narrow symmetrical structure" (NSS), consists of two spectral peaks, symmetrically located around the pump frequency f_{pump}. The frequency offset of the peaks from f_{pump} are between 15 and 30 kHz.

5.0.1 Experimental Results

The experimental results were obtained in nighttime in February and March, 2003 at the HIPAS heating facility. Three different heating schedules were introduced to investigate the SEE spectral structure excited near $2f_{ce}$. Preconditioning experiments used a similar schedule to that described in the previous chapter for only one frequency in the low power sequence (T1, T2, and T3). The high power sequence used 2.85 MHz, and the low power sequence, 2.875 MHz. The second schedule was stepping the pump frequency between 2.84 MHz and 2.88 MHz in steps of 1 kHz every 10 sec. The last schedule was power stepping experiment conducted immediately after the frequency stepping schedule. The total output power was stepped by means of increasing or decreasing the number of transmitters every 25 sec and at a frequency determined by the frequency stepping

experiment.

Figure 5.1 shows the spectrogram from using the preconditioning schedule. No SEE spectral structure is observed during any of the high power heating at 2.85 MHz. However, both upper and lower sidebands are excited during the 100 kW low power heating at 2.875 MHz, even before preconditioning. By varying the output power of the low power sequence, no sidebands are excited at all with an output power of 50 kW (Figure 5.2). Lower sidebands are excited only after preconditioning at output power of 75 kW (Figure 5.3). The observed sidebands, however, are neither the DM, BC nor the BUM. They are symmetric sidebands with multiple peaks and stronger in the lower sidebands at 100 kW power. The sidebands peaks are $\sim$ 15 kHz apart, $\sim$ 5 kHz wide and 5 dB above noise. The lower sidebands have intensity stronger than the upper sidebands. Only a single lower sideband peak at $\sim$ 22 kHz below the pump is observed at 75 kW power level.

The narrow symmetric sideband peaks (NSS) are excited within a narrow range from the pump frequencies (Figure 5.4). These peaks are within 15-30 kHz from f_{pump}. The NSS are also excited at a different range of pump frequencies (Figure 5.5).

The results from the power stepping measurement suggest a threshold level about 56 kW in order to excite the SEE. Figure 5.6 shows the pump frequency at 2.88 MHz, while the NSS is excited 28 kHz from it. The lower sideband is more intense and has a wider bandwidth than the upper sideband.

5.0.2 Discussion

The anomalous absorption at a frequency near an electron gyroharmonics is minimal and the generation of the FAS and the UH waves are suppressed [81, 86].

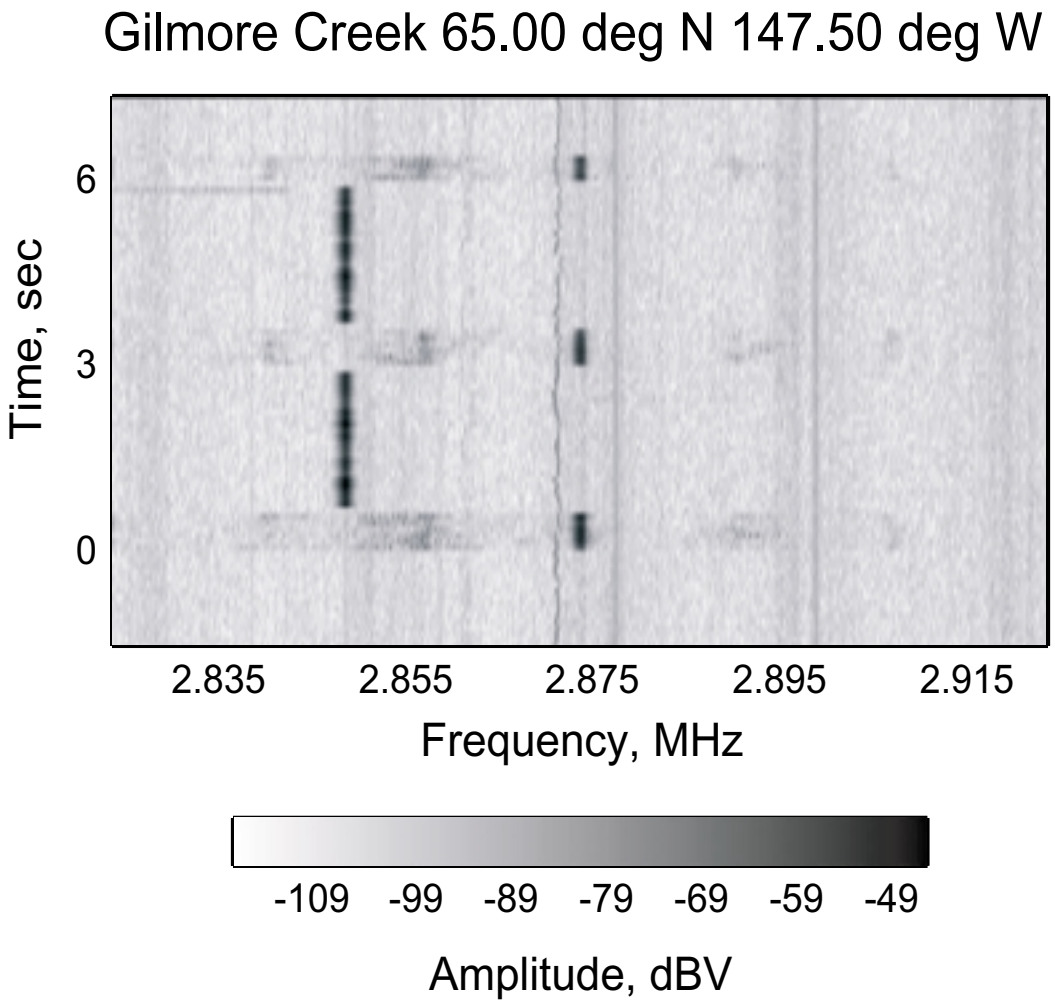

Figure 5.1: A spectrogram taken on February 13, 2003 using the HIPAS heater at 2.85 MHz during the 800 kW high power heating and 2.875 MHz during the 100 kW low power heating.

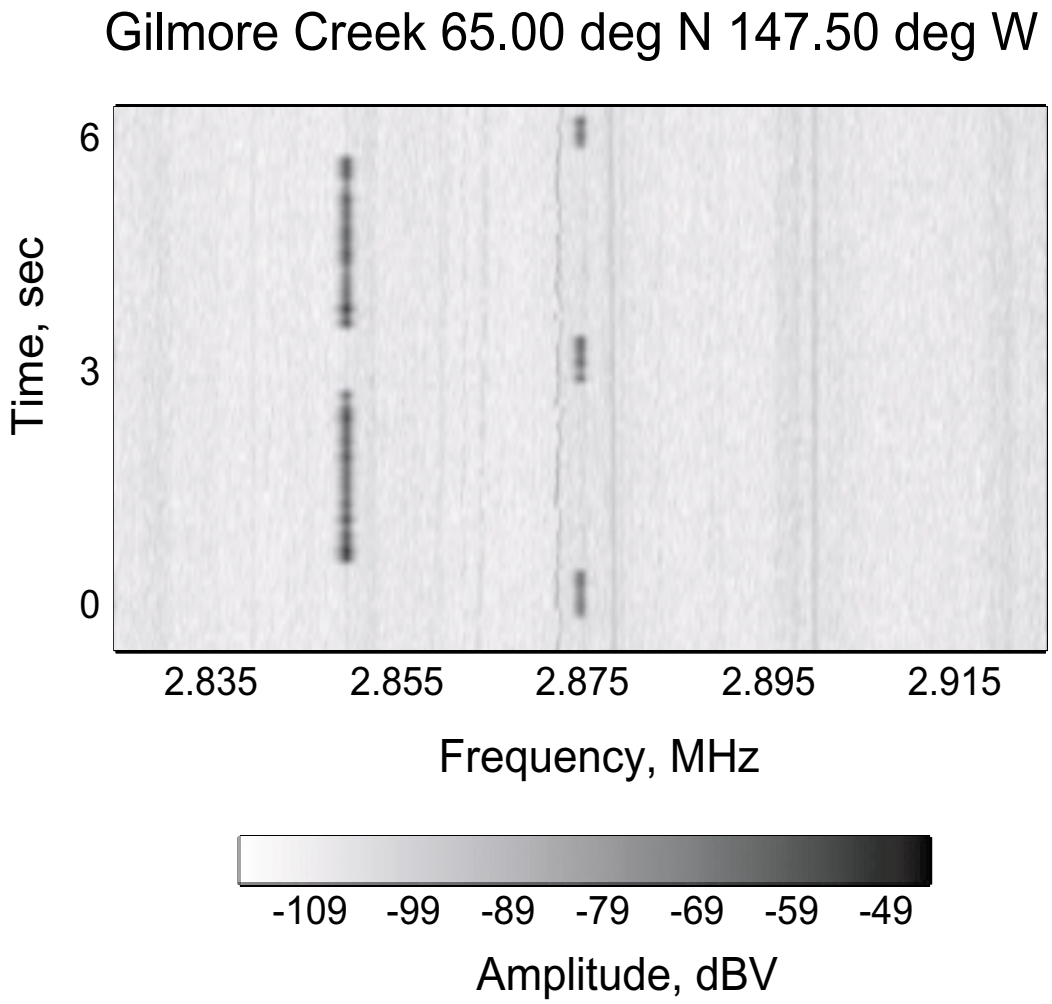

Figure 5.2: A spectrogram taken on February 13, 2003 using the HIPAS heater at 2.85 MHz during the 800 kW high power heating and 2.875 MHz during the 50 kW low power heating.

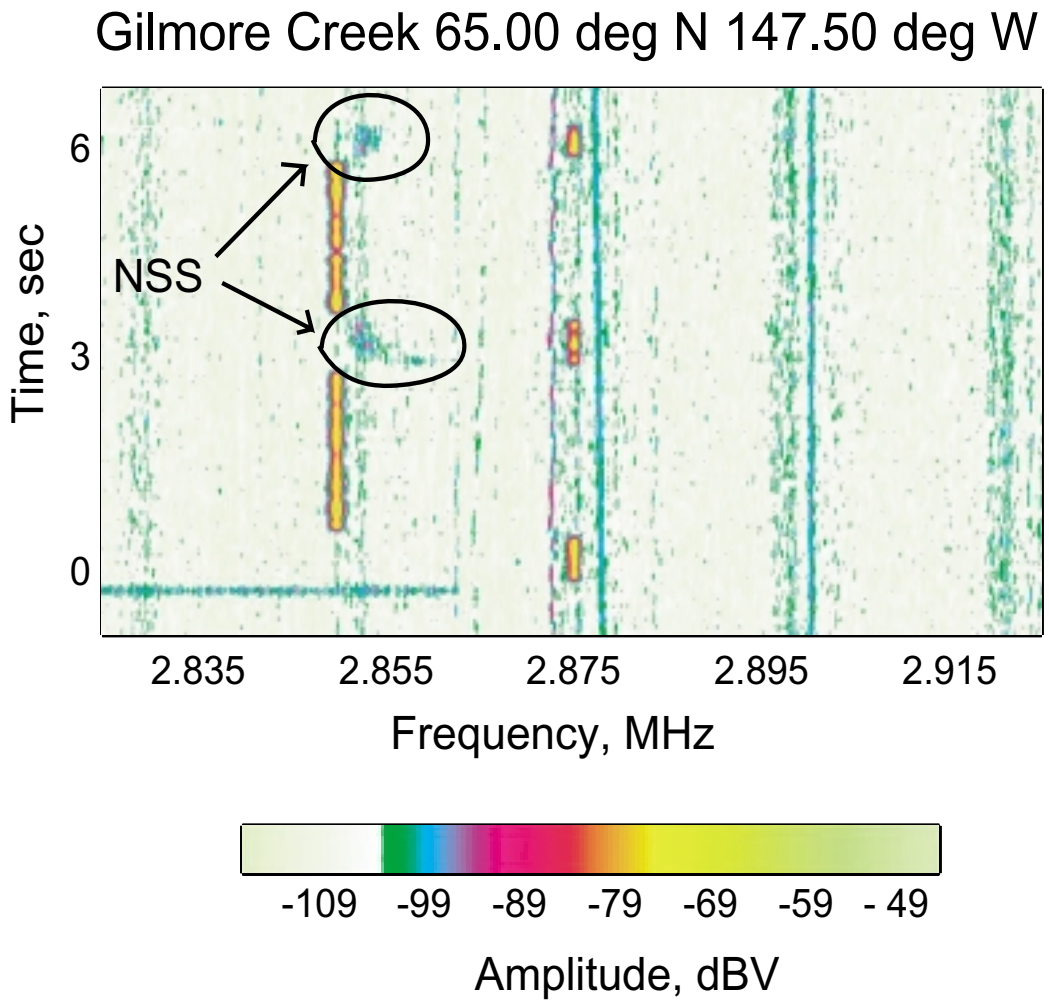

Figure 5.3: A spectrogram taken on February 13, 2003 using the HIPAS heater at 2.85 MHz during the 800 kW high power heating and 2.875 MHz during the 75 kW low power heating.

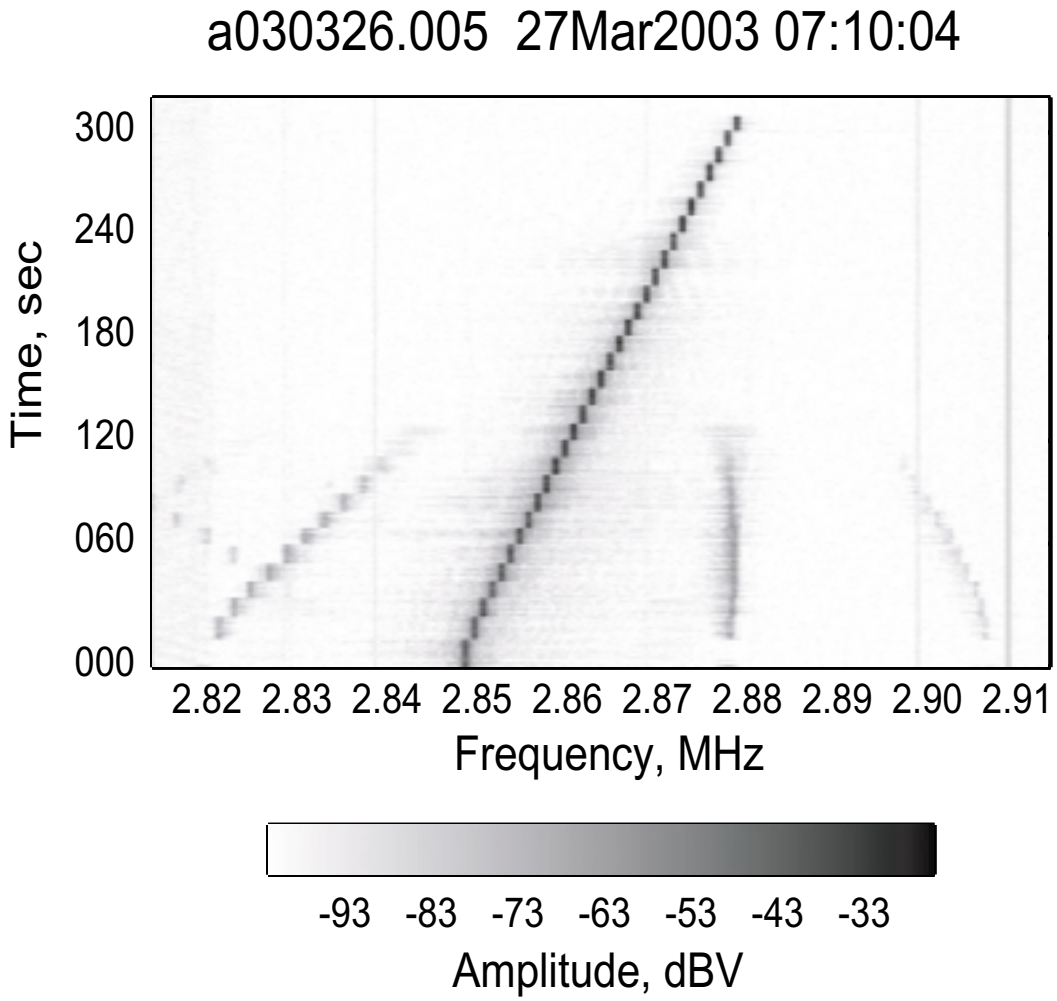

Figure 5.4: A spectrogram taken on March 27, 2003 during the frequency stepping between 2.85 and 2.88 MHz. Both stepping up and down are shown. Sidebands are observed between 2.851 and 2.860 MHz.

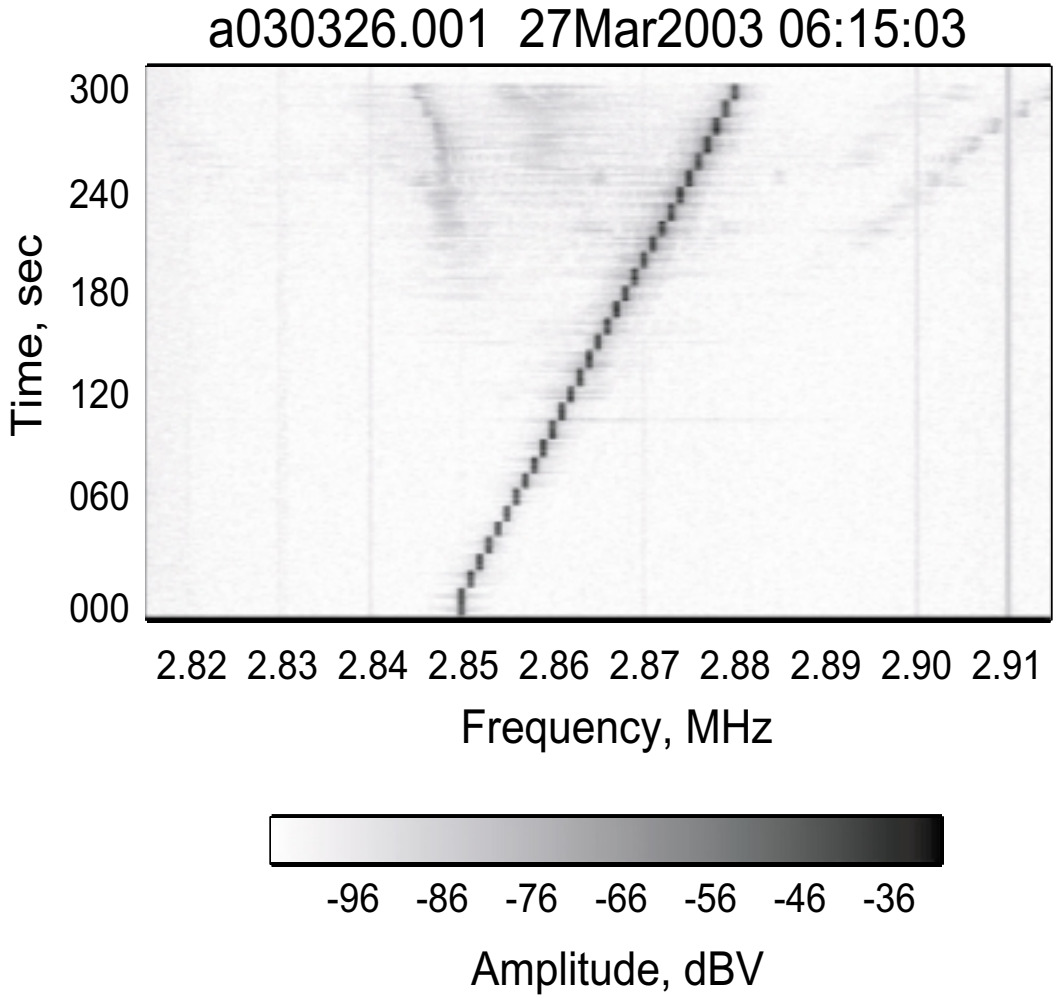

Figure 5.5: Spectrogram taken on March 27, 2003 during the frequency stepping between 2.85 and 2.88 MHz. Both stepping up and down are shown. Sidebands are observed between 2.872 and 2.880 MHz.

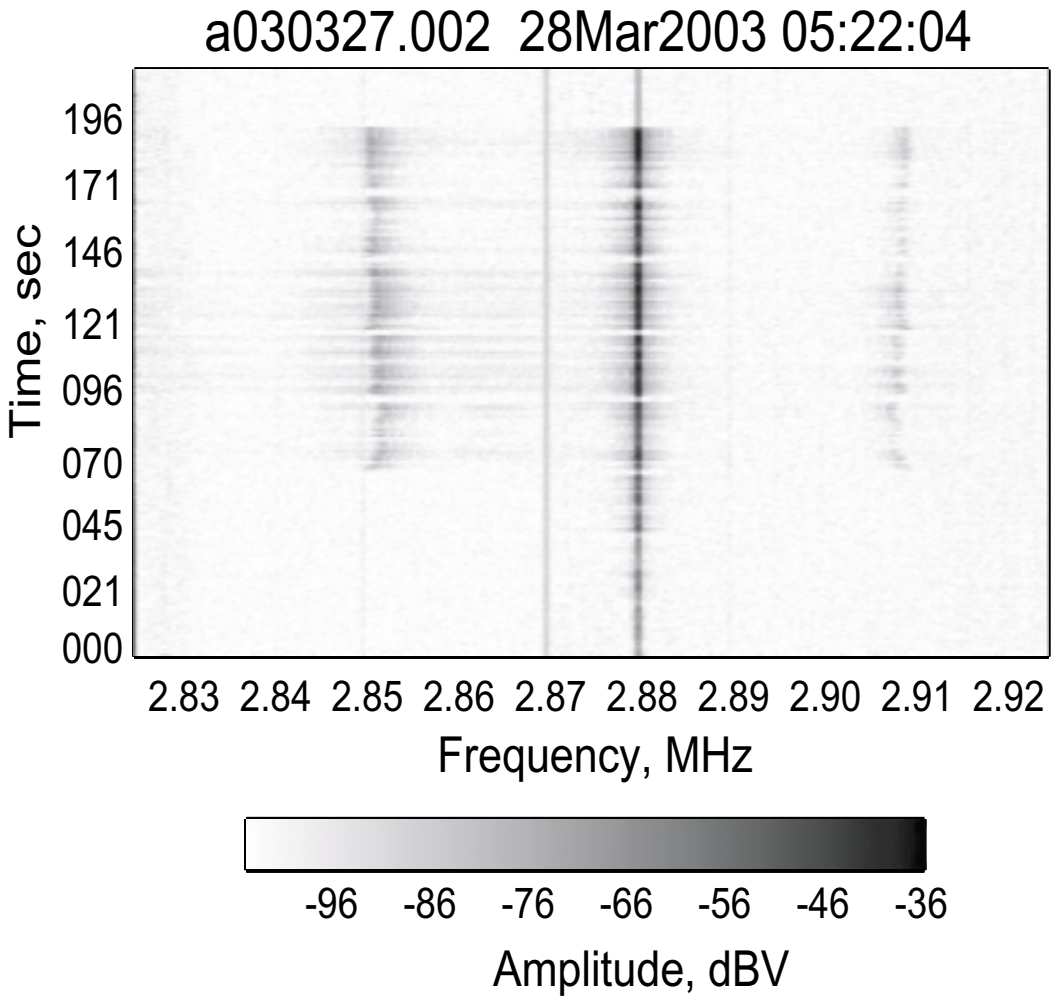

Figure 5.6: A spectrogram taken on March 28, 2003 during the transmitter stepping experiments. The pump frequency was at 2.88 MHz.

The SEE features are closely related to the UH waves and therefore very sensitive to the pump frequency when it is near a harmonic of the ionospheric electron cyclotron frequency. Many detailed measurements of the SEE spectra at pump frequencies equal to or greater than the third electron cyclotron harmonic in the ionospheric plasma have been reported extensively in the past [57, 83, 59, 56, 48, 30, 81]. The commonly observed DM and BC disappear in the SEE spectrum and a BUM develops as f_{pump} becomes slightly above nf_{ce} for n = 4 to 7. The frequency shift of the BUM is highly dependent on n and f_{pump}, and $2f_{pump} = f_{BUM} + nf_{ce}$.

A substantial enhancement appears in the cross section of the FAS when the pump frequency is approximately the second gyroharmonics in the F-region [26]. Strong SEE features are, therefore, expected when $f_{pump} \approx 2f_{ce}$. Our data and results, however, does not show any sign of FAS enhancement. The data only show two distinct peaks in the spectrum. The absence of the DM feature suggests the UH waves are strongly damped at the second gyroharmonics.

The offset frequency of the NSS from the pump is within 15 to 30 kHz range. This offset frequency suggests a Doppler motion with speed $\sim$ 1.57 x10^6 m/s occur at the resonance layer. This speed corresponds to an electron with energy level of 7 eV. The energies needed to excite optical emission of OI $2p^4$ ground state are 2 eV for 646.4 nm (green line) and 4 eV for 557.7 nm (red line). With our calculation of 7 eV, it is enough to excite both green and red lines. Airglow at 557.7 nm are observed only at near the second gyroharmonics [75] that shows electrons are accelerated at the second gyroharmonics resonance region. We, therefore, propose that matching the pump frequency with the second gyroharmonics can accelerate the electrons to an energy level higher than 4 eV. It is the motion of these energetic electrons interacts with the pump wave and excites

the downshifted and upshifted peaks.

Figure 5.7 shows the plot of the second harmonics of the ionospheric electron cyclotron frequency versus height. The pump frequency matches with the second gyroharmonics only at a specific height and depend on the density profile. This explains why the excitation of NSS only occurs within a narrow range of pump frequencies and varies with the ionospheric conditions.

5.0.3 Conclusion

In summary, we have found a new SEE feature called narrow symmetrical structure when the pump frequency is near the second harmonic of the electron cyclotron frequency. The NSS consists of two distinct lower and upper sidebands, roughly symmetric about the pump frequency. The frequency offset $\mid \Delta f_{NSS} \mid$ is within the range of 15 to 30 kHz. The NSS has only been observed for pump frequencies within $\sim 20\ kHz$ from $2f_{ce}$. With the airglow observations at 557.7 nm, we have proofed electrons are accelerated at the second gyroharmonics. We have proposed that it is these energetic electrons than interact with the pump wave and excited the NSS. It is not obvious that the proposed mechanism should fully responsive to the generation of the NSS. It appears necessary to await a quantitative analysis before firm conclusions regarding the physical nature of the NSS can be drawn.

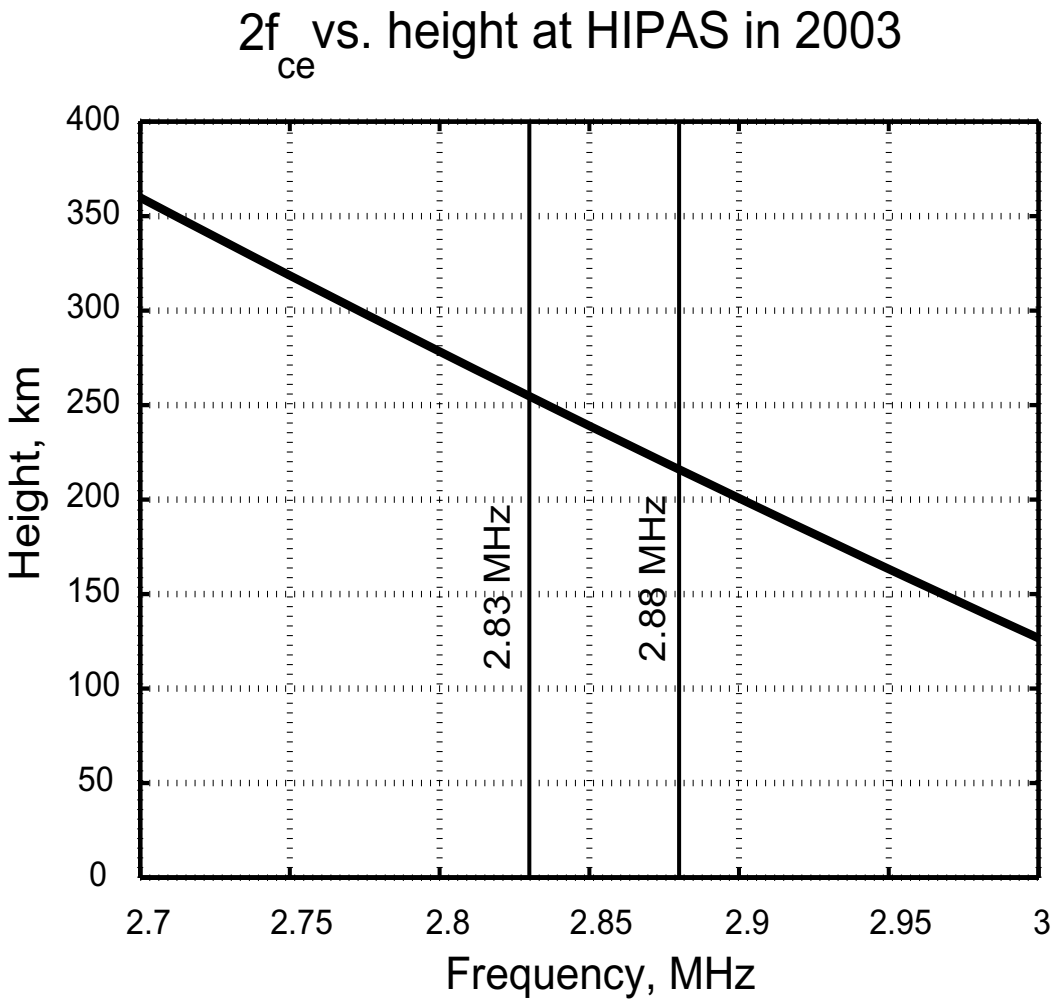

Figure 5.7: Second harmonics of the ionospheric electron cyclotron frequency versus height at HIPAS.

CHAPTER 6

Summary and Suggestions for Future Research

The purpose of this thesis is an experimental investigation at the peak of the ionospheric electron density profile, f_oF_2, and at a region where $f_{pump} \approx f_{pe} \approx 2f_{ce}$ using high power radio EM waves. The particular condition that f_{pump} matches the local plasma frequency at f_oF_2, is referred to as a "matching" condition. Turbulence, local heating, density perturbation, and field-aligned striations (FAS) are results at the resonance layer where the f_{pump} matches the local f_{pe}. At this resonance layer, non-linear processes such as the parametric decay instabilities and UH instabilities are excited. As a result, the resonant layer can stimulate the emission of EM waves that appear as the sidebands of the reflected EM wave, the SEE.

To be able to study the perturbation created at the resonance layer, we have introduced a special heating sequence. This sequence first pre-conditioned the ionosphere with a high power pump wave, then probes the perturbed layer with alternate low and high power pump waves. During the low power transmission, a series of short pulses at three different frequencies were used. Using this heating sequence, we have found the density perturbations created under the matching condition are larger than those under the overdense conditions. With the presence of the density perturbations created by pre-conditioning, the SEE sidebands excited using the low power pump waves can be sustained over a period of ~ 40 sec, twice as longer near the f_oF_2 than at a lower region of the density profile. This re-

sult infers density perturbation created under the matching condition is large and needs a longer time to recover after the high power pump wave is off. Secondly, the threshold of the SEE spectral features is lowered after pre-conditioning. SEE can now be excited with an effective radiation power (ERP) level of 24 dB less than the normally required power.

The FAS created at the resonance region can initiate a non-linear feedback mechanism that leads to mode conversion and anomalous absorption of the pump wave. The effect of anomalous absorption is strongest when the O-mode pump frequency matches the f_oF_2. In addition, anomalous scattering of the pump wave with enhanced low frequency fluctuations, parametric decay, and mode coupling processes under a matching condition appeared in the spectral broadening of the reflected pump wave and the spread of the short pulses return. In comparison, the frequency shift observed in the reflected pump frequency indicates opposite motion of the resonance layers between the X- and O-modes. The frequency shift becomes more significant under the matching condition.

In summary, figure 6.1 shows both a summary of and an explanation for our observations. All the observations mentioned in this thesis and computer model support the concept that large scale density perturbations can be created at the f_oF_2 region which enhances the non-linear processes [103].

Since the condition of the auroral ionosphere varies with the solar activity and also the $2f_{ce}$ varies with height (Figure 5.7) , we have used a frequency stepping schedule to study the EM interactions near the $2f_{ce}$. This is a first time investigation of the SEE spectral features at the second harmonic using the HIPAS heating facility. New observations are reported that are different from the emissions at higher harmonics. Both the spectral widths and the frequency dependence are different. The new feature, called narrow symmetrical structure

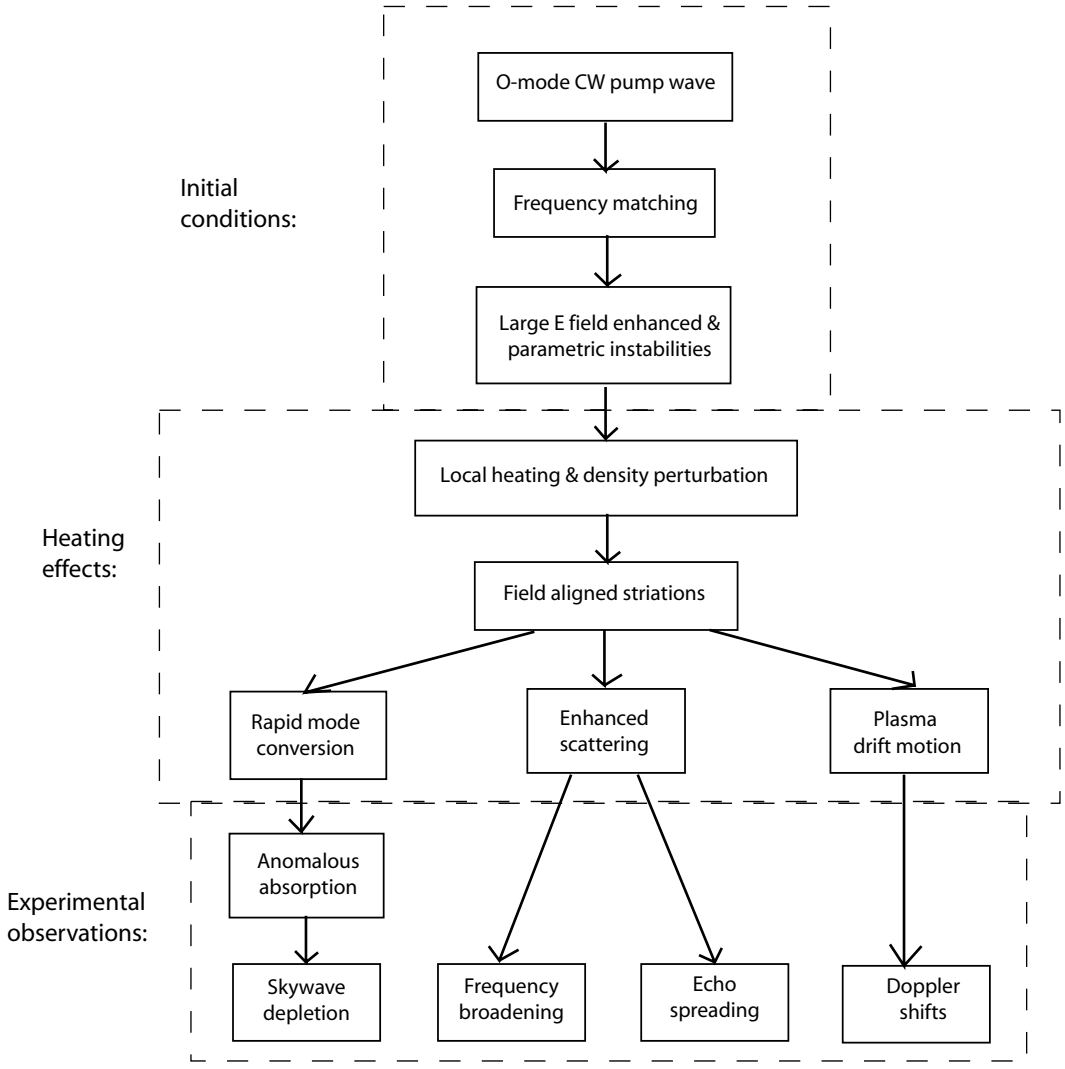

Figure 6.1: Block diagram of a self-consistent physical model to explain the results of EM wave interact with the ionosphere at the peak of the ionospheric density profile. The model includes the initial conditions, heating effects, and experimental observations.

(NSS), consists of two spectral peaks, symmetrically located around the pump frequency f_{pump}, at offset frequencies of 15 to 30 kHz. It bears some resemblance to the broad symmetric structure (BSS) excited at a pump frequency near the third electron cyclotron harmonics. A simple model is put forward to explain the generation mechanism of the NSS. We propose the matching of the pump frequency with the second gyroharmonics accelerate the ionospheric electrons to higher energy level and interact with the pump to generate the NSS.

Regarding future experimental work, it appears important to further explore the matching at the second cyclotron harmonic. High time resolution measurements of the evolution of the NSS at the turn-on and turn-off of the pump wave should be made. The NSS dependence on different propagation direction of the pump wave should be measured. Particularly along the magnetic field line. A quantitative analysis and computer modeling are necessary to confirm the model presented in this thesis.

It would be interesting to match the pump frequency with the second gyroharmonic and with the peak of the ionospheric electron density profile, i.e. $f_{pump} = 2f_{ce} = f_oF_2$.

It is the belief of the author that with improved data taking techniques and simultaneous measurements of the SEE radiated from the perturbed ionosphere with several receivers at different locations could provide valuable information on the physical processes taking place. In particular with the collaborations of other diagnostic such as the ionosonde, SuperDARN, coherent and incoherent radars.

APPENDIX A

Reprint of “Controlled ionospheric preconditioning and stimulated electromagnetic radiation” by P. Y. Cheung, A. Y. Wong, J. Pau, and E. Mjølhus, Phys. Rev. Lett., 80, 4891–4 (1998)

Controlled Ionospheric Preconditioning and Stimulated Electromagnetic Radiation

P. Y. Cheung, A. Y. Wong, and J. Pau
Department of Physics and Astronomy, University of California, Los Angeles, California 90095

E. Mjølhus
Institute of Mathematical Sciences, University of Tromsø, N-9037 Tromsø, Norway
(Received 22 January 1998)

New results of stimulated electromagnetic emissions (SEE) from the HIPAS Observatory are reported. A novel hf heating sequence was used to first precondition the ionosphere, and SEE was then excited with low-amplitude test pulses. Through this approach, the nonlinear physics of SEE was studied. The correlation between small-scale field-aligned density striations and SEE generation was demonstrated, and SEE was excited at power density of 24 dB less than normally required. The results compare well with theoretical predictions of SEE generation via trapped upper hybrid oscillations decay and cavitation within striations. [S0031-9007(98)06204-8]

PACS numbers: 94.20.Tt, 52.35.Mw, 52.35.Ra

The ionosphere provides an "outdoor laboratory" [1] ideally suited for the study and excitation of thermal and nonlinear plasma instabilities through high frequency (hf) ionospheric modification experiments. A manifestation of thermal instabilities is the observation of magnetic field-aligned density striations detected via radar scattering [2–4] and *in situ* rocket measurements [5]. A manifestation of nonlinear plasma processes is the observation of stimulated hf radiation from the heated ionosphere, commonly called stimulated electromagnetic emissions (SEE), through frequency analysis of the returned hf signal after its transit through the ionosphere [6–16]. Two of the more robust SEE spectral features observed under high duty cycle hf heating are a broad, diffuse, and down-shifted (with respect to the heating frequency, $f_{\rm hf}$) continuum, with frequency extension of tens of kilohertz or more, called the broad continuum; and a discrete, narrow, down-shifted peak, called the down-shifted maximum, with an offset frequency near the lower hybrid frequency, $f_{\rm lh}$ [11,12].

It has been suggested that these SEE features are associated with the occurrence of heater-induced small-scale (meter-size) striations [17–21] which act as resonators for electrostatic oscillations at the upper hybrid frequency, $f_{\rm uh}$. In contrast to Langmuir oscillations near the reflection layer where $f_{\rm hf} \sim f_p(z_o)$ [$f_p(z_o)$ is the plasma frequency at the reflection layer z_o], these oscillations have wave vectors predominantly perpendicular to the ambient magnetic field. Recently, Mjølhus [22,23] proposes a SEE theory including the presence of striations and has calculated the radiation source current spectra. Trapped upper hybrid oscillations or eigenstates, with frequency of $f = f_{\rm hf} = f_{\rm uh}(z)$, are first generated via conversion of pump wave off meter-size striations. The parametric decay of these states, with $f' = f_{\rm hf} - f_{\rm dm}$ (f' is the decay wave frequency), results in the generation of the down-shifted maximum feature. Optimum growth of this trapped upper hybrid decay instability is predicted to occur when the frequency offset, $f_{\rm dm}$ ($f_{\rm hf} - f'$), is near $f_{\rm lh}$. The resultant radiation source current spectrum contains discrete spectral peaks that can be identified with the down-shifted maximum feature. As the pump field increases, the discrete peaks change to a broad diffuse continuum. A new cavitation process within the striations has also been suggested for the generation of the broad continuum feature.

The physics of nonlinear SEE generation, in short, encompasses fundamental processes such as the conversion of electromagnetic waves to electrostatic waves off striations, the excitation of trapped eigenmodes, parametric instabilities, and stimulated radiation of electrostatic waves. These issues are topics of active research not only in ionospheric experiments but also in laboratory studies. It is of general interest and great importance, then, that these issues be studied in relation to SEE, that the correlation of striations and SEE be demonstrated, and that details of theoretical predictions be tested under controlled experiments. A survey of past experiments, however, yields inconclusive results.

In this Letter, new results of SEE from a series of controlled ionospheric preconditioning experiments are presented. Specifically, our experimental procedure allows (i) each heating sequence to initiate from or to approach that of a cold start condition; (ii) the complete history of temporal evolution of SEE, from its initial growth to its long-time evolution, be recorded; (iii) the correlation of striations and SEE be clearly demonstrated; and (iv) the low threshold requirement of SEE generation via the trapped upper hybrid decay instability and cavitation be verified. Our results demonstrate unambiguously that, in a preconditioned ionosphere with striations, SEE feature such as the down-shifted maximum can be excited and observed readily with test hf pulses that can be 24 dB weaker in power density than normally required without preconditioning. We have also found that the most dramatic data were observed under the conditions when hf

0031-9007/98/80(22)/4891(4)$15.00

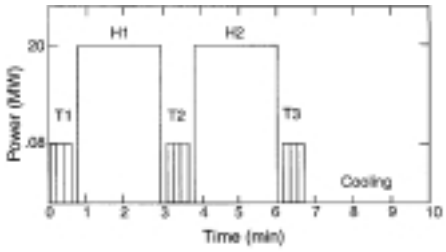

FIG. 1. Schematic of one heating sequence. The sequence consisted of a series of test pulses (T_1, T_2, and T_3) at an effective radiated power ~80 kW, two heating pump pulses (H_1 and H_2) at ~20 MW, and a cooling period.

heater pump frequency, $f_{\rm hf}$, is near the maximum plasma frequency, f_oF_2, of the ionosphere [24,25].

To accomplish our objectives, a novel heating sequence was used instead of transmitting at maximum power continuously. Figure 1 shows one cycle of the heating sequence (10 min long) consisting of three series of short test pulses (T_1, T_2, and T_3), two main heating pump pulses (H_1 and H_2), and a long cooling period. Each series of test pulses further consisted of three separate pulses (10 s each) at three different test frequencies. Test pulses, T_1, were first transmitted to check the background ionospheric conditions and to ensure a cold start condition, i.e., a clean ionosphere with no prior heating effects. This was accomplished by monitoring the spectra of returned signals of test pulses at multiple frequencies. The duration of each pump pulse, 136 s, was chosen to facilitate the growth of small-scale (meter-size) striations while avoiding the excitation of larger scale perturbations. The effects of heating from the first pump pulse, H_1, were monitored by a second sequence of test pulses, T_2, and the effects of H_2, which can also be considered as a test pulse with large amplitude, were monitored by a final sequence of test pulses, T_3. The heating cycle was then repeated after the long cooling period of 200 s when all hf transmission was off.

Experiments were performed periodically from late February to early November 1997 at HIPAS Observatory [26]. The results presented here were selected from the June experiment and are representative of the overall data collected. Measurements of returned hf waves were made at the NOAA facility at Gilmore Creek, 33 km away from the HIPAS Observatory. For this particular set of experiments, the effective radiated power of the main heater wave was ~20 MW while that of the test pulses was ~80 kW. Both the transmitted main pump wave with $f_{\rm hf} = 4.53$ MHz and the test pulses with frequencies of $f_t = 4.50$, 4.53, and 4.56 MHz were at ordinary (O) mode polarization. These heating and test frequencies were near f_oF_2 but were sufficiently away from the nearest multiples of electron cyclotron frequency f_{ce} that gyroharmonic effects are minimized [10]. Specifically, $(f_{\rm hf}, f_t) - 3f_{ce} >$ 300 kHz at the reflection layer of ~220 km.

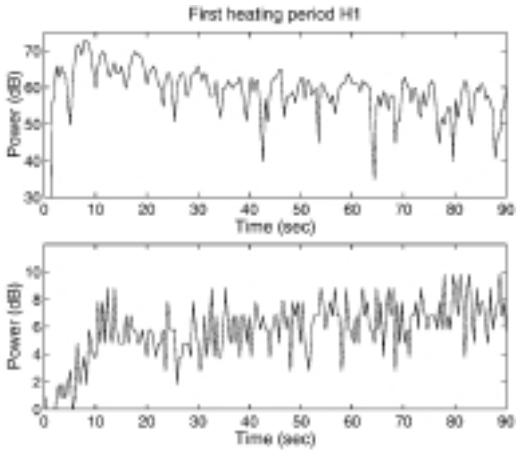

FIG. 2. Temporal evolution of returned hf signal of the first pump pulse H_1 which shows a gradual decline (top panel) and the SEE signal at −9 kHz from $f_{\rm hf}$ which shows a gradual increase (bottom panel).

The temporal evolution of the returned hf power of pump H_1 and its spectral (or SEE) power at a down-shifted frequency of −9 KHz are shown in Fig. 2. Cold start condition was first confirmed by monitoring the return of T_1 [see Fig. 4(a)]. After turn-on at $t = 2$ s, the return pump signal (top panel) drop 10 dB from a range of ~72 dB to a range of ~62 dB within a span of 20 s. This drop in return pump strength is generally attributed to the anomalous absorption of the pump signal as a result of the formation of striations and the subsequent scattering and conversion of pump wave to electrostatic oscillations [10,27–29]. The SEE signal at −9 kHz (bottom panel), on the other hand, displays a rapid rise within the first 10–15 s after turn-on. These two figures clearly show that the growth of SEE is correlated with the decline of pump signal and the excitation of striations.

Sample spectra of returned hf signal of pump H_1 at two discrete times, one near turn-on and the other 88 s into the heating pulse, are shown in Figs. 3(a) and 3(b), respectively. Following past convention, the broad diffuse structure extending from the pump signal peak to negative frequencies is labeled the broad continuum, while the broad peak riding on the continuum at about 9–10 kHz is labeled the down-shifted maximum. The center frequency of the down-shifted maximum feature is close to the lower hybrid frequency of $f_{\rm lh} \sim 8$ kHz. Comparison of Figs. 3(a) and 3(b) illustrates the relatively slow growth of SEE during this first heating period initiating from cold start. For this set of data, the down-shifted maximum feature is barely noticeable in Fig. 3(b).

Preconditioning by pump H_1 makes a significant impact on subsequent test pulse results. This is illustrated by the difference in SEE spectra of returned signals of test pulses T_1 and T_2 before and after H_1 shown

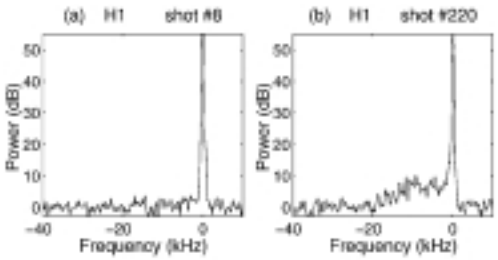

FIG. 3. Frequency spectra of returned hf signal of first pump pulse H_1. Panel (a) shows the spectrum near turn-on of H_1. Panel (b) shows the spectrum 88 s into heating. The horizontal frequency scale is offset from $f_{\rm hf}$.

in Figs. 4(a) and 4(b) for $f_t = 4.56$ MHz. Figure 4(a) shows, as expected, no SEE from the turn signal of T_1. This is consistent with the cold start condition and the result of the much reduced effective radiated power of 80 kW. After preconditioning, however, the results are very different. Figure 4(b) shows a sample spectrum from the return signal of T_2 transmitted 4 s after H_1 was turned off. First, good SEE was observed even at the reduced radiated power. Second, the spectrum shows a very strong and discrete down-shifted maximum feature. This is in distinct contrast to the down-shifted maximum features observed from main pump pulses H_1 and H_2 which are frequently superposed on a continuum background. The discreteness of the down-shifted maximum feature also appears to be more robust when $f_{\rm hf} \sim f_o F_2$.

Preconditioning effects can also persist past the turn-on time of second pump pulse H_2 (transmitted 44 s after H_1 is shut off), and the results are shown in Fig. 5. The returned power of H_2 (top panel), in contrast to that from H_1 shown in Fig. 2, is at a depressed level of $\sim$62 dB due to anomalous absorption from preexisting striations immediately at turn-on, and remains depressed throughout the heating period. The evolution of SEE power at -9 KHz (bottom panel) is also in contrast to that of H_1. It has a strong overshoot at turn-on which is followed by a quick drop with the signal level settling into the same range as that during H_1. This overshoot is very reproducible and occurs consistently during the second heating period with the combination of a large heating pump and preexisting striations.

The overshoot also leads to large frequency broadening in SEE spectra of return signal of second pump H_2. Figure 6(a) shows the spectrum during the overshoot. It shows strong SEE that has a relatively sharp down-shifted maximum peak riding on top of a very broad continuum with frequency extension of over 30 kHz. Figure 6(b) shows the spectrum 9 s into the heating period. It shows weaker SEE with a broader down-shifted maximum peak riding on a much narrower continuum background. Comparison of the two sets of spectra shown in Figs. 3 and 6 clearly contrasts the systematic growth of SEE from cold start condition with pump H_1 and the overshoot phenomenon of SEE with pump H_2 after preconditioning.

Many of our observed results can now be compared with theoretical predictions of Mjølhus [22,23] and be explained. First, the presence of meter-size striation is required in the model. As pointed out earlier, this is inferred experimentally with results from H_1 where the growth of the SEE signal is correlated with the anomalous decay of the pump signal [10,27–29]. Second, the model predicts a very low threshold for the excitation of trapped under hybrid decay instability. This is confirmed by our test pulses data that show the power threshold can be more than 20 dB lower with respect to H_1 and H_2 that generate the striations. Converting experimental parameters into the same scaled units as in the model and comparing with the instability threshold, the test

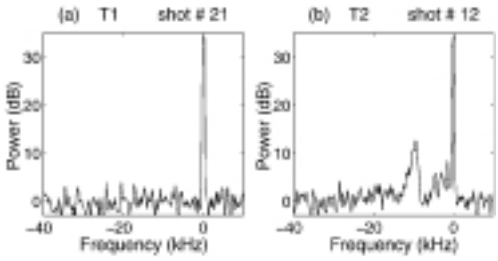

FIG. 4. Frequency spectra of returned signal of test pulses T_1 and T_2. Panel (a) shows no SEE for T_1 before H_1. Panel (b) shows SEE with a discrete down-shifted maximum feature for T_2 after H_1. The frequency scale on each panel is offset from $f_t = 4.56$ MHz.

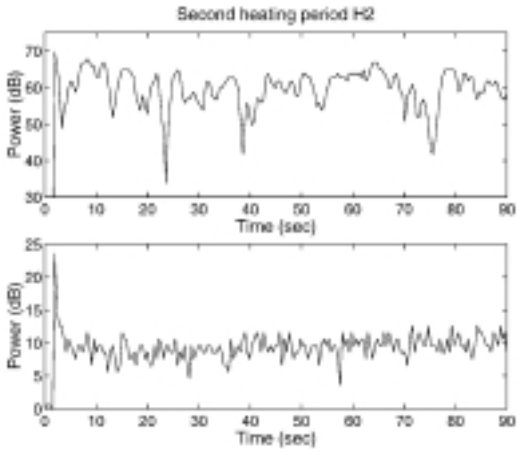

FIG. 5. Temporal evolution of returned hf signal of second pump pulse H_2 (top panel) and the SEE signal at -9 kHz from $f_{\rm hf}$ (bottom panel) that shows a strong overshoot immediately after turn-on.

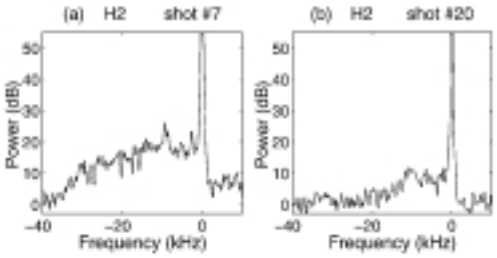

FIG. 6. Frequency spectra of returned hf signal of second pump pulse H_2. Panel (a) shows the spectra during overshoot with strong frequency broadening. Panel (b) shows the spectrum 9 s into heating after broadening has subsided. The frequency scale is offset from f_{hf}.

wave amplitude of $\mathcal{E} \sim 0.025$ gives a striation depth of $\sim 1.5\%$ which is within previous estimates and observations [3,5,19]. For comparison, the scaled main pump wave amplitude is $\mathcal{E} \sim 0.4$. Third, the model predicts the continuum feature requires a higher excitation threshold. This is demonstrated by comparing SEE spectra of H_1 and H_2 with spectra from T_2 (and T_3). In general, superposed spectra with both down-shifted maximum and broad continuum are observed during main heating, while discrete down-shifted maximum with very little broad continuum are observed with the test waves. Fourth, the model predicts that cavitation can occur within striations which leads to a very broad continuum. This appears to be demonstrated from the observation of strong overshoot of the continuum feature with H_2 after preconditioning. The highly nonstationary behavior and the associated wideband spectra agree with general features of cavitation [30]. Further experiments and modeling are needed to confirm this point.

In summary, we have studied the nonlinear physics of SEE and have confirmed the correlation between striations, trapped upper hybrid decay instability, and SEE through our controlled preconditioning experiment. We have demonstrated unambiguously that, in a preconditioned ionosphere with striations, the down-shifted maximum feature can be excited and observed readily with test hf pulses that are 24 dB weaker in power density than the main hf pump wave that preconditions the ionosphere. The results also compare well with predictions from a recent theoretical model of SEE generation via trapped upper hybrid decay instability and cavitation within striations.

This research was supported by ONR Contract No. N00014-96-C-0040, NSF Grant No. PHY-9421693, and partially supported under the auspices of DOE by LLNL Contract No. W-7405-ENG-48. One of the authors (P. Y. C.) acknowledges useful discussions with Dr. Thomas Leyser.

[1] A. Y. Wong, J. Santoru, and G. Sivjee, J. Geophys. Res. **86**, 7718 (1981).
[2] P. A. Fialer, Radio Sci. **9**, 923 (1974).
[3] J. Minkoff, P. Kugelman, and I. Weissman, Radio Sci. **9**, 941 (1974).
[4] S. T. Noble and F. T. Djuth, J. Geophys. Res. **95**, 15 195 (1990).
[5] M. C. Kelley *et al.*, J. Geophys. Res. **100**, 17 367 (1995).
[6] B. Thidè *et al.*, Radio Sci. **18**, 851 (1983).
[7] G. N. Boiko *et al.*, Radiophys. Quantum Electron. **28**, 259 (1985).
[8] B. Thidè *et al.*, J. Geophys. Res. **100A**, 23 887 (1995).
[9] P. Stubbe *et al.*, J. Geophys. Res. **89**, 7523 (1984).
[10] P. Stubbe *et al.*, J. Geophys. Res. **99**, 6233 (1994).
[11] T. B. Leyser *et al.*, J. Geophys. Res. **95**, 17 233 (1990).
[12] T. B. Leyser *et al.*, J. Geophys. Rev. **99**, 19 555 (1994).
[13] H. Derblom *et al.*, J. Geophys. Res. **94**, 10 111 (1989).
[14] W. T. Armstrong *et al.*, Radio Sci. **25**, 1283 (1990).
[15] M. Waldenvik, Ph.D. thesis, Swedish Institute of Space Physics, Uppsala, Sweden, 1994.
[16] P. Bernhardt *et al.*, Phys. Rev. Lett. **72**, 2879 (1994).
[17] T. B. Leyser, Geophys. Res. Lett. **18**, 408 (1991); Phys. Plasmas **1**, 2003 (1994).
[18] E. Mjølhus, J. Atmos. Terr. Phys. **55**, 907 (1993).
[19] A. V. Gurevich, A. V. Lukyanov, and K. P. Zybin, Phys. Lett. **206A**, 247 (1995); V. Gurevich, K. P. Zybin, and A. V. Lukyanov, Phys. Rev. Lett. **75**, 2622 (1995).
[20] Ya. N. Istomin and T. B. Leyser, Phys. Plasmas **4**, 817 (1996).
[21] S. M. Grach *et al.*, Phys. Rev. Lett. **78**, 883 (1997).
[22] E. Mjølhus and E. Helmersen, in *Strong Microwaves in Plasmas*, edited by A. G. Litvak (Institute of Applied Physics, Nizhny Novgorod, 1997), Vol. 2, p. 449.
[23] E. Mjølhus, J. Geophys. Res. (to be published).
[24] A. Y. Wong *et al.*, Phys. Rev. Lett. **63**, 271 (1989).
[25] A. Y. Wong *et al.*, Bull. Am. Phys. Soc. **42**, 1889 (1997).
[26] A. Y. Wong *et al.*, Radio Sci. **25**, 1269 (1990).
[27] K. N. Graham and J. A. Fejer, Radio Sci. **11**, 1057 (1990).
[28] T. B. Jones, T. Robinson, P. Stubbe, and H. Kopka, J. Atmos. Terr. Phys. **46**, 147 (1984).
[29] E. Mjølhus, J. Geophys. Res. **90A**, 4269 (1985).
[30] P. Y. Cheung *et al.*, Phys. Rev. Lett. **79**, 1273 (1997).

References

[1] W. T. Armstrong, R. Massey, P. Argo, R. Carlos, D. Riggin, P. Y. Cheung, M. McCarrick, J. Stanley, and A. Y. Wong. Continuous measurement of stimulated electromagnetic emission spectra from hf excited ionospheric turbulence. Radio Sci., 25:1283–1289, 1990.

[2] B. S. Bauer, A. Y. Wong, L. Scurry, and V. K. Decyk. Efficiency of caviton formation as a function of plasma density gradient. Physics of Fluids B (Plasma Physics), 2(8):1941–1943, 1990.

[3] V. N. Belyakova, I. V. Berezin, V. V. Vas kov, Yu. V. Gruzdev, Yu. S. Dimant, V. A. Zyuzin, O. P. Kapustina, G. P. Komrakov, L. A. Lobachevskiy, G. A. Mikhaylova, V. A. Panchenko, V. P. Polimatidi, A. V. Prokof ev, V. A. Puchkov, and V. Ryzhov. The features of excitation of plasma turbulence by a high-power radio wave field under even-order gyroresonance conditions. Geomagn. Aeron., 31:367–370, 1991.

[4] I. V. Berezin, V. B. Belyanskiy, N. I. Bud ko, V. V. Vas kov, Yu. S. Dimant, V. A. Zyuzin, O. P. Kapustina, G. P. Komrakov, L. A. Lobachevskiy, G. A. Mikhaylova, V. A. Panchenko, A. V. Prokof ev, and V. Ryzhov. Diagnostics of processes of excitation of plasma oscillations by the field of a powerful radio wave. Geomagn. Aeron., 31:702–706, 1991.

[5] P. A. Bernhardt, M. Wong, J. D. Hube, B. G. Fejer, L. S. Wagner, J. A. Goldstein, C. A. Selcher, V. L. Frolov, and E. N. Sergeev. Optical remote sensing of the thermosphere with hf pumped artificial airglow. J. Geophys. Res., 105:10,657–10,671, 2000.

[6] N. F. Blagoveshchenskaya, V. A. Kornienko, M. T. Rietveld, B. Thidè, A. Brekke, I. V. Moskvin, and S. Nozdrachev. Stimulated emissions around second harmonic of troms heater frequency observed by long-distance diagnostic hf tool. Geophys. Res. Lett., 25(6):873–876, 1998.

[7] G. N. Boiko, L. M. Erukhimov, V. A. Zyuzin, G. P. Komrakov, S. A. Metelev, N. A. Mityakov, V. A. Nikonov, V. A. Ryzhov, Yu. V. Tokarev, and V. L. Frolov. Dynamic characteristics of stimulated radio emission from ionospheric plasma. Radiophys. Quantum Electron. Engl. Transl., 28:259–268, 1985.

[8] K. G. Budden. The propagation of radio waves. Cambridge University Press, London, 1985.

[9] H. C. Carlson, W. E. Gordon, and R. L. Showen. High frequency induced enhancements of the incoherent scatter spectrum at arecibo. J. Geophys. Res., 77:1242–1250, 1972.

[10] J. Carroll, E. Violette, and W. Utlaut. The platteville high power facility. Radio Sci., 9:889–894, 1974.

[11] P. Y. Cheung, D. F. DuBois, T. Fukuchi, K. Kawan, H. A. Rose, D. Russell, T. Tanikawa, and A. Y. Wong. Investigation of strong langmuir turbulence in ionospheric modification. J. Geophys. Res., 97:10,575–10,600, 1992.

[12] P. Y. Cheung, E. Mjølhus, D. F. DuBois, J. Pau, H. Zwi, and A. Y. Wong. Stimulated radiation from strong langmuir turbulence in ionospheric modification. Phys. Rev. Lett., 79:1273–1276, 1997.

[13] P. Y. Cheung, A. Y. Wong, J. Pau, and E. Mjølhus. Controlled ionospheric pre-conditioning and stimulated electromagnetic radiation. Phys. Rev. Lett., 80:4891–4894, 1998.

[14] R. A. Close, B. S. Bauer, A. Y. Wong, A. B. Langdon, W. L. Kruer, and E. Mjølhus. Computer simulation of ionospheric radio frequency heating. Radio Sci., 25(6):1341–1349, 1990.

[15] R. Cohen and J. D. Whitehead. Radio-reflectivity detection of artificial modification of the ionospheric f layer. J. Geophys. Res., 75:6439–6445, 1970.

[16] K. Davies. Ionospheric Radio Waves. Blaisdell Publishing Company, 1969.

[17] D. F. DuBois and M. V. Goldman. Radiation induced instability of electron plasma oscillations. Phys. Rev. Lett., 14:544, 1965.

[18] J. R. Dudeney and M. J. Jarvis. A simple graphical method for dealiasing digital ionosonde echo location data. Radio Sci., 21:101–105, 1986.

[19] M. H. Jarvisand J. R. Dudeney. Reduction of ambiguities in hf radar results through a revised receiving antenna array and sounding pattern. Radio Sci., 21:151–158, 1986.

[20] L. M. Duncan and W. E. Gordon. Ionospheric modification by high power radio waves. J. Atmos. Terr. Phys., 44:1009–1017, 1982.

[21] K. B. Dysthe, E. Mjølhus, H. Pecseli, and K. Rypdal. Thermal cavitons. Physica Scripta, T2/2:548–559, 1982.

[22] L. M. Erukhimov, S. A. Metelev, E. N. Myasnikov, N. A. Mityakov, and V. L. Frolov. Artificial ionospheric turbulence (review). Radiophys. Quantum Electron. Engl. Transl., 30:156–171, 1987.

[23] J. A. Fejer. Generation of large-scale field-aligned density irregularities in ionospheric heating experiments. In AGARD Conf. Proc., volume 138, pages 13–1 – 13–6, 1973.

[24] J. A. Fejer. Ionospheric modification and parametric instabilities. Reviews of Geophysics and Space Physics, 17(1):135–53, 1979.

[25] J. A. Fejer and Y. Y. Kuo. Structure in the nonlinear saturation spectrum of parametric instabilities. Phys. Fluids, 16:1490, 1973.

[26] P. A. Fialer. Field-aligned scattering from a heated region of the ionosphere observations at hf and vhf. Radio Sci., 9:923–940, 1974.

[27] V. L. Frolov, G. N. Boiko, S. A. Metelev, and E. N. Sergeev. On the study of artificial ionospheric turbulence by means of stimulated electromagnetic emission. Radiophys. Quantum Electron. Engl. Transl., 37:593–603, 1994.

[28] V. L. Frolov, E. N. Ermakova, L. M. Erukhimov, G. P. Komrakov, E. N. Sergeev, and P. Subbe. A new upshifted spectral stimulated electromagnetic emission strcture, observed between electron cyclotron harmonics. GRL, 24:1647–1650, 1997.

[29] V. L. Frolov, E. N. Ermakova, L. M. Kagan, G. P. Komrakov, E. N. Sergeev, and P. Subbe. Features of the broad upshifted structure in stimulated electromagnetic emission spectra. JGR, 105:20919–20933, 2000.

[30] V. L. Frolov, E. N. Ermakova, L. M. Kagan, G. P. Komrakov, S. N. Sergeev, and P. Stubbe. Features of the broad upshifted structure in stimulated electromagnetic emission spectra. J. Geophys. Res., 105(A9):20919–33, 2000.

[31] V. L. Frolov, L. M. Erukhimov, S. A. Metelev, and S. N. Sergeev. Temporal behaviour of artificial small-scale ionospheric irregularities: Review of experimental results. J. Atmos. Sol. Terr. Phys., 59(18):2317–2333, 1997.

[32] V. L. Frolov, S. M. Grach, L. M. Erukhimov, G. P. Komrakov, E. N. Sergeev, B. Thidè, and T. Carozzi. Preculiarities in the evolution of the bum of stimulated radio emission of the ionosphere. Radiophys. Quantum Electron, 39:241–254, 1996.

[33] V. E. Golant and A. D. Piliya. Linear transformation and absorption of waves in a plasma. Sov. Physics. Uspekhi, 14:413–437, 1972.

[34] W. E. Gordon, R. Showen, and H. C. Carlson. Ionospheric heating at arecibo: First test. J. Geophys. Res., Space Phys., 75:6436–6438, 1971.

[35] S. M. Grach. Electromagnetic radiation from artificial ionospheric plasma turbulence. Radiophys. Quantum Electron. Engl. Transl., 28:470–477, 1985.

[36] S. M. Grach, M. M. Shvarts, E. N. Sergeev, and V. L. Frolov. Broad continuum feature of stimulated electromagnetic emission. J. Atmos. Sci., 60:1233–1246, 1998.

[37] K. N. Graham and J. A. Fejer. Anomalous raio wave absorption due to ionospheric heating effects. Radio Sci., 11:1057–1063, 1976.

[38] A. V. Gurevich. Nonlinear phenomena in the ionosphere. Springer-Verlag, New York, 1978.

[39] A. V. Gurevich, H. Carlson, A. V. Lukyanov, and K. P. Zybin. Parametric decay of upper hybrid plasma waves trapped inside density irregularities in the ionosphere. Phys. Letts. A, 23:97–108, 1997.

[40] A. V. Gurevich, A. V. Lukyanov, and K. P.Zybin. Stationary state of isolated striations developed during ionospheric modification. Phys. Lett. A, 206:247–259, 1995.

[41] A. V. Gurevich, A. V. Lukyanov, and K. P.Zybin. Anomalous absorption of powerful radio waves on the striations developed during ionospheric modification. Phys. Lett. A, 211:363–372, 1996.

[42] A. V. Gurevich, K. P. Zybin, and A. V. Lukyanov. Stationary striation developed in the ionospheric modification. Phys. Rev. Lett., 75(13):2622–2625, 1995.

[43] P. N. Guzdar, P. K. Chaturvedi, K. Papadopoulos, M. J. Keskinen, and S. L. Ossakow. The self-focusing instability in the presence of density irregularities in the ionosphere. J. Geophys. Res., 101:2453–2460, 1996.

[44] P. N. Guzdar, P. K. Chaturvedi, K. Papadopoulos, and S. L. Ossakow. The thermal self-focusing instability near the critical surface in the high-latitude ionosphere. J. Geophys. Res., 103:2231–2237, 1998.

[45] T. Hagfors, W. Kofman, H. Kopka, P. Stubbe, and T. Äijänen. Observations of enhanced plasma lines by eiscat during heating experiments. Radio Sci., 18:861–866, 1983.

[46] Å. Hedberg, H. Derblom, B. Thidè, H. Kopka, and P. Stubbe. Observations of hf backscatter associated with the heating experiment at tromsø. Radio Sci., 18:840–850, 1983.

[47] D. E. Hinkel-Lipsker, B. D. Fried, and G. J. Morales. Analytic expression for mode conversion of langmuir and electromagnetic waves. Phys. Rev. Lett., 62:2680–2682, 1989.

[48] F. Honary, A. J. Stocker, T. R. Robinson, T. B. Jones, and P. Stubbe. Ionospheric plasma response to hf radio waves operating at frequencies close to the third harmonic of the electron gyrofrequency. J. Geophys. Res., 100(A11):21489–501, 1995.

[49] R. D. Hunsucker. Radio Techniques for Probing the Terrestrial Ionosphere, volume 22 of Physics and Chemistry in Space. Springer-Verlag Berlin Heidelberg, 1991.

[50] Ya. N. Istomin and T. B. Leyser. Small-scale magnetic field-aligned density irregularities excited by a powerful electromagnetic wave. Phys. Plasmas, 4(3):817–828, 1997.

[51] Ya. N. Istomin and T. B. Leyser. Parametric interaction of self-localized upper hybrid states in quantized plasma density irregularities. Phys. Plasmas, 5(4):921–931, 1998.

[52] Ya. N. Istomin and T. B. Leyser. Quantization of plasma density irregularities under the action of a powerful electromagnetic wave: Spectrum of upper hybrid oscillations self consistently trapped in the density cavities. Radiophys. Quantum Electron. Engl. Transl., 42:641–650, 1999.

[53] T. B. Jones, T. Robinson, P. Stubbe, and H. Kopka. Frequency dependence of anomalous absorption caused by high power radio waves. J. Atmos. Terr. Phys., 46:147–153, 1984.

[54] W. L. Kruer. Model of resonance absorption with profile modification. Phys. Fluids, 25(12):2324–2325, 1982.

[55] W. L. Kruer. The Physics of Laser Plasma Interactions. Addison-Wesley Publishing Company, New York, 1988.

[56] T. B. Leyser, B. T hidè, M. Waldenvik, S. Goodman, V. L. Frolov, S. M. Grach, A. N. Karashtin, G. P. Komrakov, and D. S. Kotik. Spectral structure of stimulated electromagnetic emissions between electron cyclotron harmonics. J. Geophys. Res., 98(A10):17597 – 17606, 1993.

[57] T. B. Leyser, B. Thidè, H. Derblom, Å. Hedberg, B. Lundborg, P. Stubbe, and H. Kopka. Stimulated electromagnetic emission near electron cyclotron harmonics in the ionosphere. Phys. Rev. Lett., 63:1145–147, 1989.

[58] T. B. Leyser, B. Thidè, H. Derblom, Å. Hedberg, B. Lundborg, P. Stubbe, and H. Kopka. Dependence of stimulated electromagnetic emission on the ionosphere and pump wave. J. Geophys. Res., 95:17,233–17,244, 1990.

[59] T. B. Leyser, B. Thidè, S. Goodman, M. Waldenvik, E. Veszelei, S. M. Grach, A. N. Karashtin, G. P. Komrakov, and D. S. Kotik. Narrow cyclotron harmonic absorption resonances of stimulated electromagnetic emission in the ionosphere. Phys. Rev. Lett., 68:3299–3302, 1992.

[60] T. B. Leyser, B. Thidè, M. Waldenvik, E. Veszelei, V. L. Frolov, S. M. Grach, and G. P. Komrakov. Downshifted maximum features in stimulated electromagnetic emission spectra. J. Geophys. Res., 99(A10):19,555–19,568, 1994.

[61] B. Lundborg and B. Thidè. Standing wave pattern of hf radio waves in the ionospheric reflection region: 1. general formulas. Radio Sci., 20:947–958, 1985.

[62] B. Lundborg and B. Thidè. Standing wave pattern of hf radio waves in the ionospheric reflection region 2. applications. Radio Sci., 21:486–500, 1986.

[63] G. M. Milikh, K. Papadopoulos, M. McCarrick, and J. Preston. Elf emission generated by the haarp hf-heater using varying frequency and polarization. Radiophys. Quantum Electron. Engl. Transl., 42:639–46, 1999.

[64] J. Minkoff. Radio frequency scattering from a heated ionospheric volume, 3, cross-section calculations. Radio Sci., 9:997–1004, 1974.

[65] J. Minkoff, P. Kugelman, and I. Weissman. Radio frequency scattering from a heated ionospheric volume, 1, vhf/uhf field-aligned and plasma-line backscatter measurements. Radio Sci., 9:941–955, 1974.

[66] E. Mjølhus. Anomalous absorption and reflection in ionospheric radio modification experiments. J. Geophys. Res., 90:4269–4279, 1985.

[67] E. Mjølhus. On linear conversion in a magnetized plasma. Radio Sci., 25:1321–1339, 1990.

[68] E. Mjølhus. Parametric instabilities of trapped upper-hybrid oscillations. J. Plasma Phys., 58:747–769, 1997.

[69] E. Mjølhus. Theoretical model for long time stimulated electromagnetic emission generation in ionospheric radio modification experiments. J. Geophys. Res., 103:14711–14729, 1998.

[70] E. Mjølhus and T. Flå. Direct access to plasma resonance in ionospheric radio experiments. J. Geophys. Res., 89:3921–3928, 1984.

[71] F. W. Perkins, C. Oberman, and E. J. Valeo. Parametric instabilities and ionospheric modification. J. Geophys. Res., 79:1478–1496, 1974.

[72] H. Rishbeth and O. K. Garriot. Introduction to ionospheric physics. Academic Press, NewYork and London, 1969.

[73] P. A. Robinson. Nonlinear wave collapse and strong turbulence. Rev. Mod. Phys., 69:507–573, 1997.

[74] P. E. Rodriguez, J. E. Kennedy, M. Keskinen, C. Siefring, Sa. Basu, M. McCarrick, J. Preston, M. Engebretson, M. Kaiser, M. Desch, K. Goetz, J. L. Bougeret, and R. Manning. The wind-haarp experiment: Initial results of high power radiowave interactions with space plasmas. Geophys. Res. Lett., 26:2351–2354, 1999.

[75] D. D. Sentman, R. F. Wuerker, M. J. McCarrick, T. Pedersen, E. M. Wescott, H. Stenbaek-Nielsen, A. Y. Wong, M. Kubota, F. T. Sao Sabbas, and D. Lummerzheim. Imaging and spectrographic observations of artificial airglow excited by haarp and hipas. In RF Ionospheric Interactions Workshop, page 632, Santa Fe, New Mexico, 2002.

[76] M. M. Shvarts and S. M. Grach. Interaction of upper and lower hybrid waves and generation of the downshifted maximum feature of stimulated electromagnetic emissions. J. Atmos. Terr. Phys., 59:2421–2429, 1997.

[77] M. M. Shvarts, S. M. Grach, V. L. Frolov, and E. N. Sergeev. Modeling of the wideband component of artificial radioemission of the ionosphere. Radiophys. Quantum Electron. Engl. Transl., 37:412–431, 1994.

[78] M. M. Shvarts, S. M. Grach, V. L. Frolov, and E. N. Sergeev. On the generation of the stimulated electromagnetic emission. the computer simulation results. Adv. Space Res., 15:59–62, 1995.

[79] V. P. Silin. Parametric resonance in a plasma. Sov. Phys. JETP, Engl. Transl., 21:1127, 1965.

[80] R. L. Stenzel, A. Y. Wong, and H. C. Kim. Conversion of electromagnetic waves to electrostatic waves in inhomogeneous plasmas. Phys. Rev. Lett., 32:654–657, 1974.

[81] A. J. Stocker, F. Honary, T. R. Robinson, and T. B. Jones. Anomalous absorption during artificial modification at harmonics of the electron gyrofrequency. J. Geophys. Res., 98:13627–13645, 1993.

[82] P. Stubbe, H. Hopka, B. Thidè, and H. Derblom. Stimulated electromagnetic emission: A new technique to study the parametric decay instability in the ionosphere. J. Geophys. Res., 89:7523–7536, 1984.

[83] P. Stubbe and H. Kopka. Stimulated electromagnetic emission in a magnetized plasma: A new symmetric spectral feature. Phys. Rev. Lett., 65:183–186, 1990.

[84] P. Stubbe, H. Kopka, T. B. Jones, and T. Robinson. Wide band attenuation of radio waves caused by powerful hf waves: Saturation and dependence on ionospheric variability. J. Geophys. Res., 87:1551–1555, 1982.

[85] P. Stubbe, H. Kopka, H. Lauche, M. T. Rieveld, A. Biekke, O. Holt, T. Robinson T. B. Jones, A. Hedberg, B. Thidè, M Crocketr, and H. J. Lotz. Ionospheric modification experiments in northern scandinavia. J. Atmos. Terr. Phys., 44:1025–1041, 1982.

[86] P. Stubbe, A. J. Stocker, F. Honary, T. R. Robinson, and T. B. Jones. Stimulated electromagnetic emissions and anomalous hf wave absorption near electron gyroharmonics. J. Geophys. Res., 99(A4):623–6246, 1994.

[87] B. Thidè, H. Derblom, Å. Hedberg, H. Kopka, and P. Stubbe. Observations of stimulated electormagnetic emissions in ionospheric heating experiments. Radio Sci., 18:851–859, 1983.

[88] B. Thidè, F. T. Djuth, T. B. Leyser, and H. M. Ierkic. Evolution of langmuir turbulence and stimulated electromagnetic emissions excited with a 3-mhz pump wave at arecibo. J. Geophys. Res., 100(A12):23887–23899, 1995.

[89] B. Thidè, Å. Hedberg, J. A. Fejer, and M. P. Sulzer. First observations of stimulated electromagnetic emission at arecibo. Geophys. Res. Lett., 16:369–372, 1989.

[90] B. Thidè, H. Kopka, and P. Stubbe. Observations of stimulated scattering of a strong high-frequency radio wave in the ionosphere. Phys. Rev. Lett., 49:1561–1564, 1982.

[91] G. Thome and D. Blood. First observation of rf backscatter from field-aligned irregularities produced by ionospheric heating. Radio Sci., 9:917–921, 1974.

[92] L. C. Tsai, F. T. Berkey, and G. S. Stiles. On the derivation of an improved parameter configuration for the dynasonde. Radio Sci., 28:785–793, 1993.

[93] W. F. Utlaut. An ionospheric modification experiment using very high power, high frequency transmission. J. Geophys. Res., 75:6402–6405, 1970.

[94] W. F. Utlaut and E. J. Violette. A summary of vertical incidence radio observations of ionospheric modification. Radio Sci., 9:895–903, 1974.

[95] V. V. Vas'kov, S. F. Golyan, Yu. V. Gruzdev, A. V. Gurevich, Ya. S. Dimant, V. Yu. Kim, L. A. Lobachevskii, V. V. Migulin, V. A. Panchenko, M. S. Petrov, V. P. Polimatidi, V. I. Sitnikov, L. D. Shoya, I. S. Shlyuger, and K. I. Yurin. Stimulated ionization of the upper ionosphere by an intense radio wave. JETP Lett., 34:558–561, 1981.

[96] V. V. Vas'kov, S. F. Golyan, A. V. Gurevich, Ya. S. Dimant, V. A. Zyuzin, V. Yu. Kim, G. P. Komrakov, L. A. Lobachevskii, V. V. Migulin, N. A. Mityakov, V. A. Panchenko, and V. P. Polimatidi. Excitation of upper hybrid resonance in the ionospheric plasma by an intense radio wave. JETP Lett., 43:663–666, 1986.

[97] E. Villalón. Ionospheric electron acceleration by electromagnetic waves near regions of plasma resonances. J. Geophys. Res., 94:2717–2720, 1989.

[98] L. S. Wagner, J. A. Goldstein, R. W. Lind, A. Y. Wong, and M. J. McCarrick. Channel probe observations of the auroral ionosphere during high-power auroral stimulation experiments. Radio Sci., 25(6):1407–1422, 1990.

[99] J. Weinstock. Enhanced airglow, electron acceleration, and parametric instabilities. Radio Sci., 9:1085–1087, 1974.

[100] R. B. White and F. F. Chen. Amplification and absorption of electromagnetic waves in overdense plasmas. Plasma Phys., 16:565–587, 1974.

[101] J. D. Whitehead. The asorption of radio waves in an ionospheric layer. J. Atmos. Terr. Phys., 9:276–281, 1956.

[102] A. Y. Wong, J. Carroll, R. Dickman, W. Harrison, W. Huhn, B. Lum, M. J. McCarrick, J. Santoru, C. Schock, G. Wong, and R. F. Wuerker. High-power radiating facility at the hipas observatory. Radio Sci., 25:1269–1282, 1990.

[103] A. Y. Wong, P. Y. Cheung, M. J. McCarrick, J. Stanley, R. F. Wuerker, R. Close, and B. S. Bauer. Large-scale resonant modification of the polar ionosphere by electromagnetic waves. Phys. Rev. Lett., 63:271–274, 1989.

[104] A. Y. Wong, G. J. Morales, D. Eggleston, J. Santoru, and R. Behnke. Rapid conversion of electromagnetic waves to electrostatic waves in the ionosphere. Phys. Rev. Lett., 47(18):1340–1343, 1981.

[105] A. Y. Wong and R. L. Stenzel. Ion acceleration in strong electromagnetic interactions with plasmas. Phys. Rev. Lett., 34:727, 1975.

[106] A. Y. Wong and R. J. Taylor. Parametric excitation in the ionosphere. Phys. Rev. Lett., 27:644–647, 1971.

[107] J. W. Wright and M. L. V. Pitteway. Real-time data acquisition and interpretation capabilities of the dynasonde 1. data acquisition and real-time display. Radio Sci., 14:815–825, 1979.

[108] J. W. Wright and M. L. V. Pitteway. Real-time data acquisition and interpretation capabilities of the dynasonde 2. determination of magnetoionic mode and echolocation using a small spaced receiving array. Radio Sci., 14:827–8356, 1979.

[109] H. L. Zhou, J. Huang, and S. P. Kuo. Cascading of the upper hybrid/electron bernstein wave in ionospheric heating experiments. Phys. Plasmas, 1:3044–3052, 1994.